Pinnacle

# Development of an Advanced Hydraulic Fracture Mapping System

## Final Report for U. S. Department of Energy DE-FC26-04NT42108

**Reporting Period Start Date:** **April 15, 2004**
**Reporting Period End Date:** **January 31, 2007**


By:

*Norm Warpinski*
*Steve Wolhart*
*Larry Griffin*
*Eric Davis*

Pinnacle Technologies, Inc.
9949 W. Sam Houston Parkway N.
Houston, Texas 77064

## Disclaimer



## Abstract

The project to develop an advanced hydraulic fracture mapping system consisted of both hardware and analysis components in an effort to build, field, and analyze combined data from tiltmeter and microseismic arrays. The hardware sections of the project included: (1) the building of new tiltmeter housings with feedthroughs for use in conjunction with a microseismic array, (2) the development of a means to use separate telemetry systems for the tilt and microseismic arrays, and (3) the selection and fabrication of an accelerometer sensor system to improve signal-to-noise ratios. The analysis sections of the project included a joint inversion for analysis and interpretation of combined tiltmeter and microseismic data and improved methods for extracting slippage planes and other reservoir information from the microseisms. In addition, testing was performed at various steps in the process to assess the data quality and problems/issues that arose during various parts of the project. A prototype array was successfully tested and a full array is now being fabricated for industrial use.

# Table of Contents

# List of Figures

# List of Tables

# 1. Introduction

Hydraulic fracturing is an essential technology for fostering economic production of hydrocarbons from oil and gas wells. It is used on most gas wells in the U.S. and also on a large percentage of the oil wells to improve connectivity with the reservoir in order to access and produce the reserves. Hydraulic fractures are created with numerous fluid systems (various gels, water, foam, $CO_2$, $N_2$), several types of proppants (sand, ceramics, bauxite) of various strengths and densities, various perforation designs, elaborate pump schedules, and different flowback and cleanup strategies. Given this diversity of treatment options, optimization has always been hindered by an inability to directly observe what the created fracture looks like and what its characteristics are. Instead, most fracture optimization has relied on indirect pressure analyses, various well-testing and production analyses, and some near-wellbore diagnostics, which provide a very limited and/or opaque view into the subsurface results.

Recent developments in hydraulic fracture mapping have resulted in a much improved window into the subsurface that gives a more comprehensive view of the created fracture. The use of downhole tiltmeters and downhole microseismic mapping, in particular, have allowed for reasonably accurate measurements of created fracture heights, lengths, azimuths, asymmetry, and elements of complexity (complexity is a particularly interesting element because its existence and prevalence was widely dismissed until microseismic mapping provided proof).

Tiltmeters are extremely sensitive devices that measure the slightest deformation of the ground, much like a carpenter's level.[1] However, the tiltmeters used in hydraulic fracture mapping are designed for much higher sensitivities and can measure tilts as small as one nanoradian. **Figure 1** shows a schematic of a tiltmeter sensor, which is an active device that uses a conductive fluid and suitably placed electrodes to achieve the required precision. Arrays of tiltmeters are used to measure the deformation (actually measured the gradient of displacement) around a fracture that is induced by the opening of the fracture. This deformation is measured and then inverted for the size and shape of the fracture that created the deformation.

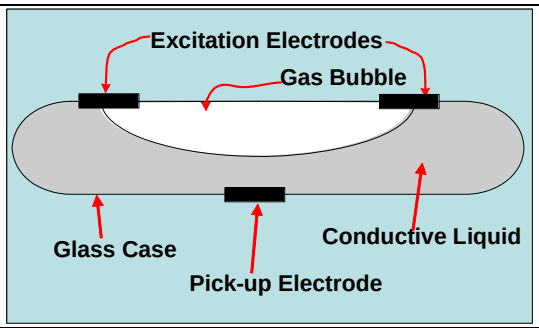


**Figure 1. Tiltmeter sensor**

Microseismic mapping is performed with an array of triaxial seismic receivers, which detect very small earthquakes that are induced by the changes in stress and pore pressure caused by the fracturing process.[2] The geophones or accelerometers in these receivers need to be extremely sensitive and also have higher frequency capabilities than typical VSP receivers, as the microseisms are generally small, high-frequency events. The receiver array detects the microseisms, and P- (compressional) and S- (shear) arrivals are determined during processing. By appropriate ray tracing, the distance and elevation to the microseism can be determined. The particle motion of the P- and S-waves (the reason why tri-axial receivers are

required) provides the information on the direction to the microseismic source. Since these microseisms are generated in a zone surrounding the fracture, the overall shape and size of the fracture can be evaluated from the spatial distribution of the microseisms.

In most fracture mapping situations, there is at most one monitor well close enough to be useful for either microseismic or downhole tiltmeter mapping. In such cases, it is currently necessary to choose one of these two technologies based upon the type of information that is required; however, there is no guarantee *a priori* that the selected technology will actually yield better results. For example, tiltmeters are insensitive to seismic noise, as induced by nearby drilling or fracturing equipment on the same pad, while microseismic receivers may be "deafened" by the noise to the point that few or no microseisms can be detected. On the other hand, microseisms gain an advantage as the monitoring distance increases because resolution from the tilt measurements decreases with distance. There may be non-seismic intervals so that microseismic monitoring misses part of the fracture, but tiltmeters respond to the deformation and will always be perturbed by fractures in such intervals. Tiltmeters average the deformation from whatever fracture or fractures are there so that complexity is difficult to deal with, whereas microseismic monitoring is ideal for mapping complex fracture treatments. There are numerous similar advantages and disadvantages of these two technologies that interplay under various circumstances, leading an observer to the obvious conclusion that it would be optimal to have both technologies in a single array in the monitoring well. This is the rationale behind the hybrid array concept.

In addition to the hybrid array, there are other activities that could be used to attempt an improvement in the data obtained by the array and in the interpretation of the results. These include improvements in the microseismic receivers, the tiltmeters, analysis procedures, and interpretation of the data.

Current microseismic receivers use geophones with relatively good characteristics; however, microseisms are events that have characteristics that should be better detected using accelerometers. Finding or developing an accelerometer with high temperature capabilities, high shock resistance, low noise, and a relatively high resonant frequency could offer advantages in detecting small and/or far events.

Current downhole tiltmeter tools have very sensitive sensors, but coupling of the sensors to walls currently uses bow spring centralizers or magnets and may not be the most noise-free method of deploying these tools. Potentially a clamp arm (as on the microseismic tools) could provide better data quality. In addition, noise generated in the tool (there are motors, amplifiers, A/D, telemetry, and various other circuits in the tool, all requiring power and all possible sources of noise) could potentially be reduced to improve data quality.

Analysis of these data sets is performed separately, resulting in a microseismic map and a tiltmeter map. If there are discrepancies in the two maps, questions can arise as to how to merge the results into the most consistent picture of the fracture. One solution is to develop a joint inversion that attempts to employ both data sets in a single inversion process of the data.

Finally, data such as microseismic events offer much information about the fracturing process and the reservoir that would be very useful in any analysis of a fracturing treatment. Developing better methods for evaluating source parameters (key elements describing the slippage) could offer an improved understanding of both the data and its relevance to the fracturing episode.

# 2. Proposed Technical Approach

*The following is the technical approach outlined in the original proposal to DOE.*

Hydraulic fracture mapping can be key to understanding and optimizing the stimulation of wells in unconventional gas reservoirs. While hydraulic fracture mapping is proving its value to the natural gas industry, this is an emerging technology that has much room for improvement. Microseismic hydraulic fracture mapping is currently performed using a multi-level (typically 12 levels) array of seismic receivers (triaxial geophones) deployed in a well offset to the treatment well. Data from the geophones is transmitted up a fiber-optic wireline to a data acquisition system for recording and then to a data processing system for analysis. Downhole tiltmeter mapping is currently performed using a multi-level (up to 15 levels) array of tiltmeters deployed in an offset well. Data from the tiltmeters is transmitted up a single-conductor wireline for data acquisition and processing. Currently, microseismic and tiltmeter arrays cannot be run concurrently and require separate observation wells offset to the treatment well.

The goal of this project is to develop and test an advanced system incorporating both seismic sensors and tiltmeters in one tool. In addition, improved instrumentation (both microseismic and tilt) will be developed and tested to improve viewing distance and accuracy. Finally, new data processing techniques will be developed and tested that can improve the information derived from hydraulic fracture mapping. These advancements will improve the quality of hydraulic fracture mapping results, reduce limits on the use of fracture mapping and make it more cost effective.

The objectives of the proposed project are to:

- Develop a combination microseismic receiver-tiltmeter system eliminating the need for two observation wells
- Improve microseismic receiver sensitivity by evaluating and testing accelerometer vs. geophone-based instruments
- Improve tiltmeter sensitivity by evaluating and testing new instruments and by assessing tiltmeter sensitivity in tools clamped in the wellbore as opposed to current tools, which are coupled to the casing-formation with bow spring centralizers or magnets
- Develop a joint-inversion routine using microseismic and tiltmeter data
- Develop a microseismic source mechanism technique offering more information for both reservoir characterization and hydraulic fracture optimization

## 2.1 Work Plan

The best means to perform this research and development was through modification of the existing seismic tool (Geospace DDS-250). The DDS-250 is a fairly new tool but it has proven to be very reliable in the field and it provides a solid platform for making these advancements; however, the DDS-250 was developed for active seismic operations (*e.g.*, crosswell seismic, VSP, etc.) and is not optimized for passive seismic monitoring like hydraulic fracture mapping. Research needs to be performed to optimize the DDS-250 for passive seismic monitoring. It will be more efficient, both time- and cost-wise, to modify the existing tool rather than develop an entirely new system. Pinnacle owns fifteen DDS-250's and will make them available to the project for development of the advanced hydraulic fracture mapping system.

The work necessary for this project includes:

- Inspection of the DDS-250 tool for power and signal input levels
- Selection or development of a triaxial accelerometer package with sufficient sensitivity and ruggedness
- Selection or development of a tiltmeter with sufficient sensitivity and ruggedness
- Design and fabrication of prototype circuitry for the seismic and tiltmeter instruments
- Design and fabrication of a prototype shuttle to hold the various components
- Installation and testing of the new instrumentation package in the receiver
- Comparison of the new combined tool performance with the current standalone tools
- Development of a joint inversion code to analyze microseismic-tiltmeter data
- Development of a rigorous source mechanism technique

The results of the work will be documented in a comprehensive final report and at least two industry publications. The improvements will be incorporated into Pinnacle's fracture mapping services. Pinnacle is the leader in providing fracture mapping services to the oil and gas industry. Project results will be featured in the multiple workshops and forums that Pinnacle conducts annually.

## 2.2 Tasks

### 2.2.1 Development of Combined Microseismic-Tiltmeter Receiver

Subtasks associated with this task are:

#### A. Inspection of Existing Tool

The types of accelerometers that will be used are constant-current devices; they typically require some bias voltage and minimum current along with some amplification. As a result, they need low-noise power, adequate voltage levels at the tools to allow full operation of the sensor, and sufficient power on the instrumentation power line. These specifications will be measured on a Geospace DDS-250 receiver to determine instrumentation constraints and design needs for power-conditioning circuitry.

### B. Selection of a Tri-Axial Accelerometer Package

Survey tri-axial accelerometer packages to find the optimal sensor. Many accelerometers are available for a wide number of applications but they need to be screened to meet the sensitivity and ruggedness requirements for standard oilfield application. Requirements are:

- ~1 volt/g sensitivity
- Minimum 1,000 g shock resistance
- Operating temperature up to 150° C
- Resonant frequency no less than 5 kHz
- Fairly flat response out to 3,000 Hz (*e.g.*, 3 dB point at least 2,500 Hz)
- Low power requirements

The objective is to find a tri-axial package, but we may find that many of the tri-axial packages have their grounds tied together. For the level of accuracy needed in this application, this is not desirable and full isolation of the three axes is required. If there is not a tri-axial package with the necessary requirement, then we will look for individual accelerometers for each of the three sensor axes.

### C. Selection or Design of a Tiltmeter Package

The current offset well dual-axis tiltmeters (optimized for a 2.875" receiver) are too large for the DDS-250 (2.5" OD) microseismic receiver. The current treatment well dual-axis tiltmeters (optimized for a 1.6875" receiver) do not have the sensitivity necessary for offset well monitoring. We will design a tiltmeter sensor packaged to fit in the DDS-250 with the sensitivity necessary for offset well fracture mapping.

### D. Design of a Power-Conditioning Circuit

Based on the tool characterization from Subtask **2.2.1** and the instruments selected in Subtasks B and C we will design and build a power-conditioning circuit to provide the correct power requirements.

### E. Design of the Accelerometer Supply & Amplification Circuit

The instruments selected in Subtask B may have their grounds all tied together and leading to noise problems and cross talk that will destroy our ability to detect microseisms. To eliminate this problem, we will design and build an accelerometer constant-current supply and amplification circuit that is fully isolated and shielded and runs on battery power.

### F. Design and Fabrication of a New Shuttle

The current sensor fixture, or shuttle, is designed to hold three SMC1850 or OMNI2400 geophones. This shuttle needs to be replaced with a new one that holds the tiltmeters, accelerometer (or accelerometers), the power regulation board, and the constant-current/amplifier board. Given the drawings for the current shuttle, we will redesign it so that we could attach the accelerometers and circuit boards in a fully compatible manner with tool assembly and performance considerations.

#### G. Installation in a Receiver

Install the new shuttle with all the components into a prototype receiver while assuring that no damage is done to any other parts or components. This will need to be done with tool system laid out and operational.

#### H. Tiltmeter Data Acquisition

The current microseismic data acquisition system will be modified to control the tiltmeter sensors and provide data acquisition. Tiltmeter data rates are very low compared to microseismic data rates and this subtask should be straightforward.

#### I. Laboratory and Benchtop Testing

Laboratory and benchtop testing will be conducted as needed to support Task **2.2.1**. Testing will be performed on sub-assemblies and the fully assembled prototype tool.

### 2.2.2 Testing of the Combined Microseismic-Tiltmeter Tool

Yard tests and field experiments will be conducted to assess the performance of the new sensor packages and combined microseismic-tiltmeter tool compared to the old tools. Comparison will be made using perforation data (for the high frequency components) as well as data from hydraulic fracture monitoring. Spectra, hodograms, noise levels, phase relationships, and other aspects of the signals will be examined and compared. This comparison should result in accelerometer spectra with much greater amplitudes at high frequencies, as opposed to the geophones with higher amplitudes at lower frequencies. This comparison would also allow us to look at signal-to-noise ratios, arrival rise times, hodogram quality, and other factors important to accurate processing. These field experiments will be conducted in onshore domestic gas reservoirs where hydraulic fracturing is a routine aspect of well completion.

Subtasks associated with this task are:

#### A. Yard Testing

Yard tests will be conducted using the fiber-optic wireline and data acquisition system running a full array of existing tools and the prototype tool. These tests are necessary to ensure the full system is operational prior to field experiments in a well. Three yards tests are scheduled, each prior to a field experiment (subtasks B and C below).

#### B. Single Receiver Field Experiments

Performance of a single prototype tool will be evaluated. The prototype tool will be run along with several existing microseismic receivers to monitor perforations and hydraulic fracturing under typical field conditions. This will allow comparison of data quality of the accelerometers in the prototype tool versus the geophones in the existing tools. Two field experiments are planned in order to troubleshoot tool operation problems and assess performance.

#### C. Multi-Receiver Field Experiment

Evaluation of the downhole tiltmeters and the joint-inversion code requires testing with multiple prototype tools in order to see the deformation pattern caused by the hydraulic fracture. One field experiment is planned to assess the downhole tiltmeter data versus the existing tools and to gather data for

running the joint-inversion code. Pinnacle will convert five additional DDS-250 receivers to combination microseismic-tiltmeter tools for this field experiment.

#### D. Build Multiple Combination Tools

Pinnacle will convert five DDS-250 to combination microseismic-tiltmeter tools using the instrumentation and design proven in single-receiver testing.

#### E. Multi-Receiver Field Experiment

Perform a field experiment monitoring a hydraulic fracture treatment using six combination tools and six existing DDS-250 tools. A hydraulic fracture treatment will be monitored from an offset observation well.

### 2.2.3 Development of Joint Inversion Routine

Analysis of microseismic and tiltmeter monitoring data is usually performed separately and the final results compared during the process of assessing the fracture or process geometry. A more accurate approach would be to jointly analyze the two types of data and arrive at a single answer that best fits both data sets. However, this is a very complex problem since tiltmeters measure earth deformation while the seismic receivers calculate the location of micro-earthquakes. Development of a "joint inversion" algorithm requires that both types of data be related to basic earth mechanics and the result be formulated in terms of these mechanisms and the rock and process (*e.g.*, fracture, waterflood, etc.) properties.

There are a number of ways to proceed with this formulation, but the most straightforward and simplest is to assume that material properties are known so that microseismic locations are as exact as possible and that the tiltmeter data are not perturbed in some unknown way by rock variations. Given this condition, the tiltmeter data can be inverted in conjunction with event location results from the microseismic data based on either probabilistic assessments or on mechanical models of microseismic development. Such an inversion would ensure that microseismic data bounds and the tiltmeter-inferred process envelope overlap as much as possible. The second step would be to invert for rock properties as well, which would require re-analysis of the microseismic locations since these are dependent on formation velocities. This step would be much more computationally intensive, given the required reevaluation of event locations, but it potentially could provide formation information as well as maximally accurate monitoring results. This second approach will obviously take considerable time to develop and will evolve as more is understood about the combined data sets.

Subtasks associated with this task are:

#### A. Develop a Microseismic Uncertainty Analysis

The most direct path for the first approach is to develop a model that assesses uncertainty of the microseismic events and to use this model in conjunction with the tiltmeter data to obtain fracture geometry. The inversion would try to maximize the fit of the tiltmeter data and minimize the total uncertainty from the microseismic data.

#### B. Develop a Joint Inversion Algorithm

An algorithm needs to be developed to handle diverse data sets with appropriate weighting for each set. It is necessary to assess the various inversion techniques, establish weighting criteria, and develop constraints, and handle other facets of the inversion process.

### C. Develop a Microseismic Mechanical Model for Use in the Inversion

A more physically attractive approach is to develop a mechanical model of where microseisms should be located given the various reservoir and process conditions and attempt to use this model in the joint inversion. An initial mechanical model is available, but it would need to be upgraded and reformulated for use in the inversion code.

## 2.2.4 Microseismic Source Mechanism Characterization

While microseismic fracture mapping is gaining acceptance by the natural gas industry, it is used on a very small number of stimulation treatments. Currently, microseismic hydraulic fracture mapping is focused almost entirely on determining the created fracture geometry (azimuth, length and height). There is certainly other information contained in the microseismic data that could also be very useful to operators. This could include information on the hydraulic fracture (such as propped fracture geometry), the reservoir (such as natural fracture characterization) and reservoir performance (depletion patterns if monitored long-term). Passive seismic monitoring has the ability to complement and augment active seismic (*e.g.*, 3D, 2D, crosswell, etc.) for reservoir characterization and performance assessment.

The fundamental basis for developing this capability is to characterize the source failure mechanism for microseismic events. A microseismic source failure mechanism is described by the specification of the failure plane orientation and dimensions, as well as the failure stress and slip direction. This is a difficult task when the event is viewed from only one location, as is typical for oilfield use, as opposed to earthquake seismology with multiple sensors for detection. Some work has been published on this topic[1-3] but has proven to be incorrect[4-5]. This task will provide a robust source mechanism methodology for the industry.

Seismic Diagnostics, Inc. (SDI) has been studying this issue recently with support from Pinnacle. This task will expand on these initial efforts and builds on work performed using data from DOE-supported projects (DOE/GRI M-Site and the Cotton Valley Fracture Imaging Project).

Subtasks associated with this task are:

### A. Development and Evaluation of Microseismic Source Characterization Capabilities

Integrating measurements of microseismic failure mechanism data with event locations and origin times can increase the usefulness of this technology to the industry. A microseismic source is characterized by the specification of its origin time, location, and failure mechanism. Its failure mechanism is described by the specification of the failure plane orientation and dimensions, as well as the failure stress and slip direction. This effort will evaluate the existing source mechanism inversion code and develop a failure stress and linear dimension component. The method will be tested using numerical simulation and data from field experiments from several types of reservoirs.

### B. Study to Improve Microseismic Signal-to-Noise Ratios

The utility of this technology will be increased by the development of reliable methods to significantly increase the effective detection range of the existing observational technology. There are two paths to increase the detection range of microseismic mapping: improve the instrument sensitivity or develop noise filtering techniques. Other tasks in this proposal deal with improving the sensor sensitivity. The effort described in this task is planned to address filtering techniques to improve signal-to-noise ratios and increase the viewing range of microseismic mapping. This supports Pinnacle's overall objective to develop an advanced hydraulic fracture mapping system.

The ambient background noise observed in monitor wells during hydraulic fracturing treatments typically limits the useful microseismic detection range to less than 1,200 feet. It also limits the angular width of the effective aperture for weak microseismic events, thus reducing the effective resolution of the methods used to characterize these events. In addition, since many gas wells are laterally offset by 2,000 feet or more, the impact of the monitor well ambient noise is to severely limit the potential for microseismic hydraulic fracture diagnostics surveys. Consequently, there is a compelling need to identify and evaluate cost-effective methods to reduce monitor well background noise levels without significantly altering the microseismic signal waveforms. This effort will acquire manufacturer's data on monitoring system electromechanical noise level and evaluate existing noise data. Time series analysis methods will be applied to the data to characterize the magnitude, polarization state, and organizational state of the monitor well noise field. Processed sample records will be representative of the noise field:

- at different times during the monitoring operations
- at different ranges
- in different geologic environments

Pending the outcomes of the noise characterization study, polarization state filters, prediction error operators, and velocity filters, as well as combinations of types of these operators, will be evaluated to determine their capabilities to reduce the magnitude of the monitor well noise field.

### 2.2.5 Technology Transfer

The objective of Task **2.2.5** is to ensure that the results of the project are effectively and efficiently transferred to the industry. A comprehensive final report will be written documenting the results of the project. At least one technical paper will be written and presented. Pinnacle conducts several hydraulic fracturing workshops annually and results from this project will be included in the workshop.

Pinnacle is the leading supplier of hydraulic fracture mapping services in the industry and can use these research results to improve fracture diagnostic services. This will make services based on this research widely available to the industry.

This task will also ensure that project progress and results are communicated to DOE for project management purposes. The periodic, topical, and final reports shall be submitted in accordance with the DOE's "Financial Assistance Reporting Checklist" and the instructions accompanying the checklist. Additionally a copy of all papers, articles and reports shall be submitted to the DOE COR for review via email in MS Word format. Periodic reports and briefings (formal and informal) will be provided to DOE as requested.

#### A. Technical Paper

Will prepare for publication and/or presentation at least two technical papers. The papers will directly involve the DOE COR participation and review. The venues for publication shall be SPE and/or other professional publications presenting and transferring the technology developed and reviewed in this project to the petroleum industry as a whole.

#### B. Progress Reports and Briefings

Will prepare at the request of the DOE COR a technical paper for the DOE/NETL Annual Contractors Review Meeting.

### C. Final Report

Will prepare a comprehensive final report for the project.

### D. Briefings/Technical Presentations

- Detailed briefings for presentation to the COR at the COR's facility in Pittsburgh, PA or Morgantown, WV
- Provide and present a technical paper at the DOE/NETL Annual Contractors' Review Meeting at a site to be determined
- Updates will be provided to the DOE Project Manager as requested

### E. Commercialization

Pinnacle can incorporate the improvements in tool technology that result from this project into our hydraulic fracture diagnostic services. Pinnacle is the leading provider of microseismic and tiltmeter fracture mapping services to the industry. Pinnacle is the only provider of tiltmeter fracture mapping.

# 3. Work Results

This section describes the results obtained in this project. These results follow the overall task numbering, but are listed by subtask because of the overlap of so many of the activities.

## 3.1 Development of Combined Microseismic-Tiltmeter Receiver

The primary result of this task was the development of a prototype hybrid array with the design and fabrication of a new housing for the tiltmeters that accommodates the various microseismic conductors that need to feed through the tiltmeter tool. In addition, development efforts were conducted to assess and build accelerometers for testing in the microseismic tools.

After extensive investigation, it was decided that the best approach to obtaining an integrated tiltmeter/microseismic array was not to place the tiltmeters inside the microseismic housing, but rather to attach a modified tiltmeter tool to a microseismic tool and allow the clamp arm on the microseismic tool to couple both instruments to the borehole wall. This approach would allow for each of the systems to retain their separate telemetry, power, leveling, and other functions. The following work results reflect that philosophy in the development of a hybrid array.

## 3.2 Tiltmeter Modifications

The problem of using a sufficiently sensitive tiltmeter in a tool small enough to match the microseismic receiver (DS250) was solved independently by modifying the existing small-diameter tiltmeter (GEN III) to achieve a much higher sensitivity. These small diameter (1.6875 inch) tiltmeters could now be used as the platform for designing a hybrid tiltmeter compatible with the DS250 receivers.

In order to use the current GEN III tiltmeters in a hybrid array with the DS250 microseismic tools, it was necessary to devise a way to pass the microseismic interconnect wires through the tilt tools. However, the current generation of tilt tools have no space internally, so it was decided to build an external housing in which the current tiltmeter tool could be inserted, along with centralizers to hold the tiltmeter rigid within the housing (as well as guide the wires) and adapters to hold and mate the tiltmeters to the end-cap connectors.

**Figure 2** shows a drawing of an assembled tiltmeter (without the outside housing), illustrating the mating of the tiltmeter into the adapters and endcaps. The end adapters (grey) connect the tiltmeter housing (blue) to the endcaps (black) and hold the tiltmeter rigidly in place. Centralizers ring the tiltmeter so that it cannot wobble within the housing and act as guides to the wires that will be fed through on the outside of the tiltmeter, but internal to the hybrid housing.

**Figure 3** shows a detailed drawing of the adapter that holds the tiltmeter within the housing. The outside diameter of the adapter is the same dimension as the centralizers and fits snugly within the external housing. There are four cutouts on the adapter for the microseismic interconnect wires and a grooved area where the tiltmeter fits into the adapter, along with screw holes to hold the tiltmeter in place. The adapter bolts on to the endcap.

**Figure 4** shows a detailed drawing of the power contact that fits within the adapter, and **Figure 5** shows a detailed drawing of the centralizers. The centralizers have an outside diameter that fits snugly within the external housing and have internal cutouts for allowing passage of the microseismic interconnect wires and for holding them in place.

In addition to these parts, male and female end connectors were also obtained from GERI. These mate directly into microseismic interconnects and receivers.

Other issues associated with the addition of a tiltmeter array to a microseismic array included power considerations and communication capabilities. The tiltmeter power and data are multiplexed on a single conductor of the fiber-optic line (all the other conductors are used for microseismic or CCL) with return on the ground.

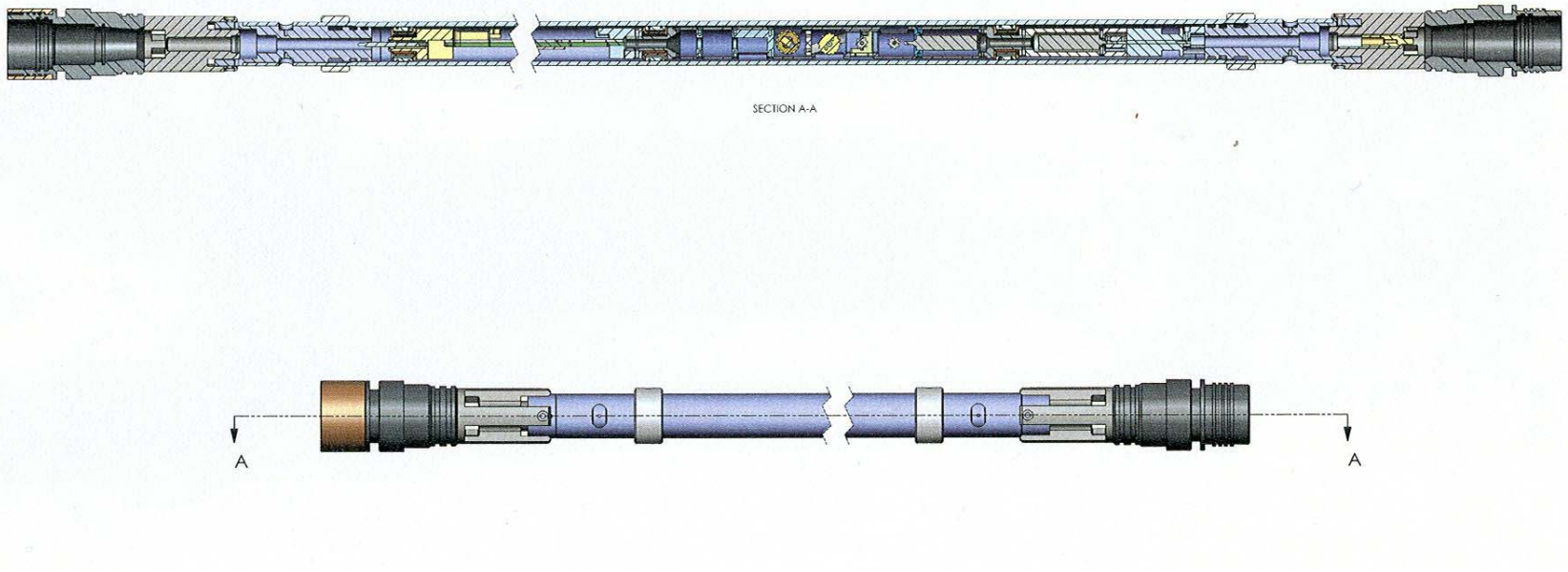


**Figure 2. Assembled hybrid tiltmeter tool**

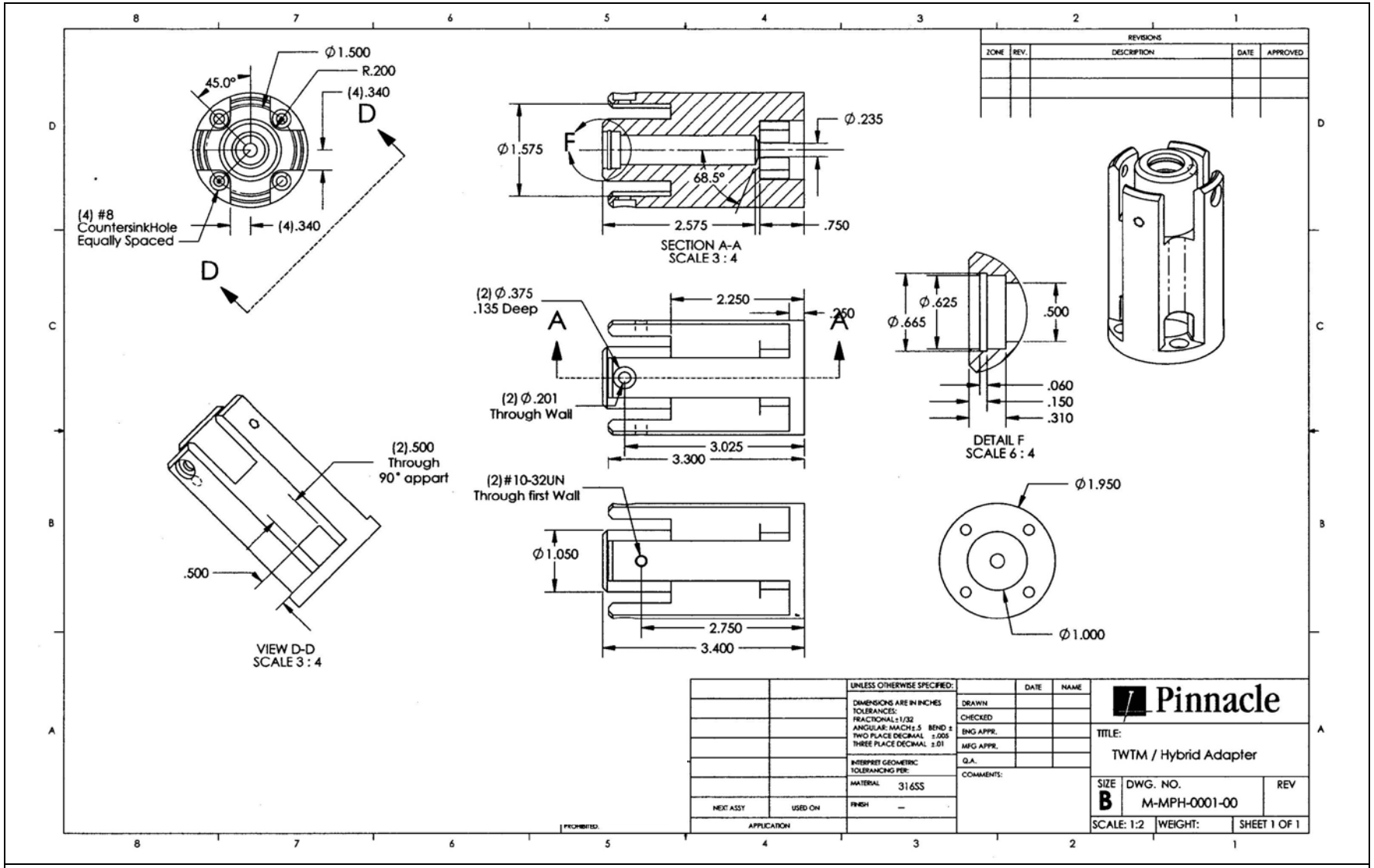


**Figure 3. Drawing of hybrid adapter**

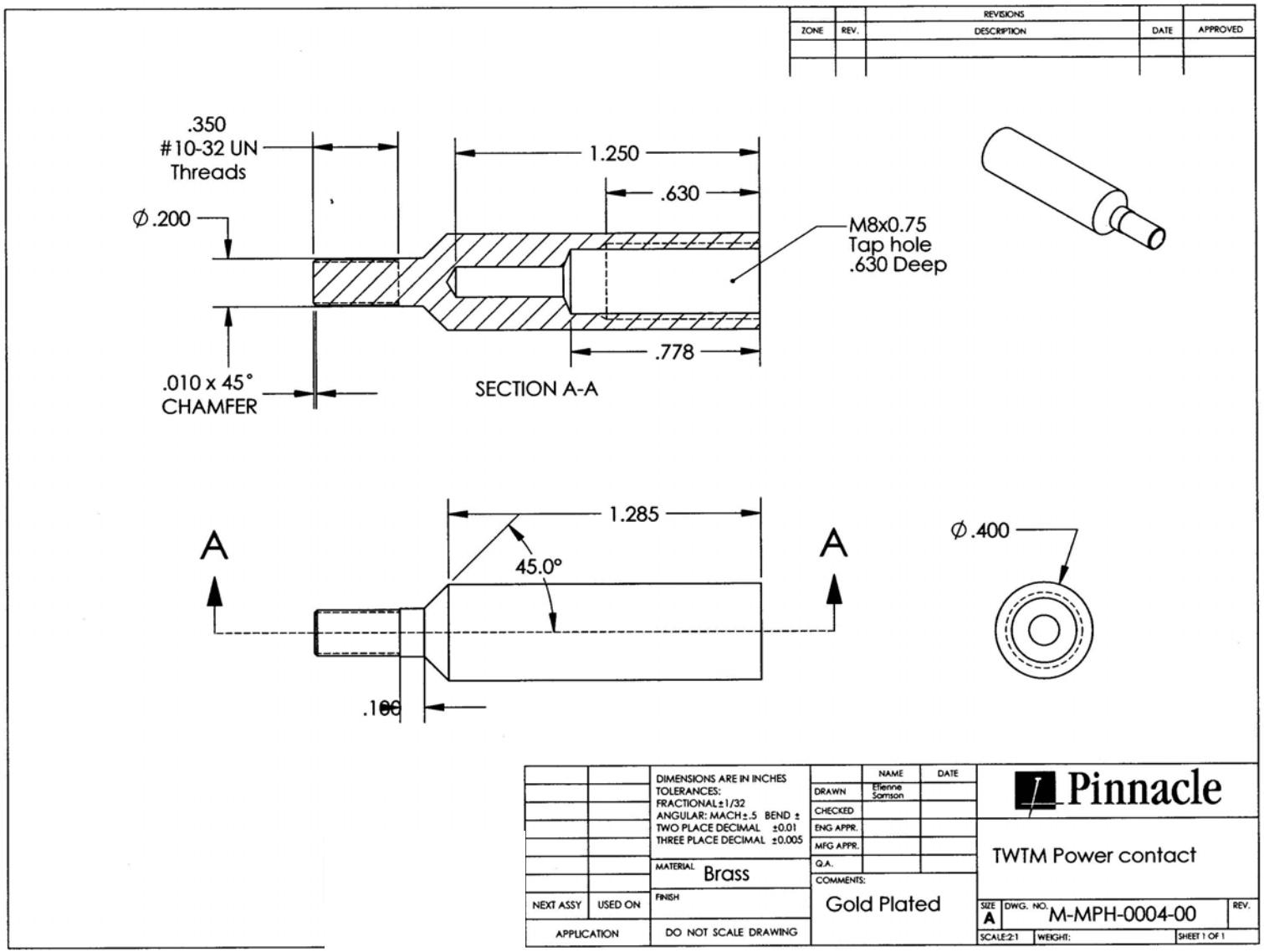


**Figure 4. Power contact for hybrid tiltmeter**

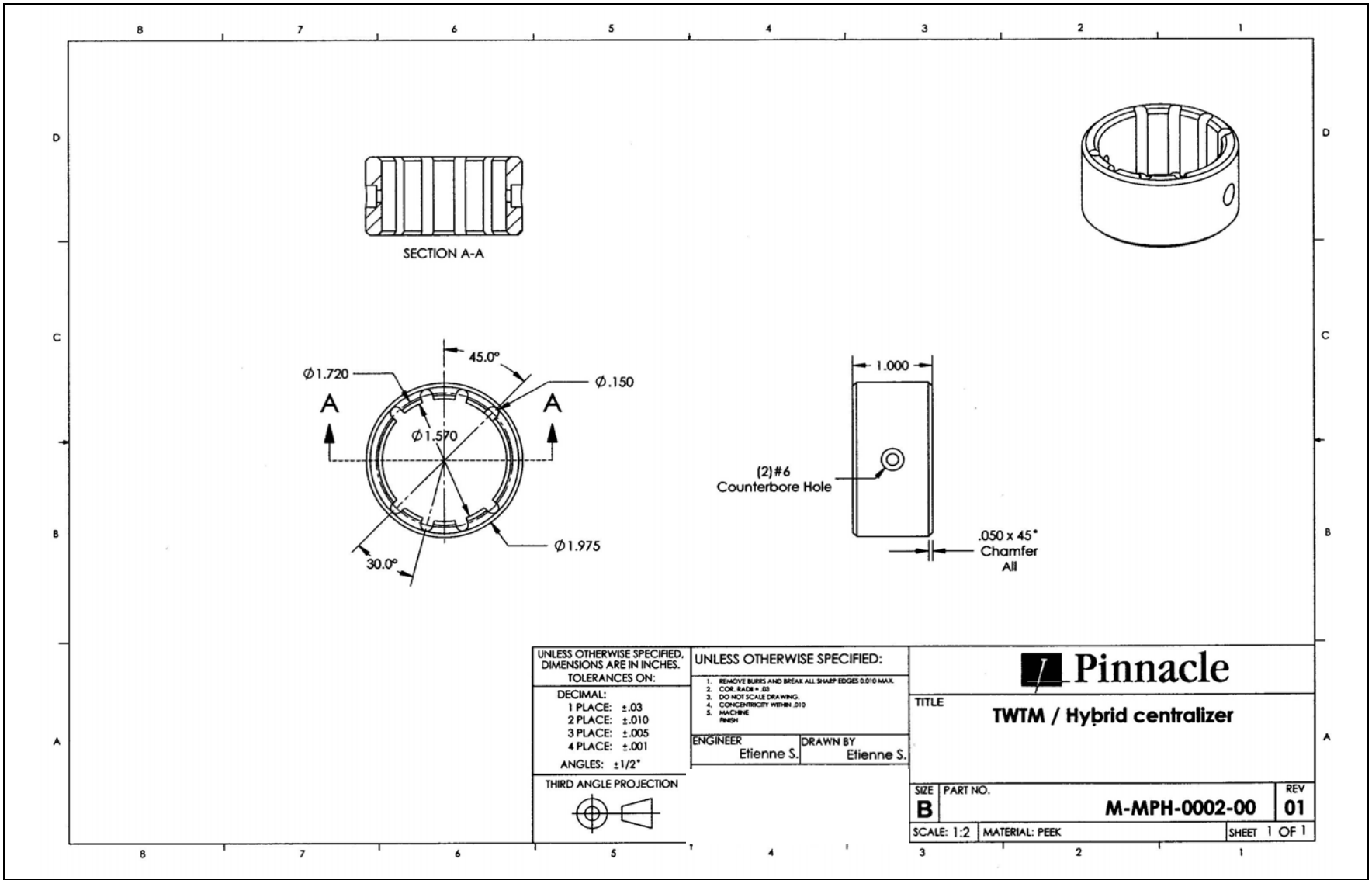


**Figure 5. Centralizer for hybrid tiltmeter**

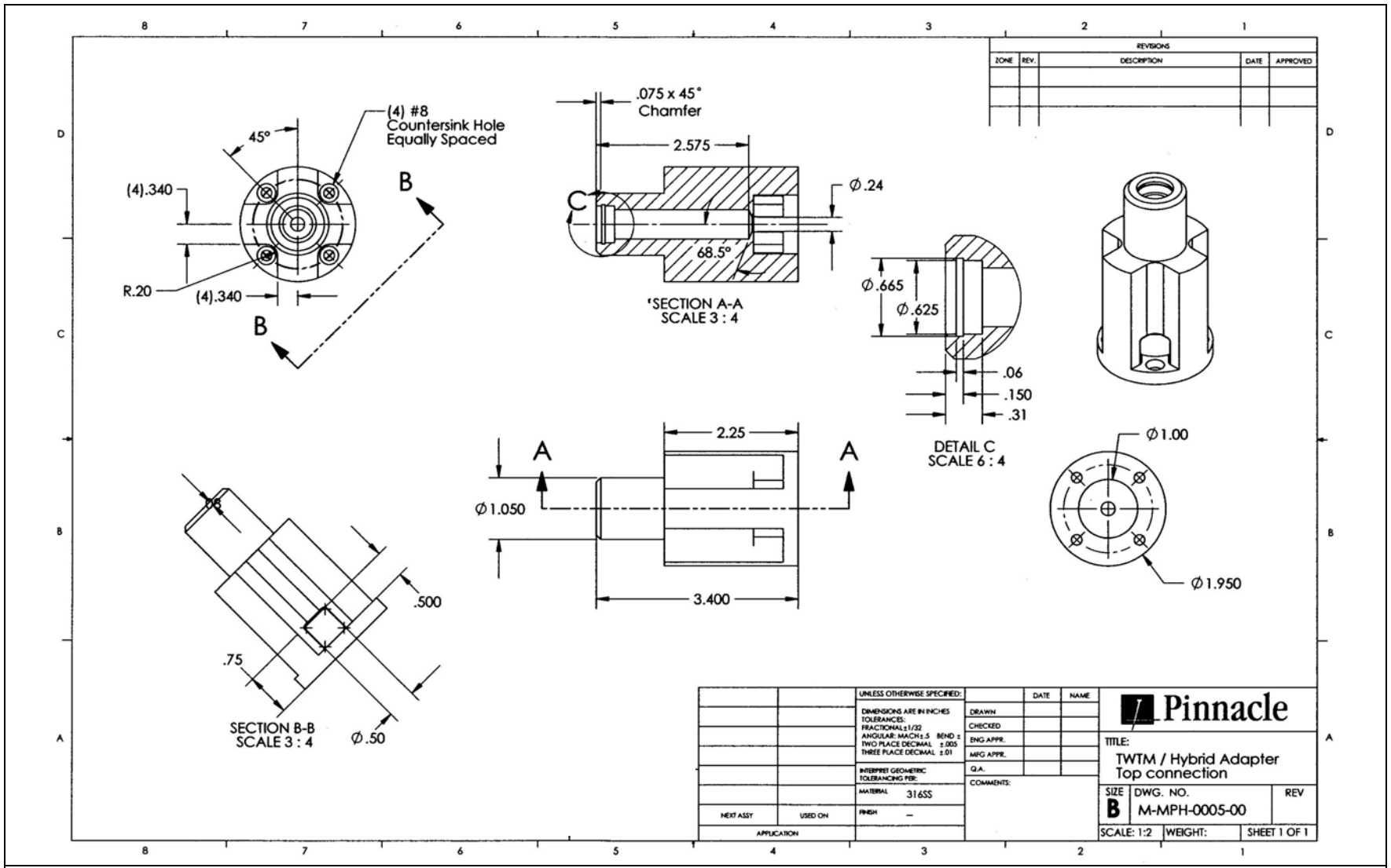


**Figure 6. Drawing of hybrid tiltmeter top connection**

## 3.3 Microseismic Modifications

Modifications made to the microseismic tools consisted of a redesign of the shuttle (the fixture that holds the geophones) to accommodate accelerometers and their associated circuitry and a replacement of the CCL negative power with the tiltmeter power. The CCL negative was attached to armor.

### 3.3.1 Inspection of Existing Microseismic Tools

Pinnacle obtained two receivers from Geospace with accelerometers in place of the geophones in order to evaluate their response. The accelerometers used were Wilcoxin 731-20 sensors, which are currently the most sensitive accelerometers on the market (also the most delicate). The tools were used in a number of fracture tests and their response was assessed in various manners. Initial examination consisted of side-by-side comparisons of the accelerometers and geophones (on adjacent tools). Spectra of the two sensors were compared for both noise and event response. In general, the response of the two systems was fairly similar, with accelerometers having a little better high-frequency response; however, some noise spikes were observed in the accelerometer data that suggested there may be some problem with the power provided to the accelerometers. In addition, the lack of significant improvement in the high-frequency response is surprising, as accelerometers have much higher response at high frequencies. This behavior suggests that something in the A/D system is filtering out the high-frequency content or the mechanical system is incapable of transmitting higher frequencies.

**Figure 7** shows an example comparison of the spectral response of adjacent levels – one geophone and one accelerometer – for a perforation shot, which should have considerable high frequency content. The spikes in the accelerometer data can be clearly seen, but the improvement at high frequencies is relatively small and centered around 1,000 Hz.

**Figure 8** shows another perforation example, but this time with a better high frequency response on the accelerometers. Two accelerometer levels are shown here, along with the adjacent geophone level. The signal-to-noise (SNR) ratios for this perforation are shown in **Figure 9** as a function of frequency. Clearly, the accelerometers are showing a much better response at the higher frequencies.

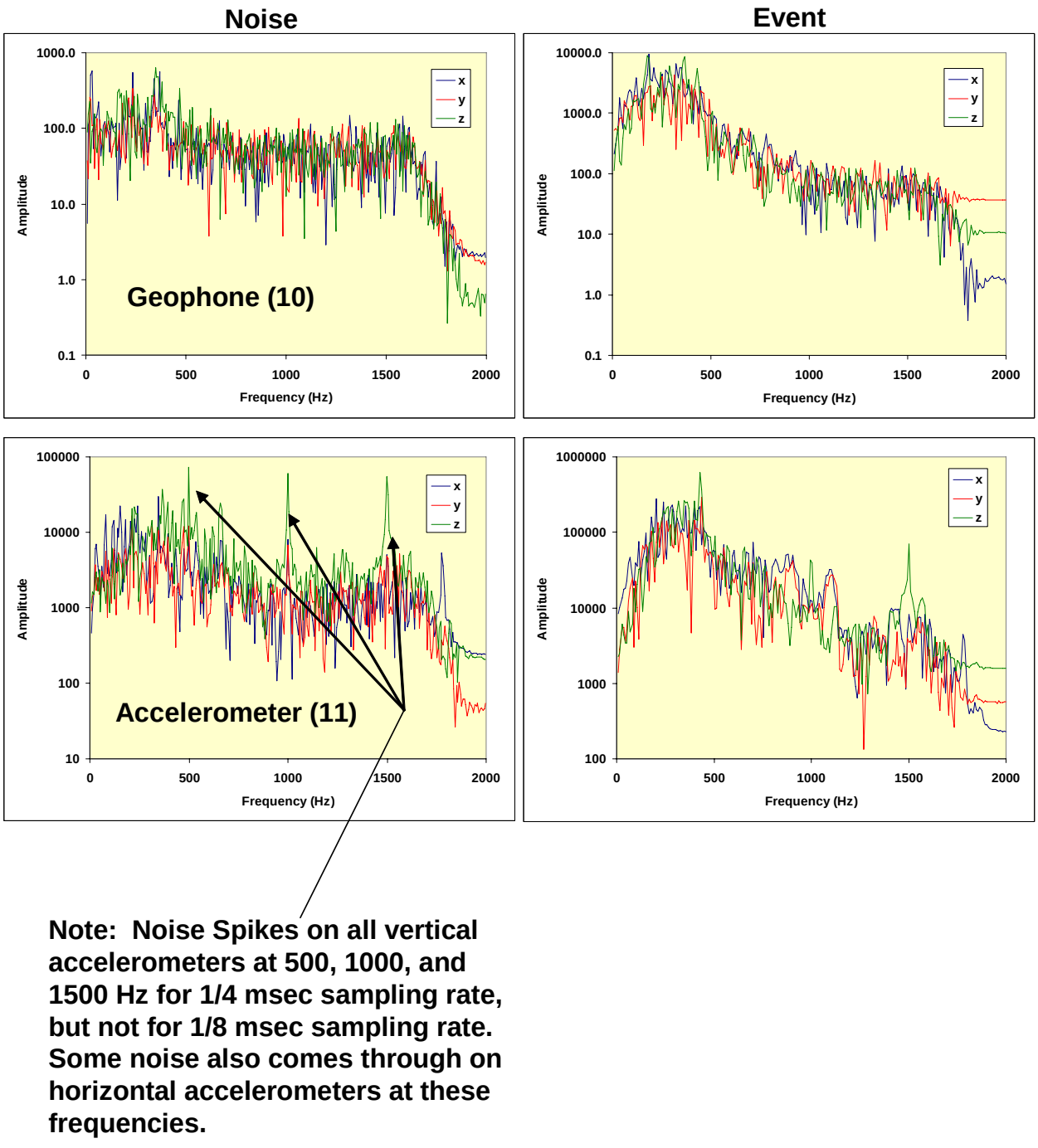


**Figure 7. Example of spectral response of adjacent geophone and accelerometer levels for a perforation shot (expected to have considerable high frequency content) at 1/4 msec sampling rate**

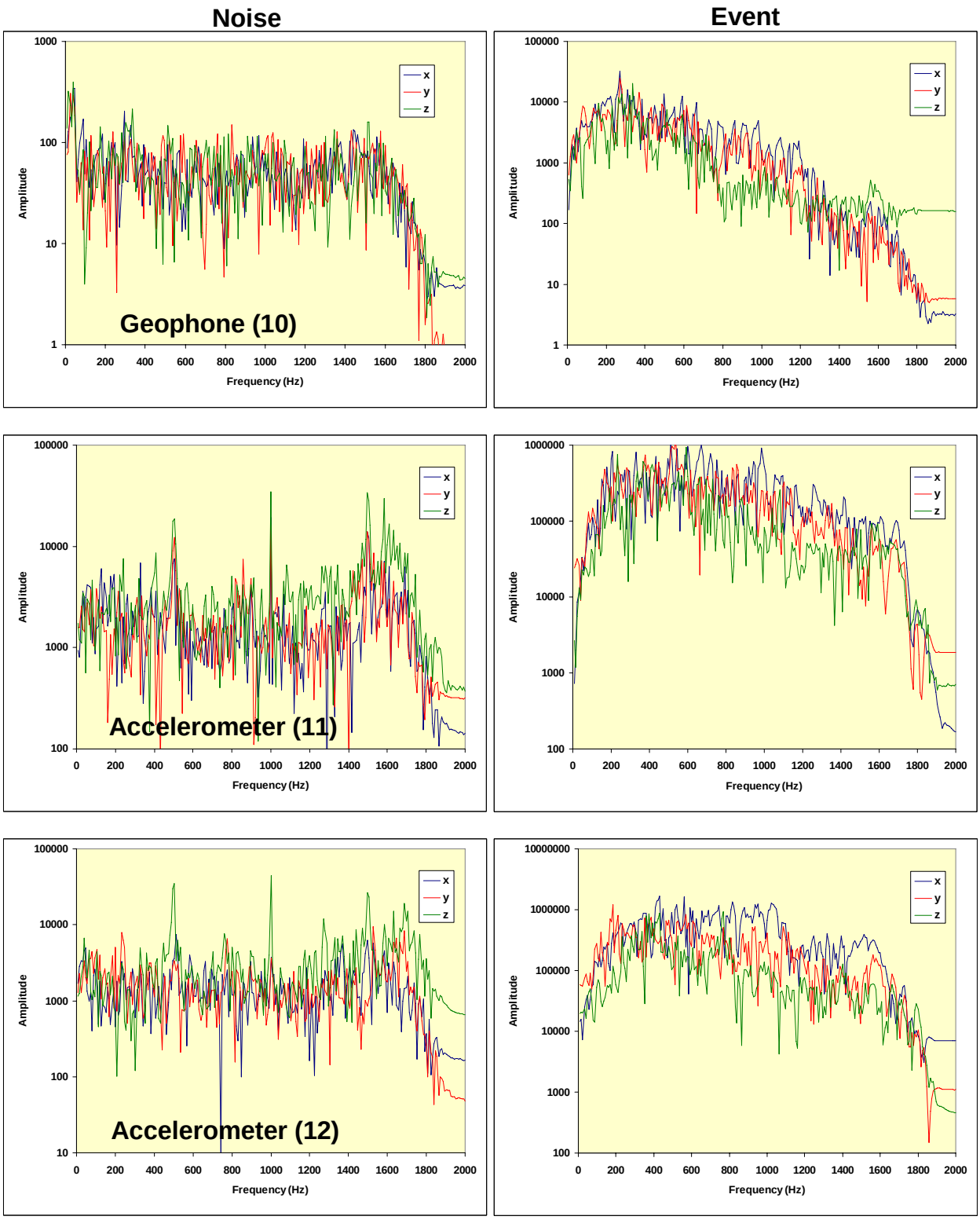


**Figure 8. Example of spectral response of geophone level (10) with two accelerometer levels (11 and 12) for a perforation at 1/4 msec sampling rate**

**Signal-To-Noise Ratios**

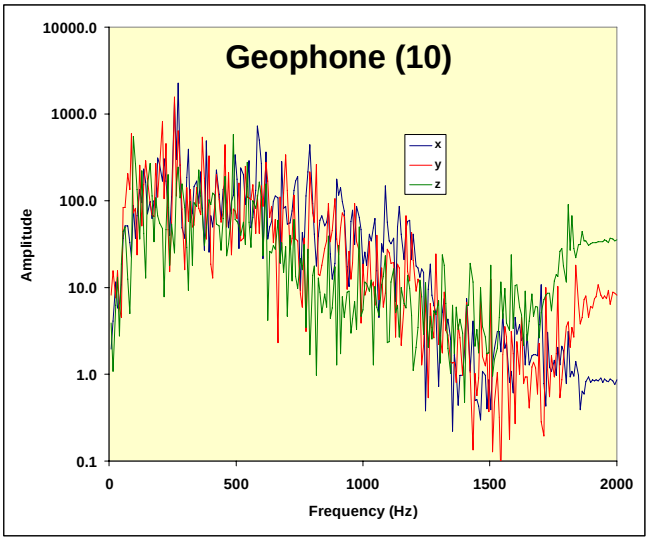


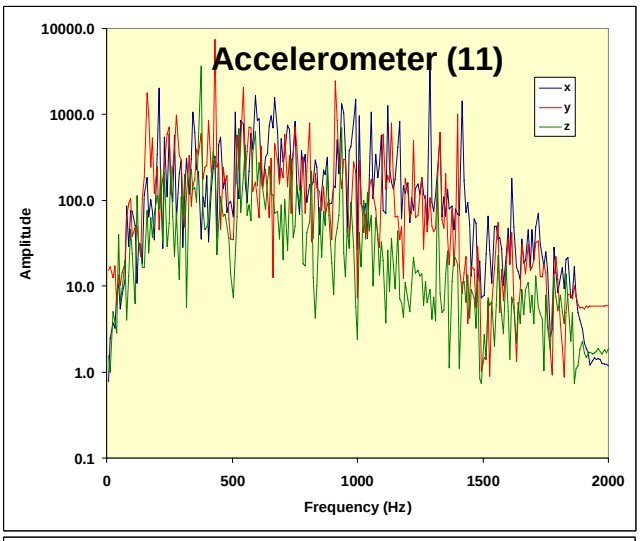


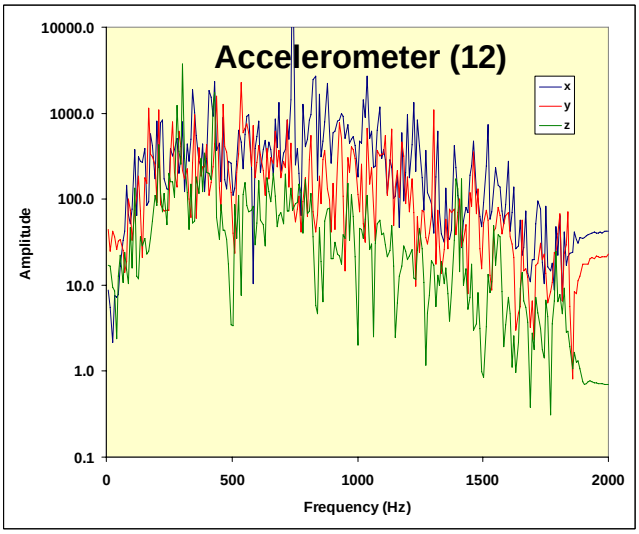


**Figure 9. Signal-to-noise ratios for example perforation of Figure 8**

In addition to the side-by-side comparison under normal conditions, a test was performed at a faster sampling rate (1/8 msec sample interval, as opposed to the normal 1/4 msec sample interval) to see if the response of the accelerometers was improved by allowing sampling of higher frequencies. However, this test showed that there was no event data at frequencies above ~1,500 Hz, that is, the event response looked just like the noise response. This was particularly surprising because the Wilcoxin 731-20 sensors have a resonance at about 2,200 Hz that provides a mechanical gain of 100. This resonance should have been evident in the data, yet it was not observed. Finally, the higher sampling rate also showed that the noise increases with frequency above about 1,200 Hz, probably due to the A/D system.

**Figure 10** shows an example of this behavior for a perforation in the Barnett Shale. The sampling rate is 1/8 msec and shows behavior similar to the previous examples for frequencies lower than about 1,200 Hz, but has no advantage at higher frequencies because the noise floor is rising. This can be seen very clearly in the SNR plot for this perforation in **Figure 11**. Above 1,500 Hz, all three sensors look the same because the system electronic noise level is so high.

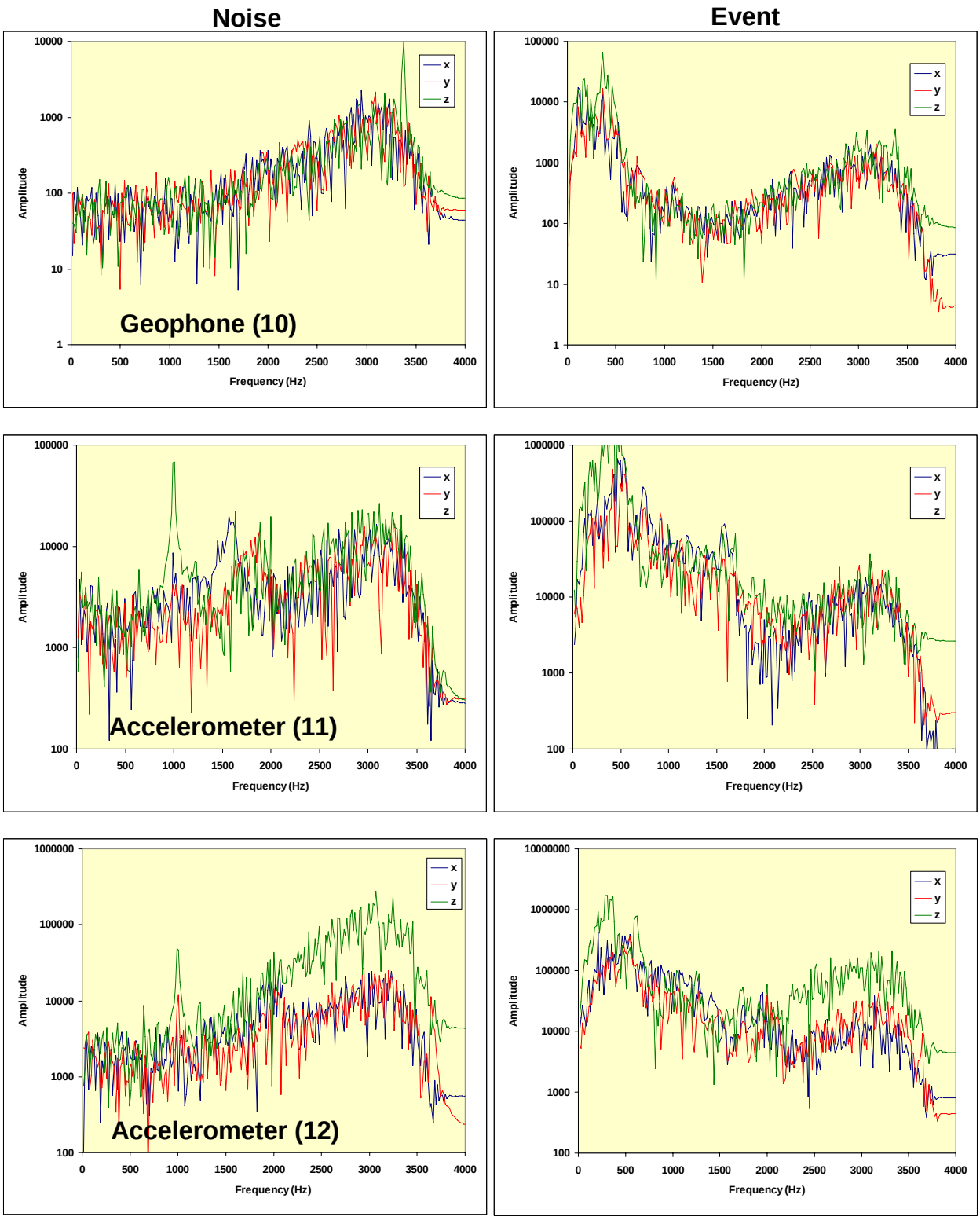


**Figure 10. Example of spectral response of geophone level (10) with two accelerometer levels (11 and 12) for a perforation at 1/8 msec sampling rate**

**Signal-To-Noise Ratios**

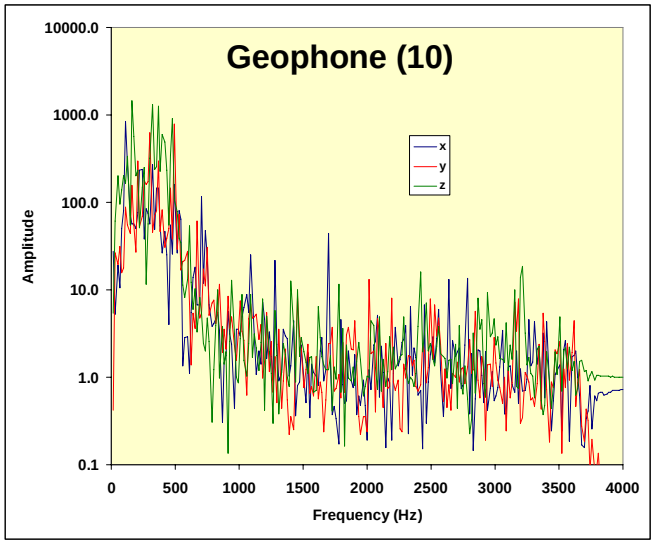


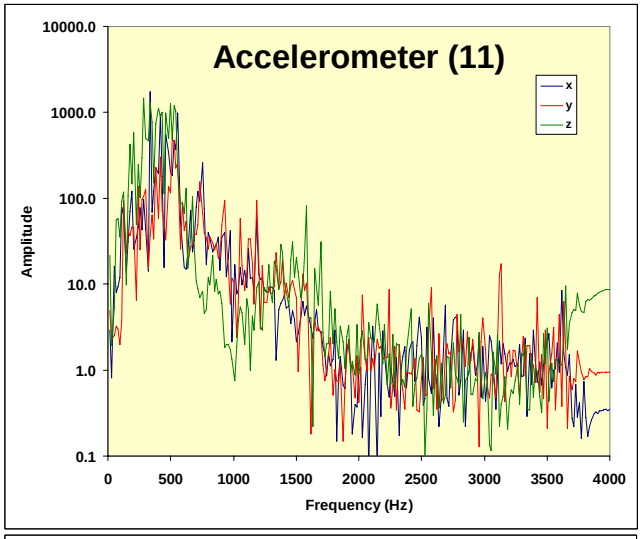


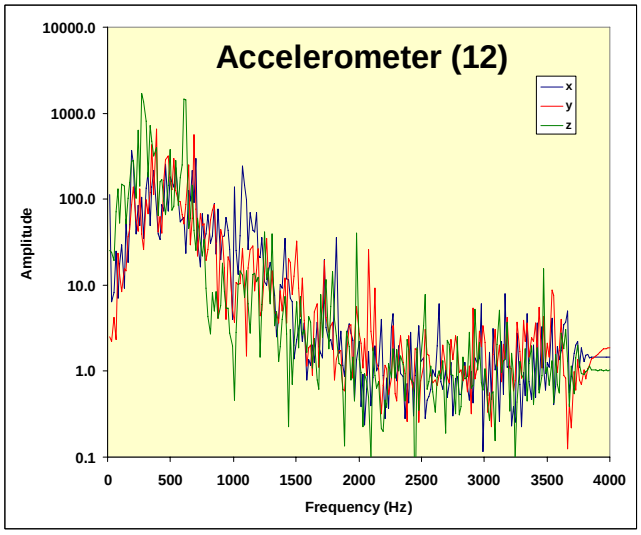


**Figure 11. Signal-to-noise ratios for example perforation of Figure 10**

These initial evaluations have provided useful information to begin detailed testing of the existing tool system in order to determine its current response limits and methods to improve the response of the system. These tests include examination of the accelerometer circuitry, inputting test signals in place of the accelerometers and monitoring the system response, excitation of the accelerometers at the shuttle fixture (the shuttle holds the accelerometers in place) and also on the housing, and various other tests of system noise and capabilities. Some of the findings are given below:

It was immediately obvious that one huge problem is that all of the grounds on the accelerometers are tied together, making the data quality less than desirable. This one feature adds noise and crosstalk between channels and is probably the most significant factor that needs to be corrected to improve the response. Crosstalk tests on the accelerometer tools and on a different geophone receiver showed that there is about -100 to -120 dB crosstalk in the electronics, -95 to -115 dB through the geophones, and -25 dB through the accelerometers. As a result, about 6% of the amplitude from one accelerometer channel bleeds over into the others, while an insignificant amount of crosstalk occurs in the geophone receivers (only 0.001 – 0.0001%), which are fully differential.

A high frequency signal was input into the A/D (by replacing the accelerometer input with a function generator input) and confirmed that the GeoRes (the data acquisition unit) can respond to high frequencies. There is no filtering or anything else limiting the data-acquisition system. Thus, the inability of this system to detect high frequencies with the tools is not due to the data-acquisition part of the system. It was noted, however, that the design of the shuttle is not conducive to detecting high frequencies. The shuttle carrying the accelerometers (or geophones) is coupled to the housing only through four O-rings. Pinnacle's tiltmeters are designed using this approach to mechanically filter out the high frequencies and the same thing is probably happening on the accelerometer receivers. Some very rudimentary tests were done to check on this and it appears that there is about a factor-of-four reduction in amplitude at high frequencies relative to low frequencies.

It was verified that the increasing noise with increasing frequency (by as much as 30 dB from 1,400 to 3,500 Hz) is a system problem that occurs with any sensor. It is probably due to some aspect of the A/D or the DSP functions. However, with the equipment on hand, it was not possible to diagnose the source of this noise and this will need to be done later.

The accelerometers in the one tool that was opened up were found to have what appears to be a degraded response. For the Wilcoxin 731-20A accelerometers, the resonant frequency should be at 2,200 ± 100 Hz and there should be a mechanical gain of ~40 dB. The response of two of the accelerometers were measured, resulting in resonant frequencies of ~1700 and ~1900 with approximate mechanical gains of 15 to 25 dB, although the gain numbers are a little rough because of the limited equipment on hand. In any case, this reduction in the resonance is exactly what happens as the tools become damaged due to continued shock and possibly other factors (*e.g.*, exposure to temperature).

At this time there is a reasonable explanation as to why the tools did not show any response at higher frequencies in the field tests. First, the accelerometers were likely degraded and the mechanical gain was considerably lower than expected. Second, the O-ring coupling limited how much high frequency energy was getting into the tools. Third, the increasing noise with frequency (about 20 dB at 1,800 to 2,200 Hz) hid any signal that might have reached the sensors. Combine them all and there is probably not much potential to improve the high frequency response.

These deficiencies in the prototype accelerometer receivers are actually a fairly positive result, as they suggest that a marginally designed accelerometer system can work as good as or better than an excellently designed geophone system. While there are still some questions and issues that need to be addressed, it is believed that sufficient information has been obtained to:

1. Assure that the performance of the receivers can be improved with accelerometers
2. Suggest improvements in the current prototype tools to correct the deficiencies in this prototype design
3. Begin searching for an optimal accelerometer for microseismic monitoring using these receivers

### 3.3.2 Accelerometer Investigation

Given the characteristics of microseisms and the cultural noise in wellbores, it is expected that accelerometers would provide a better sensor for detecting microseisms in the downhole environment. Microseisms are typically very small, high frequency, events, with the smaller events usually being higher frequency. In addition, the cultural noise in a borehole typically decreases with increasing frequency. Thus, a sensor that performs better at higher frequencies has a better chance of detecting these events. Accelerometers, which measure acceleration, have an amplitude that is $2\pi f$ greater than the velocity amplitude, where $f$ is the frequency. In this way, accelerations are much greater amplitude at higher frequencies if the sensor system can function appropriately at high frequencies. Negating this to some extent is attenuation, which is greater at higher frequencies.

The general philosophy at the start of the project was to obtain a complete tri-axial accelerometer because it would be guaranteed to be balanced (*e.g.*, all three channels having the same sensitivity and resonance). However, most of the tri-axial units that were found have their grounds tied together, which essentially results in a single-ended configuration instead of the fully differential configuration that is needed.

Sandia National Laboratories performed most of the work on developing a new accelerometer for the microseismic tools. After conducting detailed searches of accelerometer products that are available, a database of several types of applicable sensors and vendors was developed. In general, applicable sensors appear to fall into the categories of: (1) charge output sensors, (2) strain resistors output sensors, and (3) MEMS sensors. However, strain resistors output sensors are not presently being considered for this use because of several factors.

The charge output sensors may or may not have internal electronics. Those sensors without internal electronics are typically ceramic composite devices with sensitivities of 10 pC/g, 100 pC/g or 1,000 pC/g (pico-Coulombs/g). Sandia would provide a first-stage, low-noise, signal conditioning circuit for these devices. Those with internal electronics typically have charge to voltage conversions that result in sensitivities of 100 mV/g to 1,000 mV/g. While use of these latter sensors would save considerable time and effort, it will be necessary to determine if the internal electronics can satisfy our particular noise requirements.

MEMS sensors are typically variable capacitance and it is the nature of the MEMS device to have the internal electronics integrated with the sensing unit in a very small physical package. Typical sensitivities for these devices are 80 mV/g, 200 mV/g and 1,000 mV/g, for devices that are being considered.

Five different sensors, all from Endevco (Endevco has bought out several companies recently and now is a huge presence in the accelerometer business) were procured for initial testing. These include the 2228C triaxial, 7201-100 single-axis, 7251HT-100 single axis, 7703A-1000 single axis, and 7250A-10 single axis accelerometers. In addition, the 2258A-10 and 7250A-2 single axis accelerometers were already on

hand for testing. Evaluation of these products allowed Sandia to assess pros and cons of sensor type, sensitivity, temperature, shock, and frequency response.

A basement lab (fewer environmental changes and vibrations) with an air table and shaker were used for the initial testing. **Figure 12** shows a photograph of the shaker table (top cylindrical device) on top of the air table. **Figure 13** shows a close-up photograph of the top of the shaker table with a reference accelerometer (Wilcoxin 731-20A) mounted in the center and four of the test accelerometers mounted around.

Test equipment for the evaluation is shown in **Figure 14** and includes a function generator, amplifiers, voltmeter, spectrum analyzer and phase-lock system.

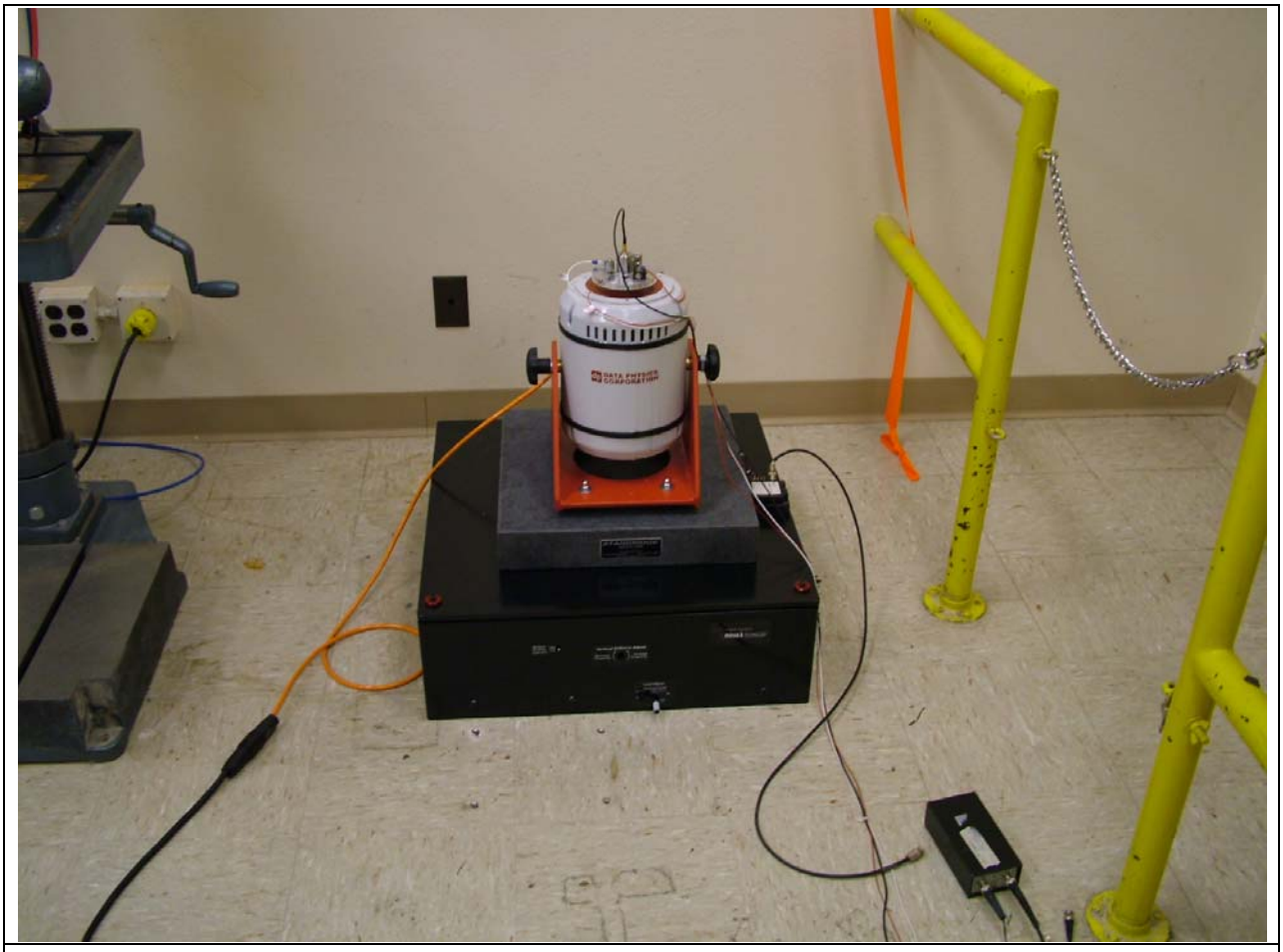

**Figure 12. Photograph of shaker table and air table in basement laboratory**

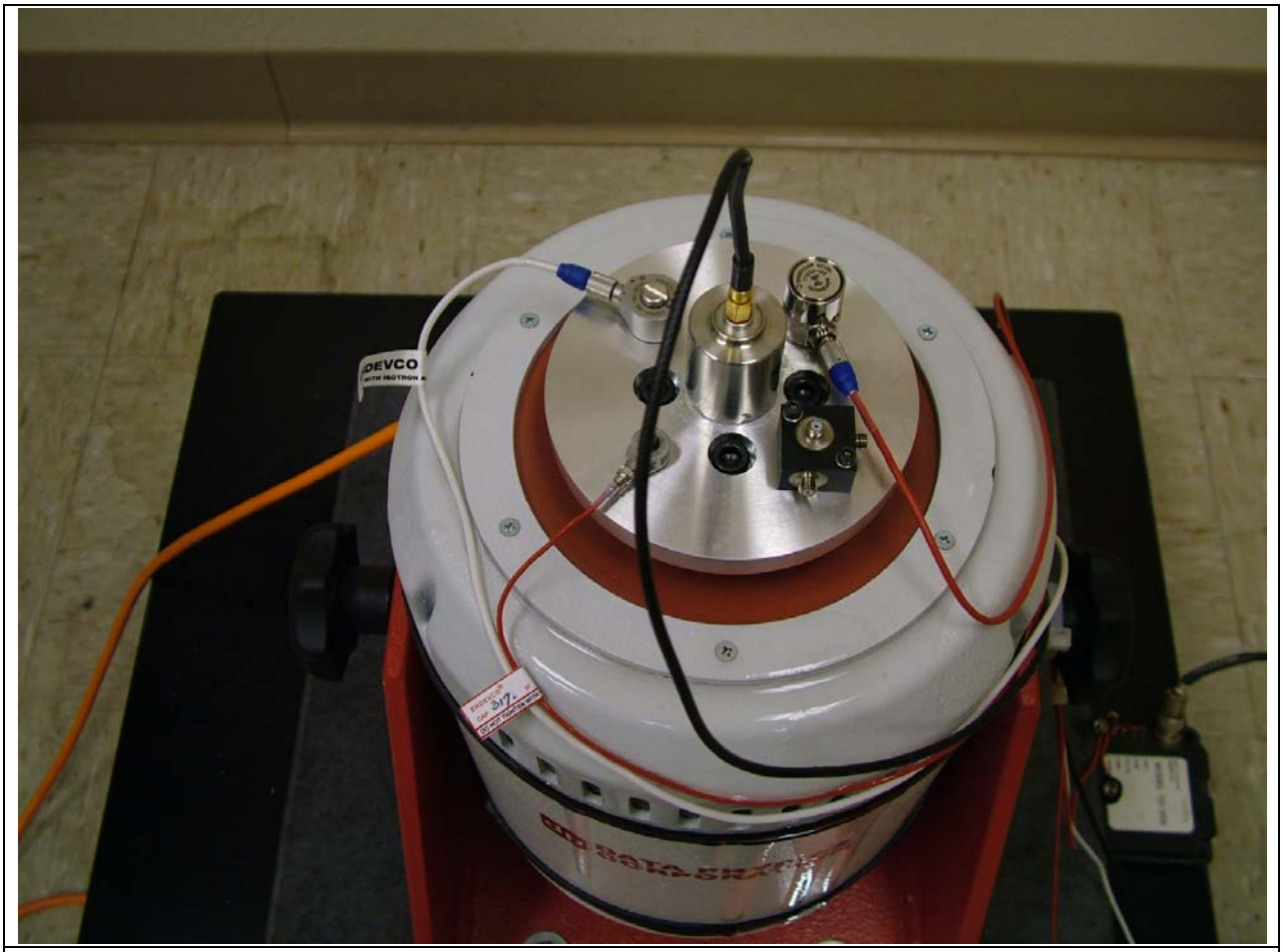


**Figure 13. Photograph of Wilcoxin reference accelerometer (center) and four test accelerometers mounted on the shaker for initial testing in basement laboratory**

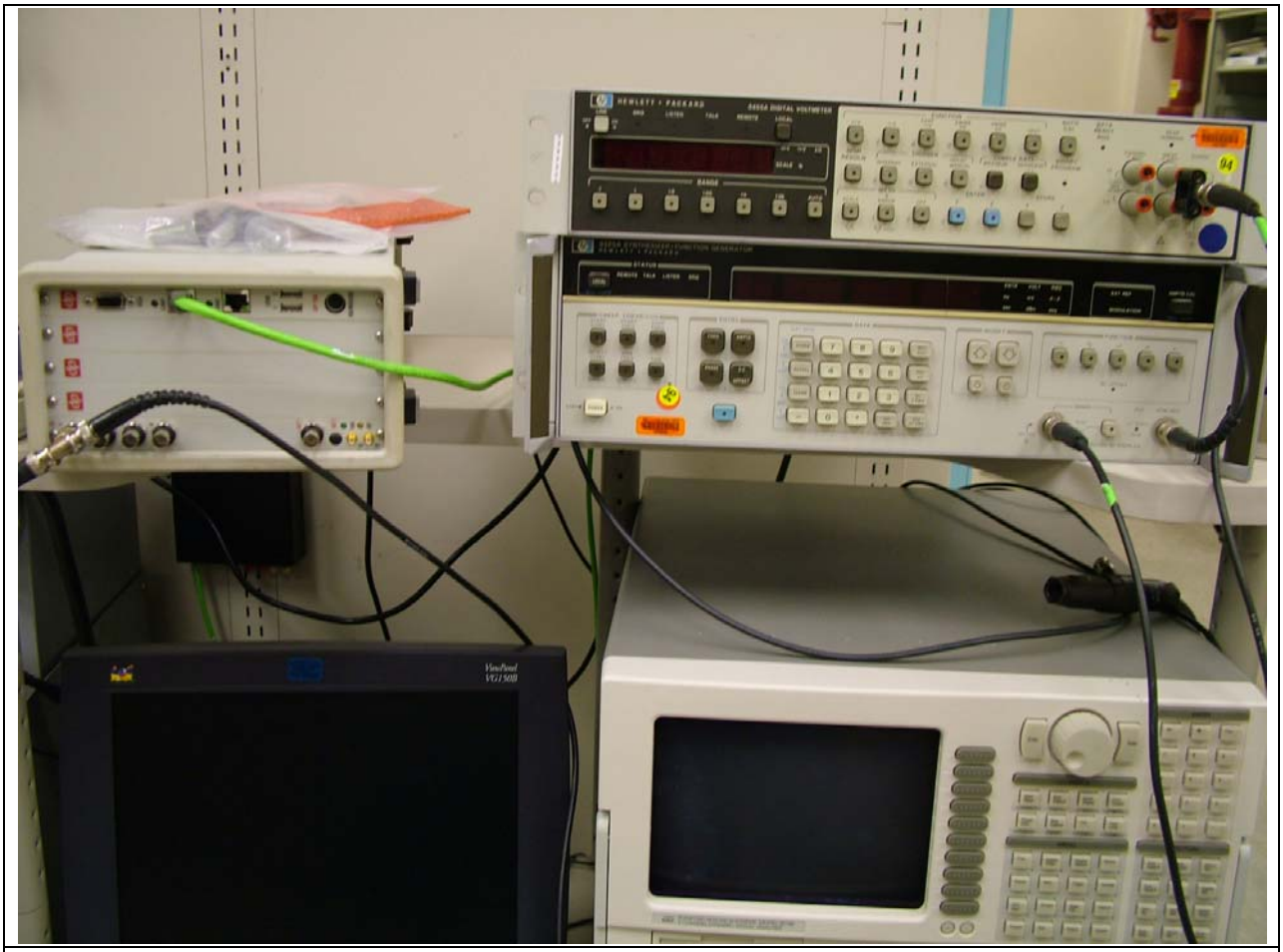

**Figure 14. Test setup for initial accelerometer evaluation**

Based upon the initial tests, it appeared that both the Endevco 7703A series piezoelectric accelerometers and the 7251HT series piezoelectric accelerometers with integral electronics would be sufficient for our needs. The 7703A series, however, is rated to 288°C and has a very flat charge sensitivity out to that temperature, thus assuring that response is not lost with increasing temperature. Thus, after initial testing the 7703A was the preferred choice. The 7251HT series is rated to 150°C, which is barely sufficient for our needs, but it also has a flat temperature response out to this temperature. The 7703A series has a relatively flat amplitude response out to about 4,000 Hz and a resonant frequency of 20,000 Hz.

Using the 7703A series accelerometer would require that we add our own electronics to the accelerometers, but this would allow us to ensure that a low-noise, high temperature, flat-response, amplifier was used. In the testing, Sandia used the amplifier that is part of the Wilcoxin 731-20 accelerometers for initial evaluation. With this configuration, it was possible to obtain the same type of output as the Wilcoxin (*e.g.*, 10's of volts per g) without any noise problems (at least qualitatively – final evaluation of noise issues will come later in quieter environments).

The 7703A series accelerometers come in 50, 100, 200, 1000 picoCoulomb/g (pC/g) output. The initial test was of a 100 pC/g model and it appears to have the best features. For example, the physical size of the 100 pC/g is less than 1 inch, whereas the 200 and 1,000 units are over 1.25 inch. In addition, the response of the 1,000 pC/g device is flat only out to about 2,000 Hz and the 200 is flat out to about 3,000

Hz. The shock resistance of the 100 pC/g is 5,000 g's, while the 200 is 2,000 g's and the 1,000 is 1,000 g.

Relative to noise levels, most of the testing was done in the 10's of mg range, which is a typical event amplitude in the Barnett Shale. Sandia was able to take it down to 0.125 mg in the lab (the lab is too noisy to go lower), which is about 3 to 4 times larger than the lowest signals that are currently event detected.

Further testing concentrated on (1) getting equipment installed in a vault area so that noise floor measurements could be made and (2) assessing the associated circuitry that would be required to power and condition the Endevco 7703A accelerometer which is the most promising of the sensors.

**Figure 15** shows a picture of the shaker table in the vault. The vault is a facility that was built underground in the foothills of the mountains near Sandia Labs, with a concrete slab base and concrete block walls. **Figure 16** shows a photograph of the test electronics.

**Figure 15. Photograph of shaker table in the underground vault**

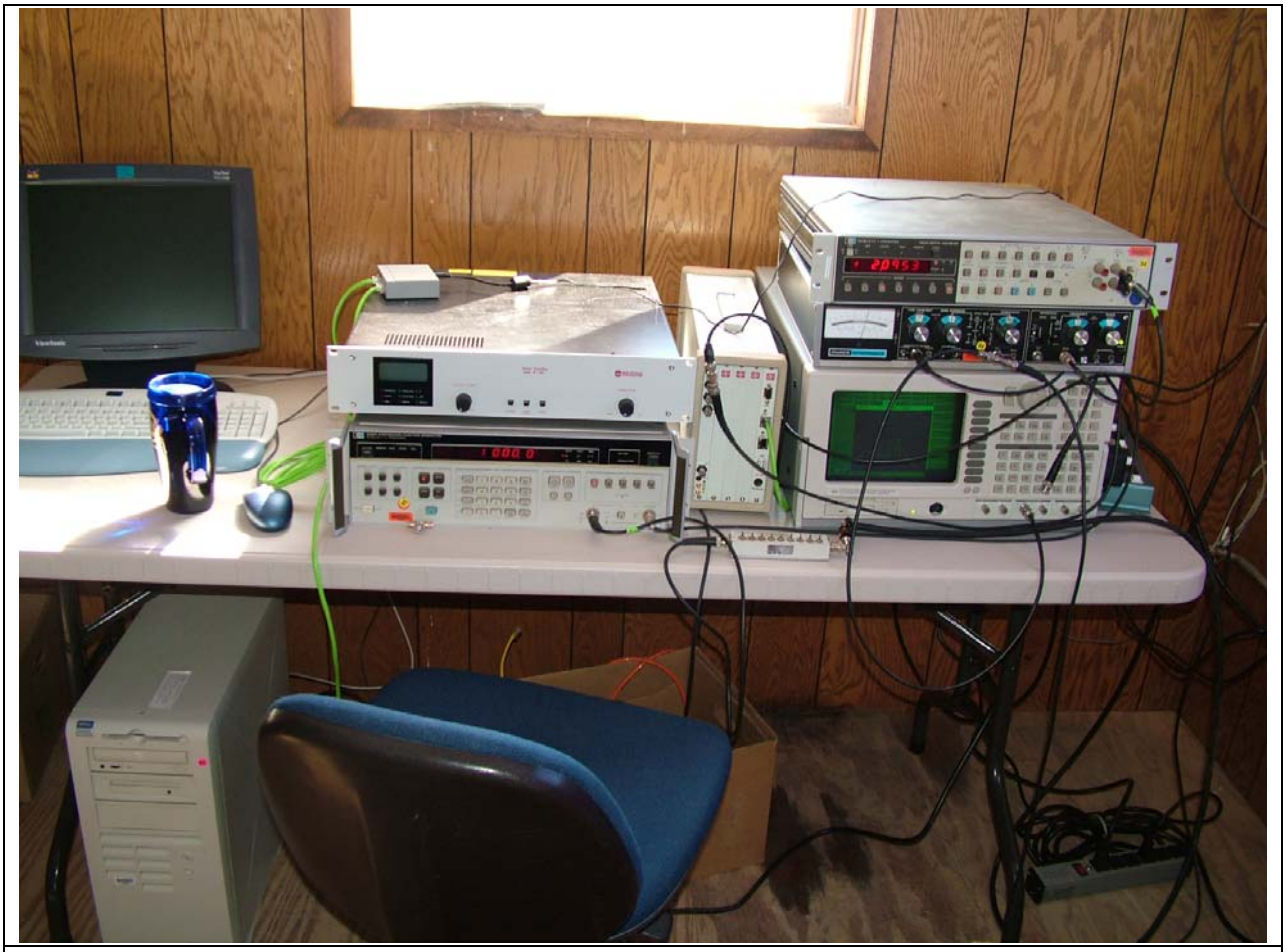

**Figure 16. Photograph of test electronic in the vault**

Initial vault testing of the selected accelerometers was very promising and suggested that the Endevco 7703A accelerometer is a very good choice for this work. Tests were run at 100 micro g, 50 micro g, and 1 micro g. The 1 micro g appeared to be right at the level of our capabilities in the vault (aircraft flying overhead, ventilation, etc.), but data at 1 micro g could be observed in some frequency ranges. Based upon the results, it appears that the sensor is good for measurements down to 1 micro g (our target) and may actually be better, but Sandia was unable to perform such measurements in any available site. The only possibility for a quieter site is probably to work downhole.

**Figure 17** shows the measured output of the 7703A and the 7251-HT transducers while attempting to hold the Wilcoxin response relatively constant. The Wilcoxin accelerometer has a resonance at about 2200 Hz and its response is continually increasing above a few hundred Hz, which is why both the input and the other accelerometers show a decrease. No data can be obtained between about 2000 and 2400 Hz due to the high mechanical gain of the Wilcoxin (potential to break the sensor). Alternately, the 7703A and the 7251-HT can be used to derive a corrected response, as shown in **Figure 18**. This figure shows the increasing sensitivity of the Wilcoxin accelerometer and the nearly flat response of the other two. The input level is approximately 50 mg.

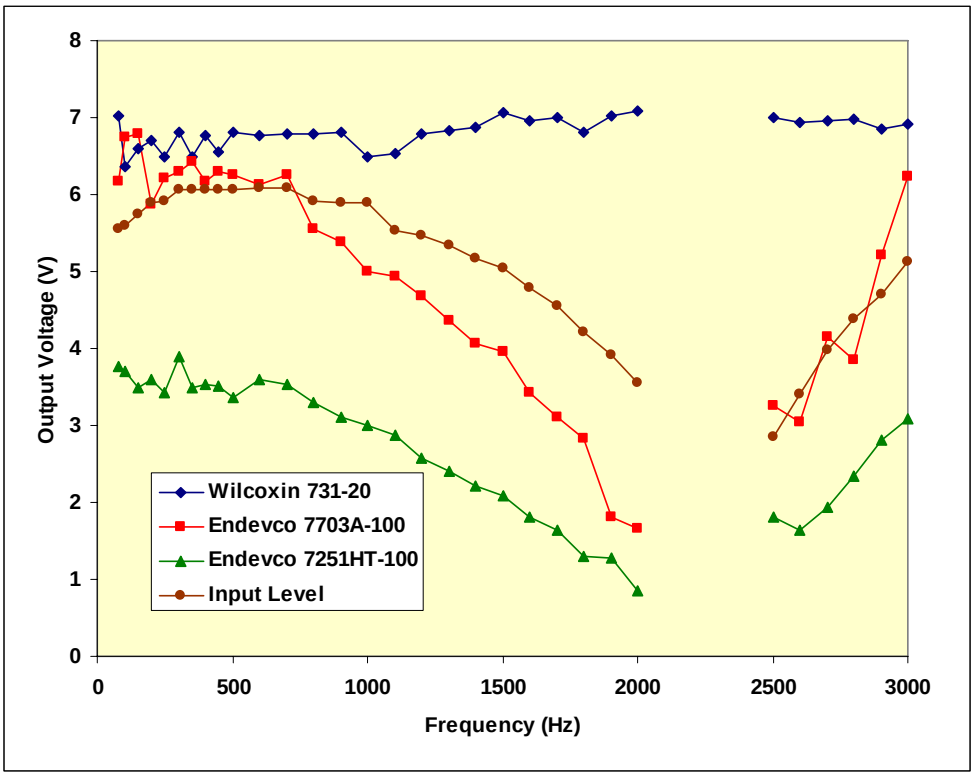


**Figure 17. Output response of sensors while attempting to hold Wilcoxin response constant**

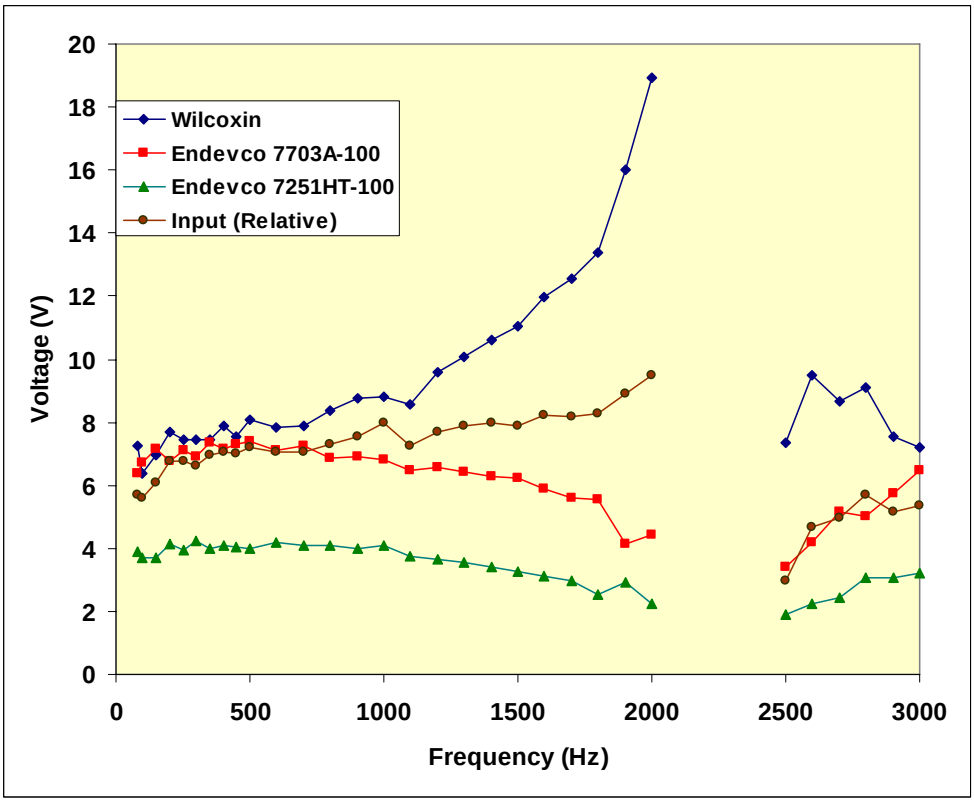


**Figure 18. Adjusted output response after correcting for Wilcoxin response**

Finally, a normalized output of the 7703A as a function of input level is shown in **Figure 19**. For input ranges from 50 µg to 50 mg, the outputs overlay very well, showing a consistent response across input levels. However, the 1 µg input is such a low level (and almost in the noise) that accurate measurements could only be made for frequencies below about 700 Hz. For higher frequencies, the behavior is less certain.

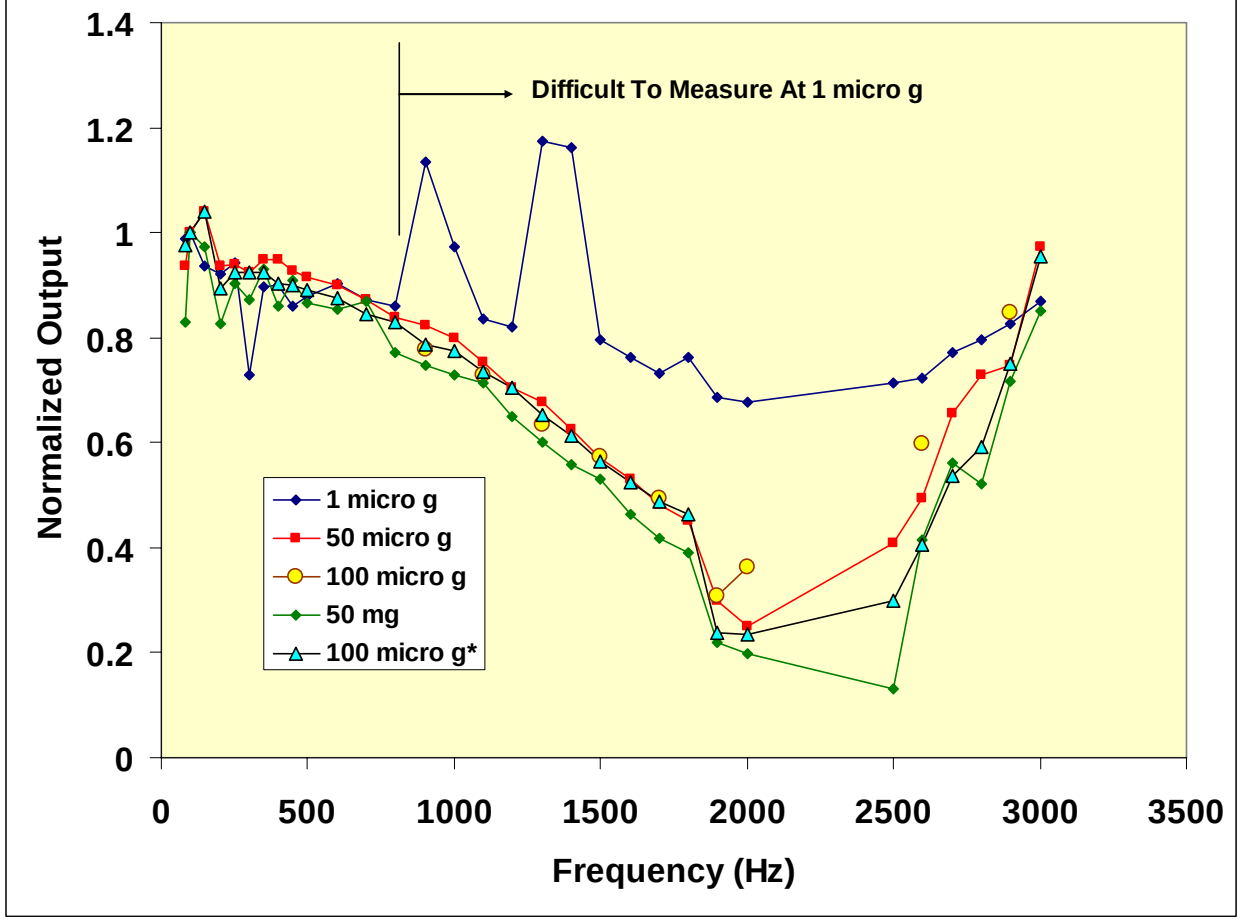


**Figure 19. Normalized output as a function of frequency for various input levels**

In summary, the results of accelerometer testing have shown that the accelerometer that was expected to be the best one (Endevco 7703A-100) was quiet down to 1 μg, which was the noise level of the buried vault in which the low-noise tests were performed. The noise floor could be lower than 1 μg, but there is no method to test it without using a primary standards laboratory. No additional tests are needed, however, because this noise floor is good enough for our needs. It was also found that this accelerometer can be amplified to give several volts per g output (maybe as much as 10). This is approaching the sensitivity of the Wilcoxin 731-20A accelerometers, which have the best response in the world (but they have no shock resistance and are temperature sensitive). The 7703A have great shock resistance (5,000 g) and can stand temperatures above 250 degrees C.

One problem with the 7703A is that it has a side mount, which makes it harder to use in the current receiver fixture. In discussions with Endevco, it was found that they make the same unit in a top mount and it is called a 7701. This unit is not in their standard catalog, but it does exist. Sandia acquired three of them for use in the prototype testing. The characteristics of the 7701 were also checked in the vault and found to be the same response as the 7703A. The final curve in **Figure 19** (100 microg*) is the response of the 7701; thus, the 7701 is our accelerometer of choice.

The next step is mating the 7701 with an amplifier. In the initial tests, Sandia decided to test the state-of-the-art low noise amplifier that is currently used in the Wilcoxin 731-20A accelerometers. One of the

reasons the 731-20A is such a good accelerometer is the very low noise amplifier. (Incidentally, the design of that amplifier was done in a joint Sandia/Wilcoxin project under DOE funding over ten years ago.) At this time, three amplifiers have been taken out of old Wilcoxin 731-20A accelerometers and have been mated to Endevco 7701 accelerometers. One of these mated units was tested in the vault and gave great response with low noise. **Figure 20** shows one of the side-mounted Endevco 7703A accelerometers with an amplifier from the Wilcoxin 731-20A mounted on top.

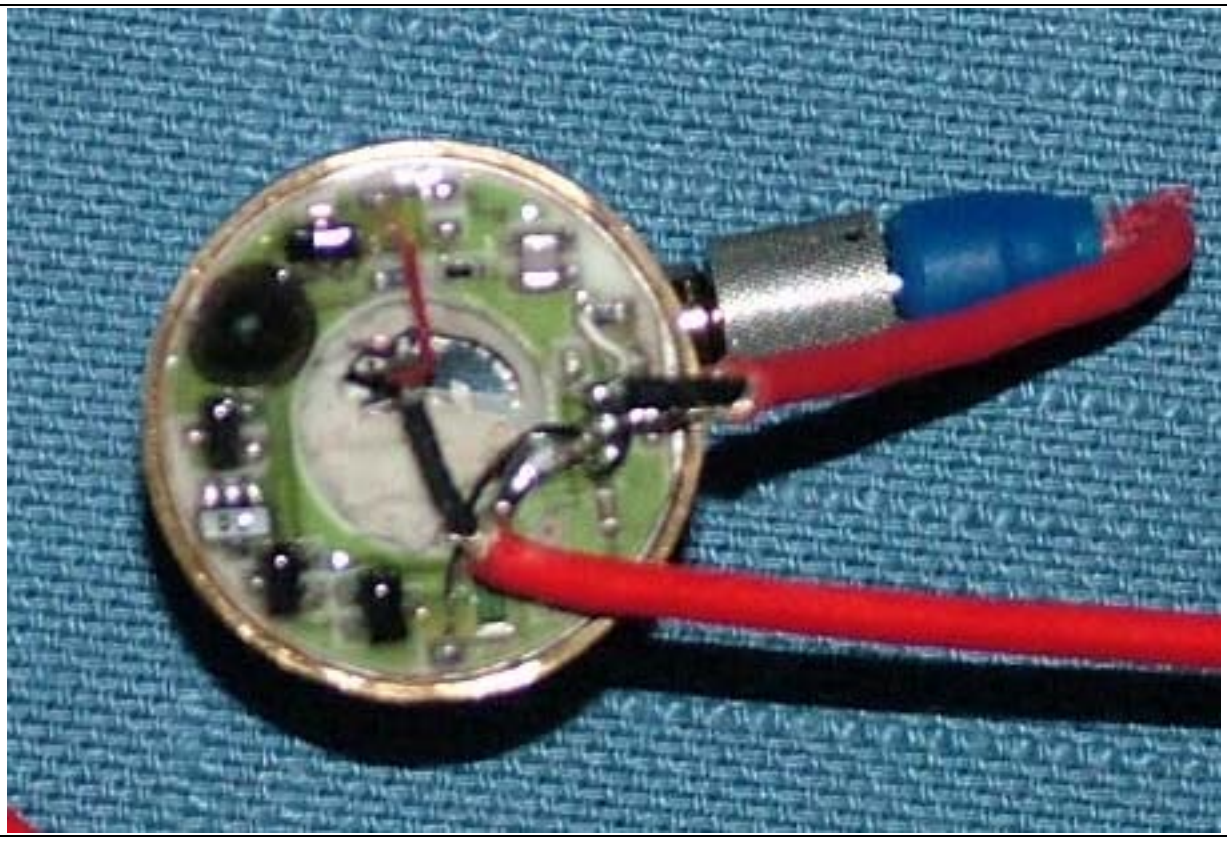

**Figure 20. Photograph of Endevco 7703A accelerometer with Wilcoxin 731-20A amplifier mounted on top**

The other additional circuitry needed for the Endevco accelerometers is a constant-current power supply circuit with amplification. **Figure 21** shows a functional block diagram of this circuit. The constant-current circuit needs clean supply power and a low-noise amplifier to perform adequately. **Figure 22** shows a circuit diagram of the power supply circuit, and **Figure 23** shows a circuit diagram of the power supply circuit with additional conditioning of the output signal to better match the A/D of the GERI system.

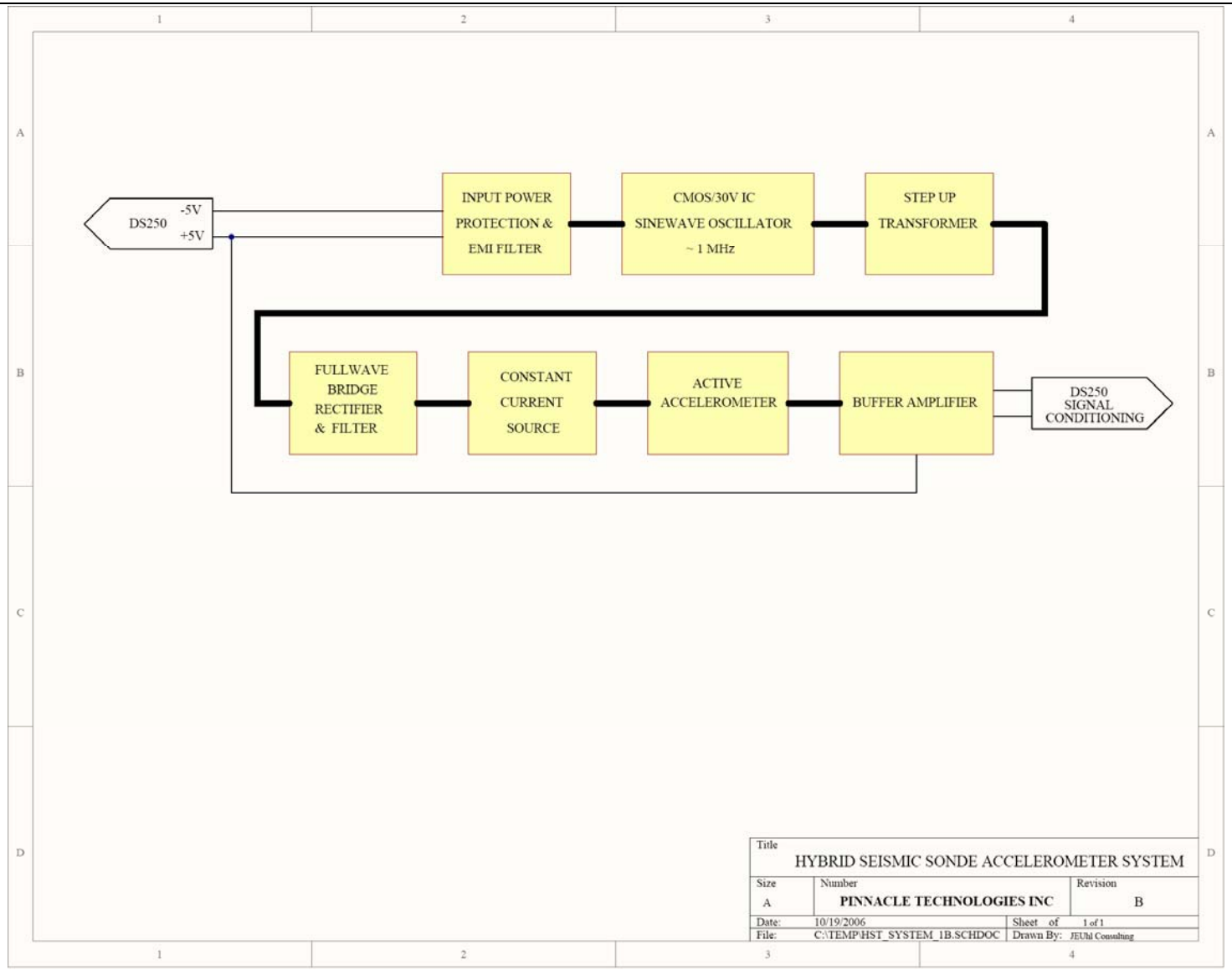


**Figure 21. Functional block diagram of constant-current power and amplification circuit**

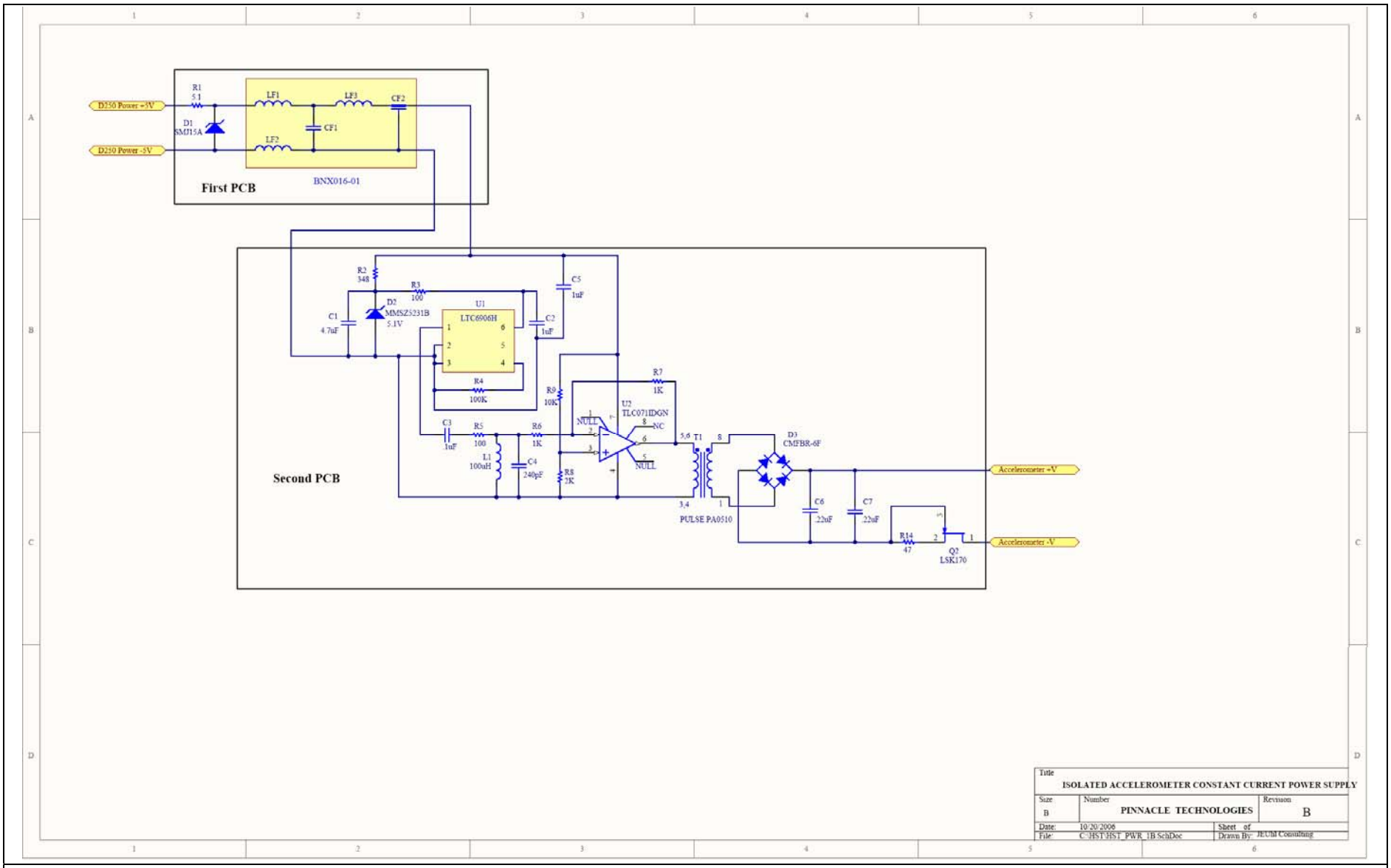


**Figure 22. Circuit diagram for constant-current power supply**

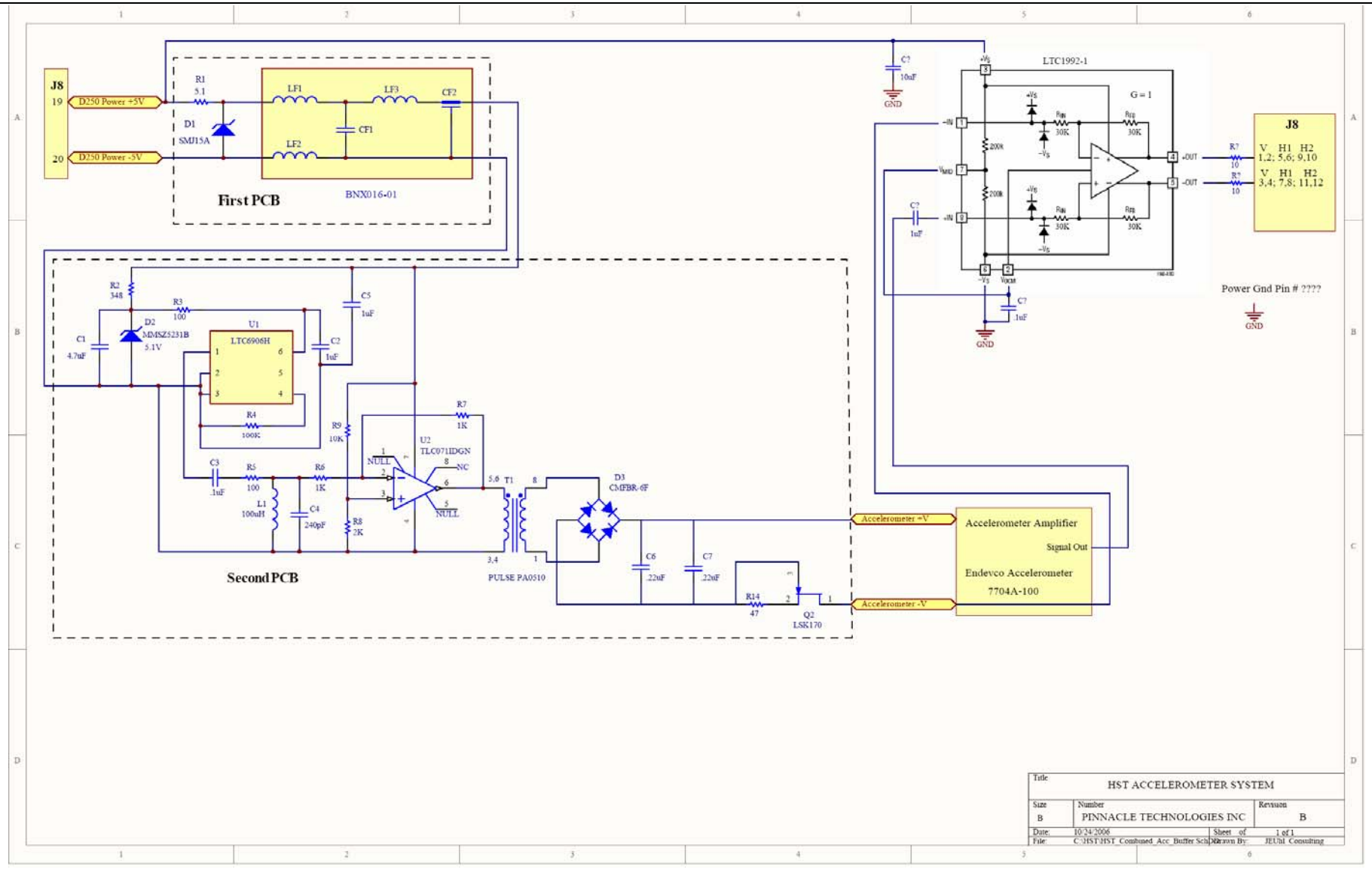


**Figure 23. Circuit diagram for constant-current power supply and additional conditioning**

## 3.4 Accelerometer Field Testing

The accelerometer sensor and associated circuitry described above was inserted into a shuttle, tested in the laboratory, and then tested in the field by placing it at the bottom of a microseismic array just a short distance from a standard geophone sensor. Both microseisms and perforations were recorded during two Barnett Shale tests; however, the perforations are the best test of the accelerometer performance because such explosive events generate considerable high frequency energy.

**Figure 24** shows an example of the traces recorded for a large perforation on the geophone tool while **Figure 25** shows the same example for the accelerometer tool. In both cases, the top trace is the vertical sensor while the two overlain traces on the bottom are the two horizontals. Only P-waves could be detected from this perforation at this particular viewing location. A comparison of **Figure 24** and **Figure 25** reveals a higher frequency content for the accelerometer than for the geophone tool. Note that the two sets of data are scaled differently and no inference should be made about the relative amplitudes of the two sets of traces.

The different frequency response can be seen more clearly in the spectra of the two sondes, as shown in **Figure 26**. The geophone spectrum is concentrated around 300 to 600 Hz, whereas the accelerometer has its maximum energy in the 700 to 1,000 Hz range. The accelerometer also has considerable energy in the 300 to 600 Hz range, matching the geophone. The response of the geophone tool clearly drops off above about 600 Hz. The accelerometer tool begins to drop off at about 1,000 Hz, but it is uncertain whether this is reflecting the true energy content of the perforation (plus attenuation effects) or is some limitation of the A/D system. The anti-aliasing filter is set at around 1700 Hz and should not be responsible for the observed drop-off.

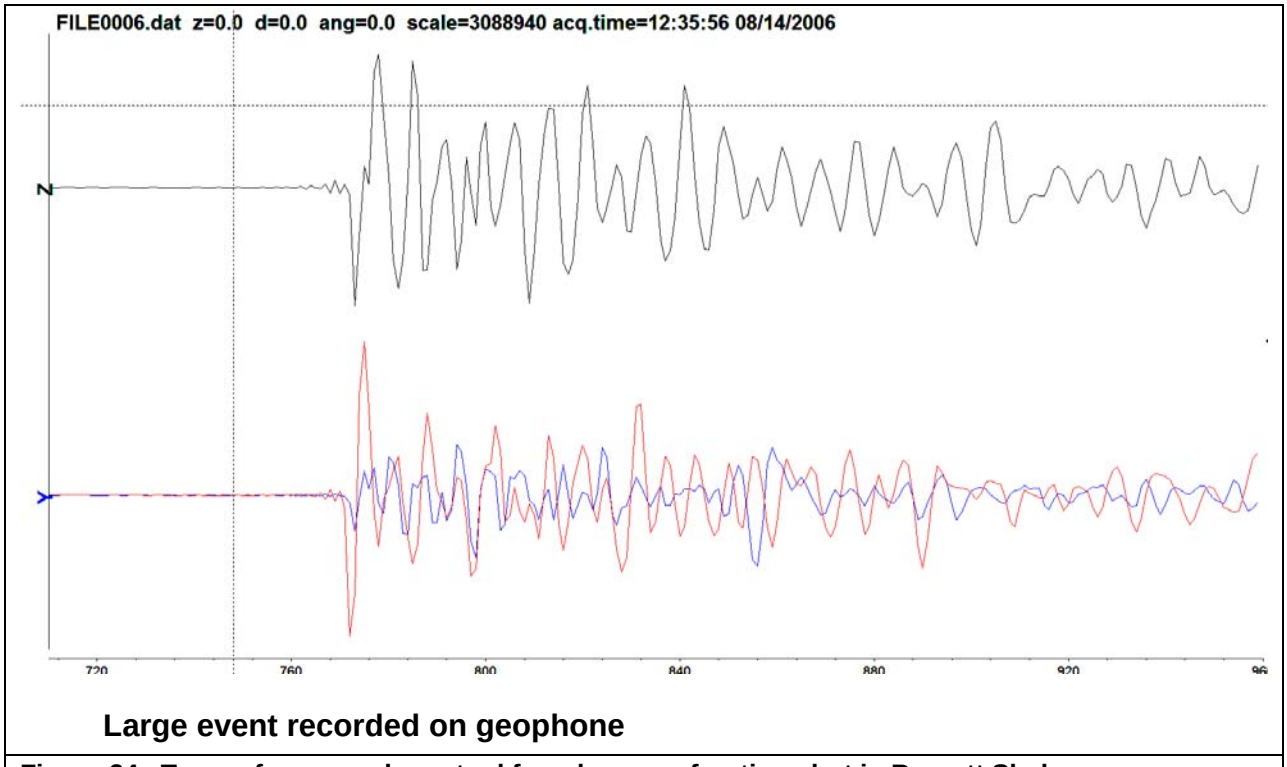


**Figure 24. Traces from geophone tool for a large perforation shot in Barnett Shale**

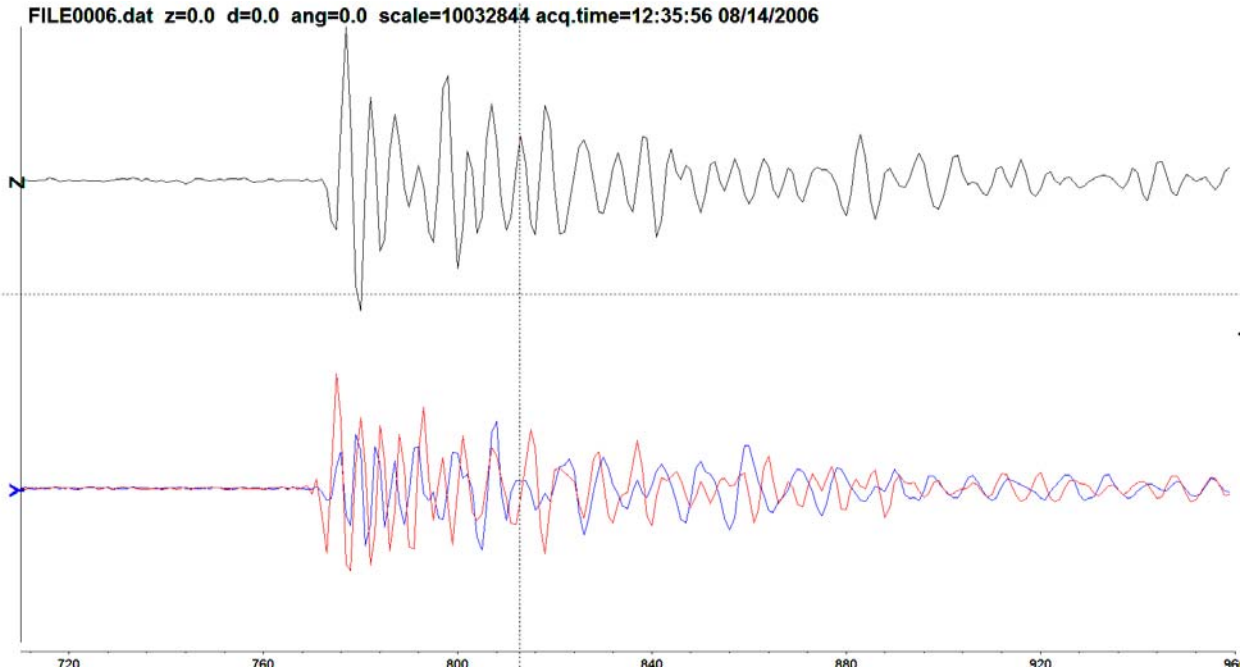


**Figure 25. Traces from accelerometer tool for a large perforation shot in Barnett Shale**

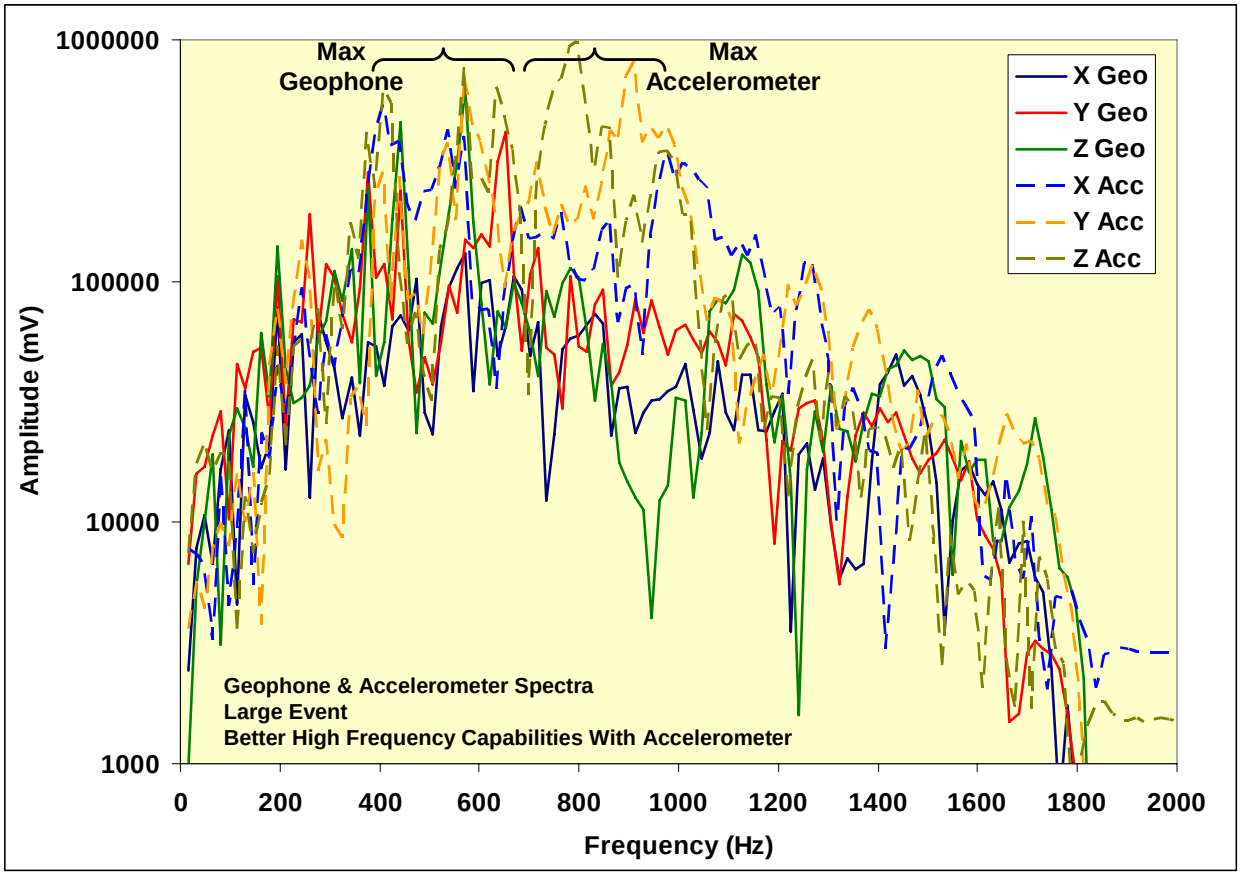


**Figure 26. Comparison of spectrum of accelerometer and geophone tools for a large perforation**

Based upon this response alone, it appears that the accelerometer is performing much better than the geophone, as there are much better high frequency capabilities with the accelerometer. However, the accelerometer performance does not look nearly as good for small events. **Figure 27** shows the traces for a small microseismic event as detected from the geophones, and **Figure 28** shows the same event as detected on the accelerometer tool. In this example, the event is clearly seen on the geophone tool but is considerably masked by noise in the accelerometer tool.

**Figure 29** shows the comparison of the spectra for the two sets of data. The noise level for the accelerometer is about 2 orders of magnitude greater than it is for the geophones. This noise is most likely due to electronic noise rather than anything cultural. **Figure 30** shows the noise spectrum for both tools (no event). The relatively constant noise across all frequencies suggests that the noise is electron rather than cultural.

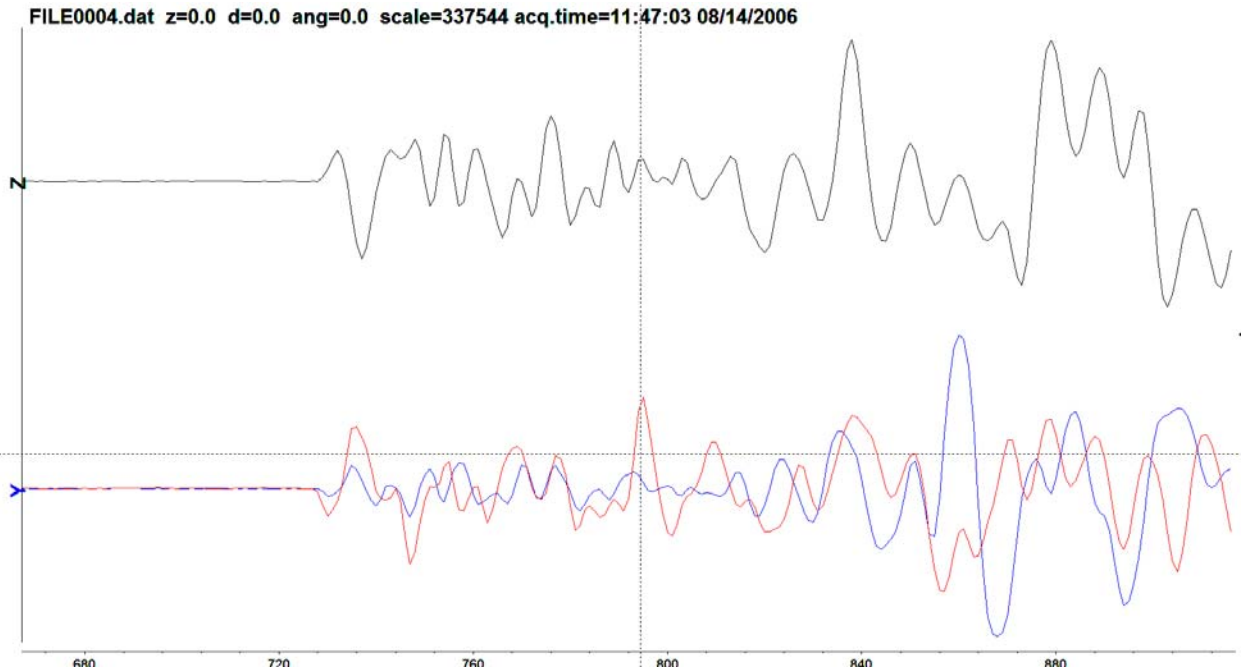


**Small event recorded on geophone**

**Figure 27. Traces from geophone tool for a small event in the Barnett Shale**

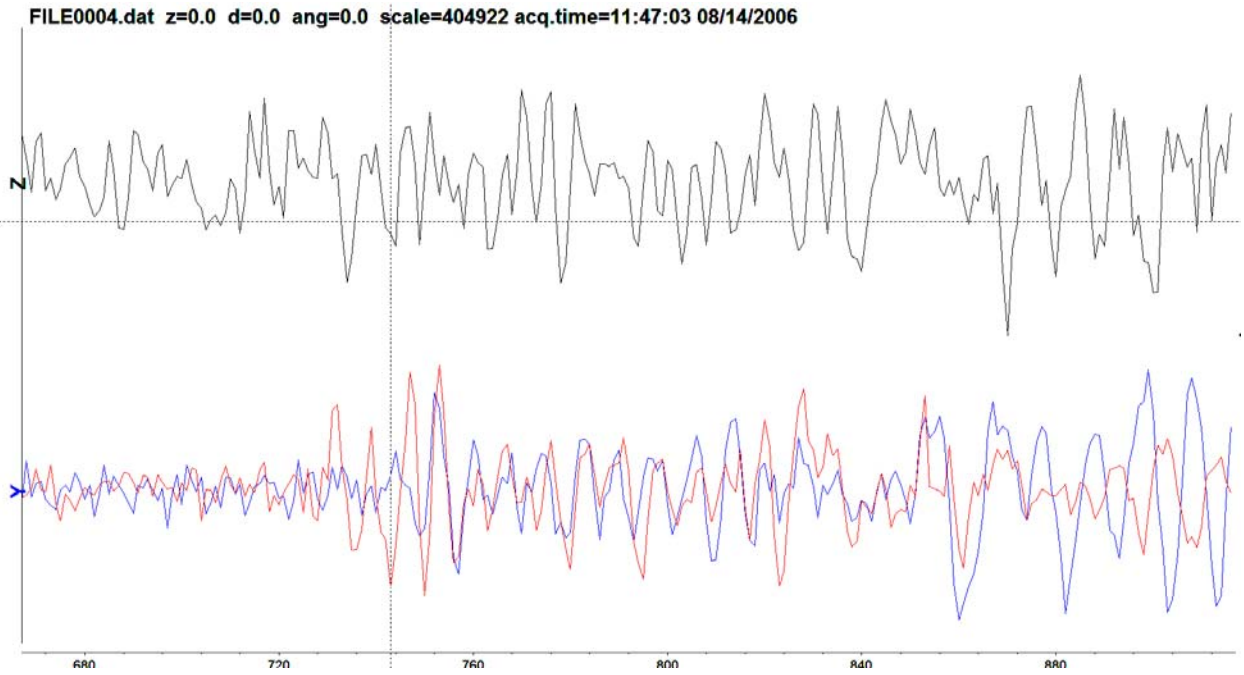


**Small event recorded on accelerometer**

**Figure 28. Traces from accelerometer tool for a small event in the Barnett Shale**

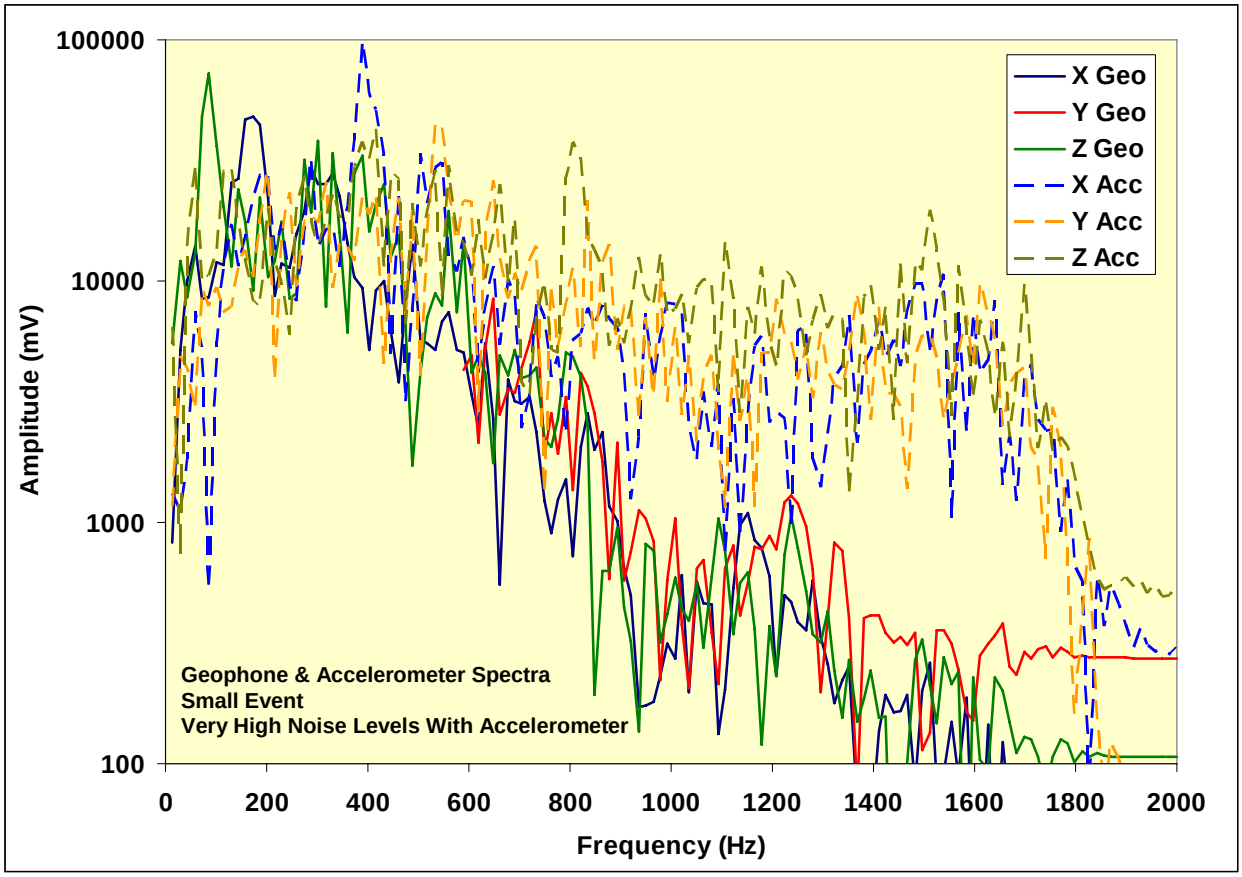


**Figure 29. Comparison of spectrum of accelerometer and geophone tools for a small event**

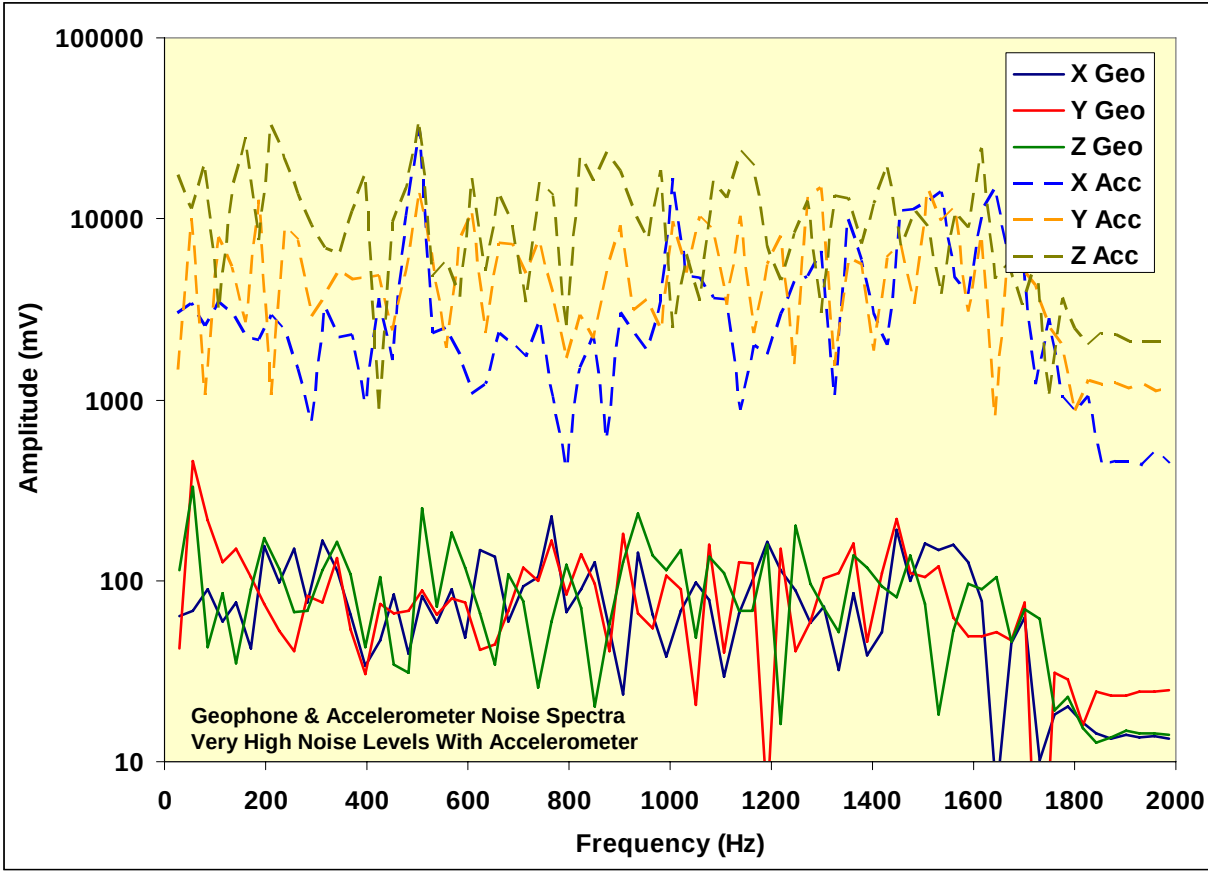


**Figure 30. Comparison of spectrum of accelerometer and geophone tools for only noise**

The observed noise levels on the accelerometer tool make it unusable for microseismic monitoring under these conditions, but the results are not entirely unexpected. This is a first attempt to mate a new sensor into a commercial tool, and much about this commercial tool is unknown and unavailable (proprietary to the manufacturer). The high noise levels suggest a mismatch between the output of the accelerometer circuit and the A/D input. Circuits can be developed (and are currently being developed) to better match the accelerometer with the A/D, but this aspect of the work is outside of the scope of this project.

The results that were obtained have shown that an accelerometer tool is capable of detecting much higher frequency energy than the geophones and will thus provide an enhanced capability to detect microseisms. However, the GERI tool system is not optimized for accelerometer data, both in its input characteristics and in the electronic noise generated at high sampling rates. Additional work will be performed to find ways to improve these operating conditions.

In summary, this development effort has convinced us that better microseismic data can be obtained with accelerometer sensors rather than geophones. Additional work will need to be performed to match the accelerometers with the A/D system or alter the A/D system to take advantage of the accelerometer capabilities.

## 3.5 Testing of the Combined Microseismic-Tiltmeter Tool

Testing of a single tiltmeter tool on the microseismic array was attempted in May 2005 in a well in North Texas. The tool malfunctioned because an electronics board failed in the well. The board rated for 80°C, which was inadequate for the well (temperature 100°C). This component was replaced with a higher temperature one for later tests.

Two additional attempts at fielding a single tiltmeter took place in August and September 2005 in North Texas as part of a microseismic monitoring test. In the second test, the tiltmeter tool worked but one of the sensor axes failed to rezero properly. The second axis worked fine and appeared to give good data. The problems with the rezero were unrelated to the hybrid issues and were found and fixed. In general, these tests showed that the combined array could function as required.

Initial fielding of an array containing both tiltmeters and microseismic receivers was performed in December of 2005. This test consisted of three tiltmeters added to a 12-level string of microseismic receivers during a test in the Barnett Shale. These tools were run on the fiber-optic wireline of the microseismic array. The purpose of the test was to assess whether (1) the tiltmeter tools would function properly using the electrical conductors of the fiber-optic wireline, (2) the tiltmeter tools would be sufficiently clamped by being attached to the microseismic receivers (with their clamp arms), and (3) the microseismic tools would be affected in any way (seismic and electrical response) by the presence of the tiltmeters. There was no attempt to extract information about the fracture from the tiltmeter data since three tiltmeters are insufficient for any inversion of the data. These initial tests were successful and showed that the combined system would function properly. The tiltmeters ran acceptably, with some issues in communication that were addressed later. The tiltmeter coupling was adequate to record the deformation. The microseismic tools were unaffected by the addition of the tiltmeters once some noise problems were addressed.

A more comprehensive test was carried out in May of 2006 during a coalbed-methane fracturing test in Colorado. However, this test was conducted in the treatment well, with the additional issues of pressure control and noise due to flowing fluids. In this test, five microseismic receivers (a typical number for a treatment well test) and three tiltmeters were deployed on the fiber-optic wireline of the microseismic system. All tools functioned correctly in this test and provided reasonable data.

**Figure 31** shows an example of a microseismic event detected with the five microseismic receivers. This is a very close event with high frequency content and difficult S-waves. The vertical sensor is shown by the black trace and the two horizontal traces are overlain in red and blue. It shows that the tool is still well coupled to the casing and is not adversely affected by the connected tiltmeter tools.

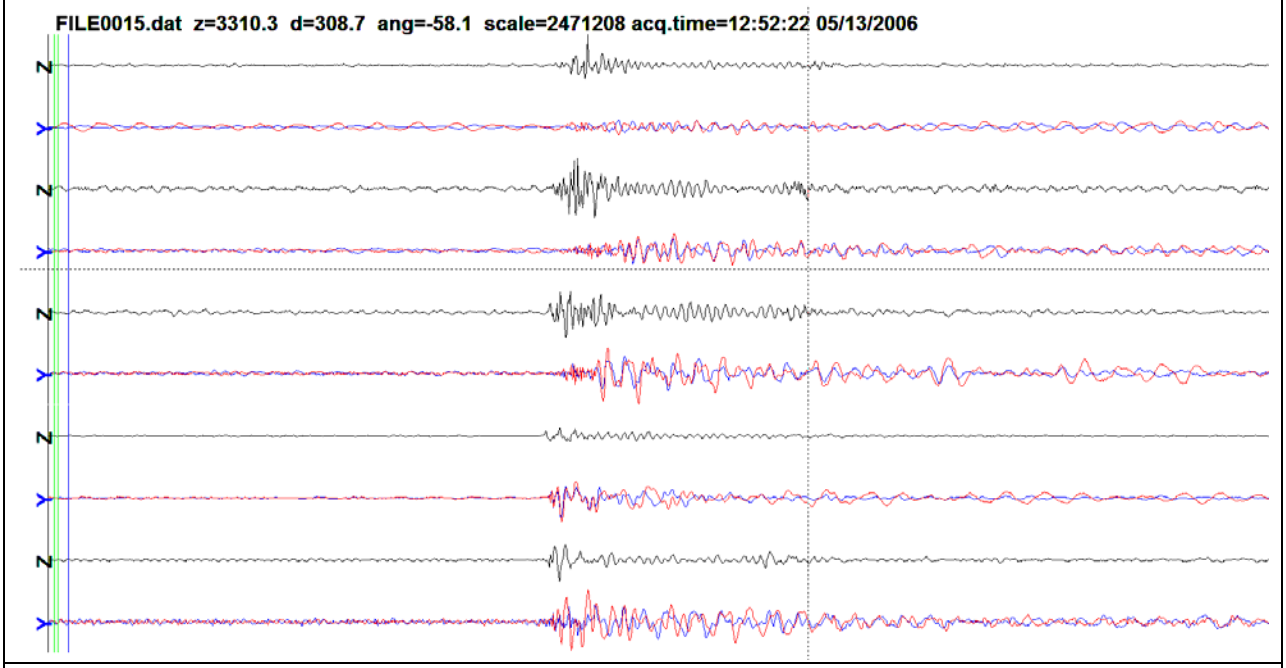


**Figure 31. Example microseismic event detected with 5-level receivers in hybrid array**

**Figure 32** shows an example of the tilt data that were obtained in this test. With only three levels, it is very difficult to make any inferences about the fracture geometry, but the tiltmeters appear to be functioning correctly. Early in the injection there are several jumps in the tiltmeter data that are probably caused by rate changes that moved one or more tools. However, once the rate stabilizes and the tools settle in, changes in the tilt field can be easily monitored. The two dashed vertical lines show start and end points where the change in tilt was calculated for each of the levels. The left-hand plot shows those tilt changes plotted against depth. In this case, the very large change in the tiltmeter at about 3,110 ft suggests that the bottom of the fracture is near this location. The small change in the tiltmeter at about 3,080 ft suggests that this level is near the center of the crack and consequently saw very little tilt. However, these results are speculative without more tiltmeters to show corresponding increases and decreases in surrounding tilt values.

This test verified that the hybrid array is operational as it is currently designed and a larger array of both microseismic and particularly tiltmeters can be deployed. As a result of these positive tests, a full array of tiltmeter housings is being fabricated so this technology can be run as a service.

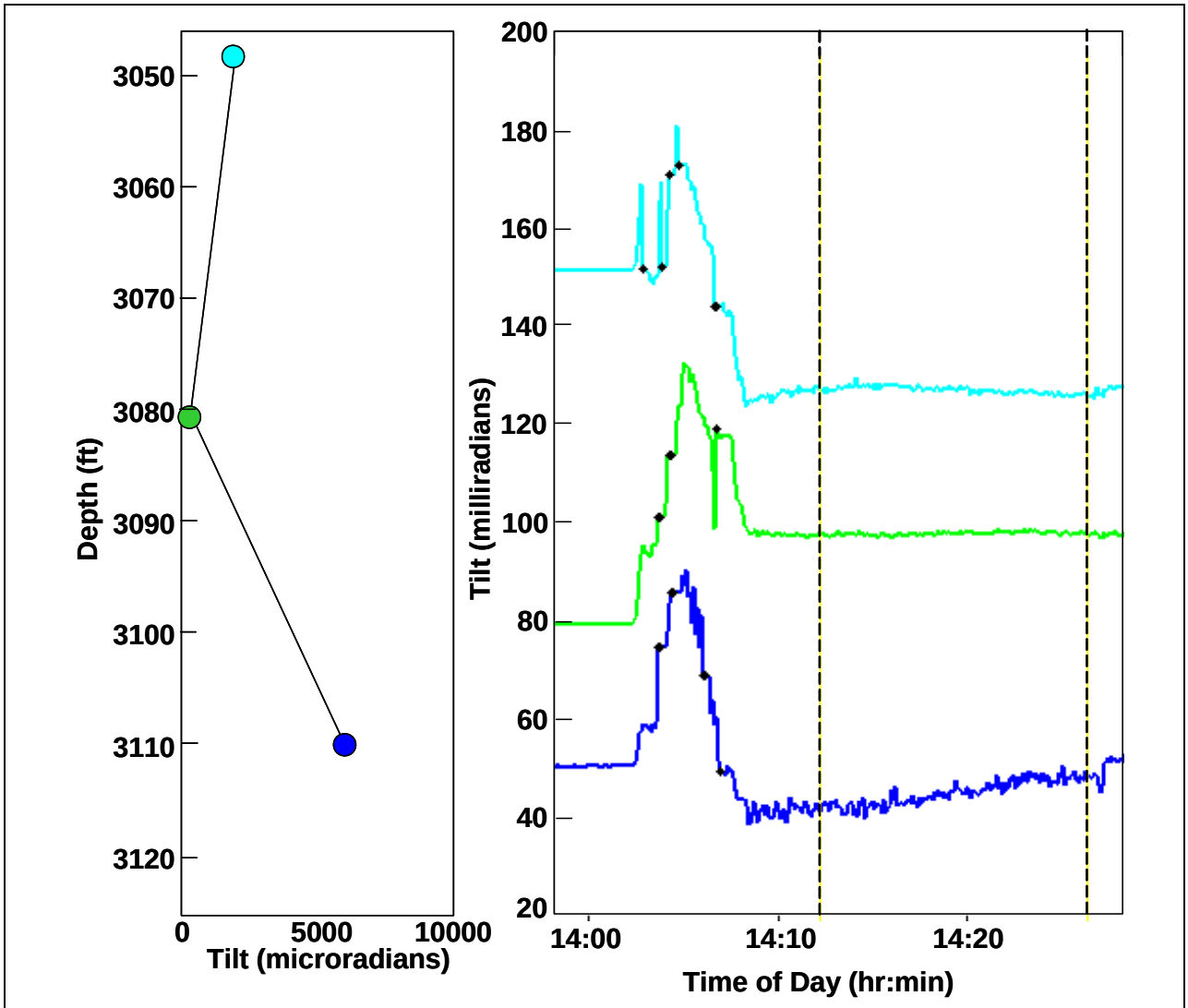


**Figure 32. Example tiltmeter data from three tiltmeter levels on hybrid array**

## 3.6 Development of Joint Inversion Routine

The development of a joint inversion analysis consisted of several potential analyses that were investigated to determine the best approach. These included an analysis of uncertainty, an evaluation of using a mechanical model to link the microseismic and tiltmeter data, and the final formulation of a joint inversion algorithm. In the end, it was decided that the link using a mechanical model was insufficiently constrained because of the lack of the necessary data for most industrial applications and a more universal distributional approach was formulated.

### 3.6.1 Joint Inversion

With two separate data sets – tiltmeter and microseismic – one has the capability of developing two separate maps and comparing the results. This is a useful approach and could provide information about the fracturing process that might not be otherwise evident. In the end, however, there is a need for a single best answer giving the most likely fracture geometry. If the results from the two data sets are very

similar, then the single best answer may be evident. More likely there will be some discrepancies in the two individual answers and some method will be required to extract the best combined solution. One approach to doing this is to jointly invert the data in some way to obtain a single, integrated solution. We call this a joint inversion.

Developing a methodology for jointly inverting the two data sets is not necessarily a simple task since the data sets are so diverse. If one starts with the raw data, the microseisms are a collection of waveforms with discrete arrivals while the tiltmeter data are similar time-series responses with discrete events on them. A final solution would marry analyses of both time series through some time-dependent mechanical model, but such a complex analysis is not feasible at this time. However, by moving farther along in the process and using the arrival time data and the tilt values at specific times, then it is possible to link the tilt model and the microseismic event locations through the velocity structure.

If the microseismic data points are treated as a distribution of events with an azimuth and standard deviation about that azimuth, a length distribution and a standard deviation associated with that distribution, a height distribution (with standard deviation), an edge distribution (with standard deviation), and dip (with standard deviation), then these distributions can be used to represent an envelope surrounding a "model" fracture. This "model" fracture will have a well defined tilt field that will need to agree with the observed tilt distribution (assuming some pressure or width). In addition, the microseismic distributions will change as the velocity structure changes (events are relocated), thus allowing the velocity structure to be refined as part of the inversion process.

The mechanism for performing the joint inversion is the Marquardt-Levenberg approach. In the Marquardt-Levenberg (M-L) analysis, a model is provided to calculate derivatives as a function of the desired output parameters and the M-L analysis uses a combined steepest descent and linearization scheme to figure out how to minimize errors and obtain the best possible solution. For the tiltmeter analysis this is straightforward, as equations describing the elastic tilt model (it could be a dislocation or the flat elliptic crack used here) can be provided in the code and the differences between the observed tilts and calculated tilts drive the algorithm toward the best-fit "model." For the microseismic data, the distributional misfit between the microseismic events and the "model" provide the rationale for changing either the "model" of the fracture or the velocity structure (or both).

It should be noted that the use of a distributional approach eliminates the need for a mechanical model to link the tiltmeter and microseismic data. This is a change of approach from the original work proposal.

### A. Tiltmeter Model

The tiltmeter model is the 3D flat elliptic crack of Green and Sneddon[3] that is in the literature. The only reason that this model was chosen is that it was already coded up and in an available program. The Okada[4] dislocation approach could replace the crack model and would provide essentially the same results.

Considering a 3-dimensional flat elliptic crack opened by internal pressure and having the geometry shown in **Figure 33**, Green and Sneddon[3] found an analytical solution for the following assumptions:

- infinite medium
- homogeneous isotropic material
- linear elastic behavior
- uniform pressure
- length > height (a > b)

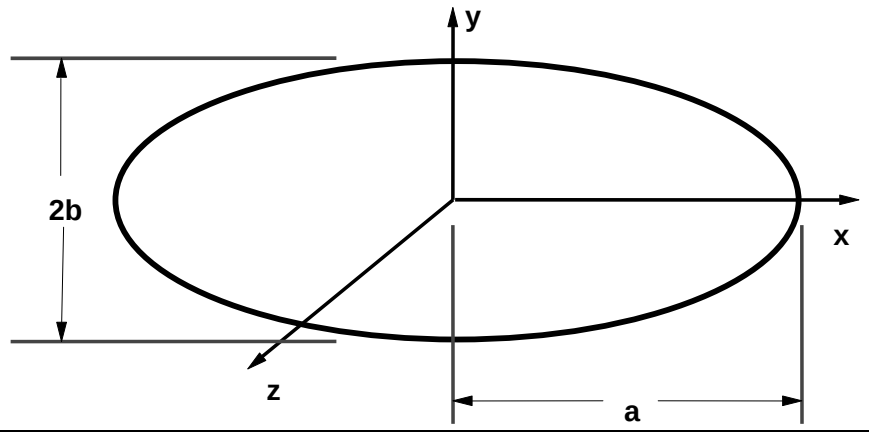


**Figure 33. Geometry of fracture for tilt calculations**

Given these restrictions, the displacements and stresses can be given by

$$D = 8\frac{\partial}{\partial \bar{z}}\left\{(1+2\nu)\phi + Z\frac{\partial \phi}{\partial Z}\right\},$$

$$u_Z = -8(1-\nu)\frac{\partial \phi}{\partial Z} + 4Z\frac{\partial^2 \phi}{\partial Z^2},$$

$$\Theta = -8G\left\{(1-2\nu)\frac{\partial^2 \phi}{\partial Z^2} + Z\frac{\partial^3 \phi}{\partial Z^3}\right\},$$

$$\Phi = 32G\frac{\partial^2}{\partial \bar{z}^{-2}}\left\{(1-2\nu)\phi + Z\frac{\partial \phi}{\partial Z}\right\},$$

$$\sigma_Z = -8G\frac{\partial^2 \phi}{\partial Z^2} + 8GZ\frac{\partial^3 \phi}{\partial Z^3}, \text{ and}$$

$$\Psi = 16GZ\frac{\partial^3 \phi}{\partial \bar{z}\partial Z^2},$$

with

$$D = u_x + iu_y,$$

$$\Theta = \sigma_x + \sigma_y,$$

$$\Phi = \sigma_x - \sigma_y + 2i\tau_{xy}, \text{ and}$$

$$\Psi = \tau_{xz} + i\tau_{yz}.$$

In these equations, G is the shear modulus of the material and ν is Poisson's ratio. Additionally, Z is the third coordinate while $z$ is the complex variable given by $z = x + iy$ and $\bar{z}$ is its complex conjugate. Given such forms of the equations, Green and Sneddon[3] found a solution of the problem by converting to an ellipsoidal coordinate system, $\lambda$, $\mu$, $\varepsilon$, given by

$$a^2\left(a^2 - b^2\right)x^2 = \left(a^2 + \lambda\right)\left(a^2 + \mu\right)\left(a^2 + \varepsilon\right)$$
$$b^2\left(b^2 - a^2\right)y^2 = \left(b^2 + \lambda\right)\left(b^2 + \mu\right)\left(b^2 + \varepsilon\right)$$
$$a^2b^2Z^2 = \lambda\mu\varepsilon$$

where

$$\infty > \lambda \geq 0 \geq \mu \geq -b^2 \geq \varepsilon \geq -a^2 \quad .$$

In this coordinate system, the solution can be found as an integration of combined coordinates as

$$\phi = \frac{ab^2 p}{32G\ \ E(k)} \int_\lambda^\infty \left\{ \frac{x^2}{a^2 + s} + \frac{y^2}{b^2 + s} + \frac{Z^2}{s} - 1 \right\} \frac{ds}{\sqrt{s\left(a^2 + s\right)\left(b^2 + s\right)}} \quad ,$$

where *E(k)* is an elliptic integral of modulus *k*, with

$$k = \frac{\sqrt{a^2 - b^2}}{a}$$

and with a complementary modulus, *k' = 1 - k*

### B. Application to a Vertical Fracture (Length > Height)

The tilts normal to the face of a long vertical fracture can be found as

$$\frac{\partial u_Z}{\partial y} = \frac{-8AZ}{ab^2}\left[ -\left(1 - 2\nu\right)\left\{ k'^2 \frac{\mathrm{sn}^2 u}{\mathrm{cn}^2 u} \right\} \frac{du}{d\lambda}\frac{\partial \lambda}{\partial y} \right.$$
$$+ Z\left\{ 2k'^2 \frac{\mathrm{sn}\,u\,\mathrm{dn}\,u}{\mathrm{cn}^3 u} \right\}\left( \frac{du}{d\lambda} \right)^2 \frac{\partial \lambda}{\partial y}\frac{\partial \lambda}{\partial Z}$$
$$\left. + Z\left\{ k'^2 \frac{\mathrm{sn}^2 u}{\mathrm{cn}^2 u} \right\}\left( \frac{d^2u}{d\lambda^2}\frac{\partial \lambda}{\partial y}\frac{\partial \lambda}{\partial Z} + \frac{du}{d\lambda}\frac{\partial^2 \lambda}{\partial y \partial Z} \right) \right],$$

where sn, dn and cn are Jacobian elliptic functions, *A* is given by

$$A = -\frac{ab^2 P}{16GE\left(k\right)} \quad ,$$

*u* is defined as

$$\lambda = a^2 \frac{\mathrm{cn}\,u}{\mathrm{sn}\,u}$$

and *E(k)* is the complete elliptic integral of the second kind. The additional derivatives are found from

$$\frac{du}{d\lambda} = \frac{-\,\mathrm{sn}^3 u}{2a^2\,\mathrm{cn}\,u\,\mathrm{dn}\,u} \ ,$$

$$\frac{d^2u}{d\lambda^2} = \frac{-\mathrm{sn}^2 u}{2a^2}\left[3+\frac{\mathrm{sn}^2 u}{\mathrm{cn}^2 u}+k^2\,\frac{\mathrm{sn}^2 u}{\mathrm{dn}^2 u}\right]\frac{du}{d\lambda} \ ,$$

$$\frac{\partial\lambda}{\partial y} = \frac{2y\lambda\left(a^2+\lambda\right)}{(\lambda-\mu)(\lambda-\varepsilon)} \ ,$$

$$\frac{\partial\lambda}{\partial Z} = \frac{2Z\left(a^2+\lambda\right)\left(b^2+\lambda\right)}{(\lambda-\mu)(\lambda-\varepsilon)} \ ,$$

$$\frac{\partial^2\lambda}{\partial y\partial Z} = \frac{yZ}{4\left(h_1^2\right)^2\lambda\left(b^2+\lambda\right)}\left[-\frac{1}{\lambda}-\frac{1}{b^2+\lambda}+\frac{1}{2h_1^2}\left\{\frac{x^2}{\left(a^2+\lambda\right)^3}+\frac{y^2}{\left(b^2+\lambda\right)^3}+\frac{Z^2}{\lambda^3}\right\}\right] \ ,$$

and

$$h_1^2 = \frac{(\lambda-\mu)(\lambda-\varepsilon)}{4\lambda\left(a^2+\lambda\right)\left(b^2+\lambda\right)} \ .$$

More information about these derivatives and other characteristics of the ellipsoidal confocal coordinate system can be found in Whittaker and Watson.[5] This same reference has extensive information about the Jacobian elliptic functions, as does Abramowitz and Stegun.[6] In addition, Sih and Liebowitz[7] provide some discussion on the 3D-elliptic-crack solution that is useful.

Similarly, the tilts parallel to the fracture face are found from

$$\begin{aligned}\frac{\partial u_x}{\partial y} = {} & \frac{8(1-2\nu)Ax}{a^3}\left\{\mathrm{sn}^2 u\right\}\frac{du}{d\lambda}\frac{\partial\lambda}{\partial y} \\ & + \frac{8AZ^2}{ab^2}\left[\left\{2k'^2\,\frac{\mathrm{sn}\,u\,\mathrm{dn}\,u}{\mathrm{cn}^3 u}\right\}\left(\frac{du}{d\lambda}\right)^2\frac{\partial\lambda}{\partial x}\frac{\partial\lambda}{\partial y}\right. \\ & \left. + \left\{k'^2\,\frac{\mathrm{sn}^2 u}{\mathrm{cn}^2 u}\right\}\left\{\frac{d^2u}{d\lambda^2}\frac{\partial\lambda}{\partial x}\frac{\partial\lambda}{\partial y}+\frac{du}{d\lambda}\frac{\partial^2\lambda}{\partial x\partial y}\right\}\right]\end{aligned}$$

where the additional derivatives are given by

$$\frac{\partial\lambda}{\partial x} = \frac{2x\lambda\left(b^2+\lambda\right)}{(\lambda-\mu)(\lambda-\varepsilon)}$$

and

$$\frac{\partial^2\lambda}{\partial x\partial y} = \frac{xy}{4\left(h_1^2\right)^2\left(a^2+\lambda\right)\left(b^2+\lambda\right)}\left[-\frac{a^2+b^2+2\lambda}{\left(a^2+\lambda\right)\left(b^2+\lambda\right)}+\frac{1}{2h_1^2}\left\{\frac{x^2}{\left(a^2+\lambda\right)^3}+\frac{y^2}{\left(b^2+\lambda\right)^3}+\frac{Z^2}{\lambda^3}\right\}\right] \ .$$

The calculation of the $\lambda$, $\mu$, $\nu$ coordinates requires the solution of the cubic equation

$$\lambda^3+\lambda^2\left(a^2+b^2-x^2-y^2-Z^2\right)+\lambda\left(a^2b^2-b^2x^2-a^2y^2-a^2Z^2-b^2Z^2\right)-a^2b^2Z^2=0$$

for $\lambda$ followed by solution of the quadratic equation

$$\mu^2\left(a^2\lambda+\lambda\right)+\mu\left(a^2b^2Z^2+b^2\lambda Z^2+a^4\lambda+a^2\lambda^2-a^2\lambda x^2+b^2\lambda x^2\right)+a^4b^2Z^2+a^2b^2\lambda Z^2=0$$

for $\mu$ and then

$$\varepsilon=\frac{a^2b^2Z^2}{\lambda\mu}$$

The procedure for using these equations is as follows:

1. Select point *x,y,Z* for which the calculation is to be made
2. Determine the appropriate $\lambda,\mu,\varepsilon$ for this point
3. Determine the value of *u*
4. Obtain tilts

### C. Non-Vertical Fracture or Height Greater than Length

The previous solution is for a vertical fracture whose height is greater than its length, which is quite a limiting constraint; however, this model can be used to also extract the tilts for a fracture with dip and for one whose height is greater than its length. To obtain the tilts for these cases, it is necessary to obtain the displacement derivatives for the seven other components. These are given as:

$$\begin{aligned}\frac{\partial u_x}{\partial x}=&\frac{8(1-2\nu)A}{a^3k^2}\{u-E(u)\}\\&+\frac{8(1-2\nu)Ax}{a^3}\left\{\mathrm{sn}^2u\right\}\frac{du}{d\lambda}\frac{\partial\lambda}{\partial x}\\&+\frac{8AZ^2}{ab^2}\left[\left\{2k'^2\frac{\mathrm{sn}\,u\,\mathrm{dn}\,u}{\mathrm{cn}^3u}\right\}\left(\frac{du}{d\lambda}\right)^2\left(\frac{\partial\lambda}{\partial x}\right)^2\right.\\&\left.+\left\{k'^2\frac{\mathrm{sn}^2u}{\mathrm{cn}^2u}\right\}\left\{\frac{d^2u}{d\lambda^2}\left(\frac{\partial\lambda}{\partial x}\right)^2+\frac{du}{d\lambda}\frac{\partial^2\lambda}{\partial x^2}\right\}\right]\end{aligned}$$

$$\begin{aligned}\frac{\partial u_x}{\partial Z}=&\frac{8(1-2\nu)Ax}{a^3}\left\{\mathrm{sn}^2u\right\}\frac{du}{d\lambda}\frac{\partial\lambda}{\partial Z}\\&+\frac{8AZ}{ab^2}\left[\left\{2k'^2\frac{\mathrm{sn}^2u}{\mathrm{cn}^2u}\right\}\frac{du}{d\lambda}\frac{\partial\lambda}{\partial x}\right.\\&+Z\left\{2k'^2\frac{\mathrm{sn}\,u\,\mathrm{dn}\,u}{\mathrm{cn}^3u}\right\}\left(\frac{du}{d\lambda}\right)^2\frac{\partial\lambda}{\partial x}\frac{\partial\lambda}{\partial Z}\\&\left.+Z\left\{k'^2\frac{\mathrm{sn}^2u}{\mathrm{cn}^2u}\right\}\left\{\frac{d^2u}{d\lambda^2}\frac{\partial\lambda}{\partial x}\frac{\partial\lambda}{\partial Z}+\frac{du}{d\lambda}\frac{\partial^2\lambda}{\partial x\partial Z}\right\}+\right]\end{aligned}$$

$$\frac{\partial u_y}{\partial x} = \frac{8(1-2\nu)Ay}{a^3}\left\{\frac{\mathrm{sn}^2 u}{\mathrm{dn}^2 u}\right\}\frac{du}{d\lambda}\frac{\partial \lambda}{\partial x} + \frac{8AZ^2}{ab^2}\left[\left\{2k'^2\frac{\mathrm{sn}\,u\,\mathrm{dn}\,u}{\mathrm{cn}^3 u}\right\}\left(\frac{du}{d\lambda}\right)^2\frac{\partial \lambda}{\partial y}\frac{\partial \lambda}{\partial x} + \left\{k'^2\frac{\mathrm{sn}^2 u}{\mathrm{cn}^2 u}\right\}\left\{\frac{d^2u}{d\lambda^2}\frac{\partial \lambda}{\partial y}\frac{\partial \lambda}{\partial x} + \frac{du}{d\lambda}\frac{\partial^2 \lambda}{\partial y \partial x}\right\}\right]$$

$$\frac{\partial u_y}{\partial y} = \frac{8(1-2\nu)A}{a^3k^2k'^2}\left\{E(u) - k'^2u - \frac{k^2\,\mathrm{sn}\,u\,\mathrm{cn}\,u}{\mathrm{dn}\,u}\right\} + \frac{8(1-2\eta)Ay}{a^3}\left\{\frac{\mathrm{sn}^2 u}{\mathrm{dn}^2 u}\right\}\frac{du}{d\lambda}\frac{\partial \lambda}{\partial y} + \frac{8AZ^2}{ab^2}\left[\left\{2k'^2\frac{\mathrm{sn}\,u\,\mathrm{dn}\,u}{\mathrm{cn}^3 u}\right\}\left(\frac{du}{d\lambda}\right)^2\left(\frac{\partial \lambda}{\partial y}\right)^2 + \left\{k'^2\frac{\mathrm{sn}^2 u}{\mathrm{cn}^2 u}\right\}\left\{\frac{d^2u}{d\lambda^2}\left(\frac{\partial \lambda}{\partial y}\right)^2 + \frac{du}{d\lambda}\frac{\partial^2 \lambda}{\partial y^2}\right\}\right]$$

$$\frac{\partial u_y}{\partial Z} = \frac{8(1-2\nu)Ay}{a^3}\left\{\frac{\mathrm{sn}^2 u}{\mathrm{dn}^2 u}\right\}\frac{du}{d\lambda}\frac{\partial \lambda}{\partial Z} + \frac{8AZ}{ab^2}\left[\left\{2k'^2\frac{\mathrm{sn}^2 u}{\mathrm{cn}^2 u}\right\}\frac{du}{d\lambda}\frac{\partial \lambda}{\partial y} + Z\left\{2k'^2\frac{\mathrm{sn}\,u\,\mathrm{dn}\,u}{\mathrm{cn}^3 u}\right\}\left(\frac{du}{d\lambda}\right)^2\frac{\partial \lambda}{\partial y}\frac{\partial \lambda}{\partial Z} + Z\left\{k'^2\frac{\mathrm{sn}^2 u}{\mathrm{cn}^2 u}\right\}\left\{\frac{d^2u}{d\lambda^2}\frac{\partial \lambda}{\partial y}\frac{\partial \lambda}{\partial Z} + \frac{du}{d\lambda}\frac{\partial^2 \lambda}{\partial y \partial Z}\right\} + \right]$$

$$\frac{\partial u_Z}{\partial x} = \frac{8AZ}{ab^2}\left[-(1-2\nu)\left\{k'^2\frac{\mathrm{sn}^2 u}{\mathrm{cn}^2 u}\right\}\frac{du}{d\lambda}\frac{\partial \lambda}{\partial x} + Z\left\{2k'^2\frac{\mathrm{sn}\,u\,\mathrm{dn}\,u}{\mathrm{cn}^3 u}\right\}\left(\frac{du}{d\lambda}\right)^2\frac{\partial \lambda}{\partial x}\frac{\partial \lambda}{\partial Z} + Z\left\{k'^2\frac{\mathrm{sn}^2 u}{\mathrm{cn}^2 u}\right\}\left\{\frac{d^2u}{d\lambda^2}\frac{\partial \lambda}{\partial x}\frac{\partial \lambda}{\partial Z} + \frac{du}{d\lambda}\frac{\partial^2 \lambda}{\partial x \partial Z}\right\}\right]$$

$$\frac{\partial u_z}{\partial z} = \frac{8(1-2\nu)A}{ab^2}\left\{E(u) - \frac{\operatorname{sn} u \operatorname{dn} u}{\operatorname{cn} u}\right\}$$
$$\frac{8(1+2\nu)AZ}{ab^2}\left[\left\{k'^2 \frac{\operatorname{sn}^2 u}{\operatorname{cn}^2 u}\right\}\frac{du}{d\lambda}\frac{\partial\lambda}{\partial Z}\right.$$
$$+ Z\left\{2k'^2 \frac{\operatorname{sn} u \operatorname{dn} u}{\operatorname{cn}^3 u}\right\}\left(\frac{du}{d\lambda}\right)^2\left(\frac{\partial\lambda}{\partial Z}\right)^2$$
$$\left. + Z\left\{k'^2 \frac{\operatorname{sn}^2 u}{\operatorname{cn}^2 u}\right\}\left\{\frac{d^2u}{d\lambda^2}\left(\frac{\partial\lambda}{\partial Z}\right)^2 + \frac{du}{d\lambda}\frac{\partial^2\lambda}{\partial Z^2}\right\}\right]$$

To calculate these derivatives, some additional partial derivatives of $\lambda$ need to be calculated. These are given by

$$\frac{\partial^2\lambda}{\partial x \partial Z} = \frac{xZ}{4\left(h_1^2\right)^2\lambda\left(a^2+\lambda\right)}\left[-\frac{1}{\lambda} - \frac{1}{a^2+\lambda} + \frac{1}{2h_1^2}\left\{\frac{x^2}{\left(a^2+\lambda\right)^3} + \frac{y^2}{\left(b^2+\lambda\right)^3} + \frac{Z^2}{\lambda^3}\right\}\right],$$

$$\frac{\partial^2\lambda}{\partial x^2} = \frac{1}{2\left(a^2+\lambda\right)H_1^2}\left[1 - \frac{x^2}{\left(a^2+\lambda\right)^2 H_1^2} + \frac{x^2}{4\left(a^2+\lambda\right)H_1^4}\left\{\frac{x^2}{\left(a^2+\lambda\right)^3} + \frac{y^2}{\left(b^2+\lambda\right)^3} + \frac{Z^2}{\lambda^3}\right\}\right],$$

$$\frac{\partial^2\lambda}{\partial y^2} = \frac{1}{2\left(b^2+\lambda\right)H_1^2}\left[1 - \frac{y^2}{\left(b^2+\lambda\right)^2 H_1^2} + \frac{y^2}{4\left(b^2+\lambda\right)H_1^4}\left\{\frac{x^2}{\left(a^2+\lambda\right)^3} + \frac{y^2}{\left(b^2+\lambda\right)^3} + \frac{Z^2}{\lambda^3}\right\}\right],$$

and

$$\frac{\partial^2\lambda}{\partial Z^2} = \frac{1}{2\lambda H_1^2}\left[1 - \frac{Z^2}{\lambda^2 H_1^2} + \frac{Z^2}{4\lambda H_1^4}\left\{\frac{x^2}{\left(a^2+\lambda\right)^3} + \frac{y^2}{\left(b^2+\lambda\right)^3} + \frac{Z^2}{\lambda^3}\right\}\right].$$

For vertical fractures that are taller than they are long, the normal tilt is given by interchanging a and b (essentially switching the length and the height) and using $\partial u_Z/\partial x$. The parallel tilt is given by $\partial u_y/\partial x$.

For fractures with dip, it is necessary to rotate the displacement gradients into the correct orientation and it is necessary to find the correct spatial parameters. Considering the transformation first, **Figure 34** shows the fracture with dip and the observation well and a rotated view of this geometry. It is observed that the two displacements of interest, the one normal to the fracture ($u_n$) and the one parallel to the fracture ($u_p$) are given by

$$u_n = u_Z \cos\gamma + u_y \sin\gamma$$

$$u_p = u_x \ ,$$

where $\theta$ is the angle of the fracture plane referenced to the vertical (*e.g.*, zero is a vertical fracture). The tiltmeter array measures the variation of the displacement derivatives along the s direction,

$$\frac{\partial u_n}{\partial s} = \frac{\partial u_n}{\partial Z}\frac{dZ}{ds} + \frac{\partial u_n}{\partial y}\frac{dy}{ds}$$

and

$$\frac{\partial u_p}{\partial s} = \frac{\partial u_p}{\partial Z}\frac{dZ}{ds} + \frac{\partial u_p}{\partial y}\frac{dy}{ds}.$$

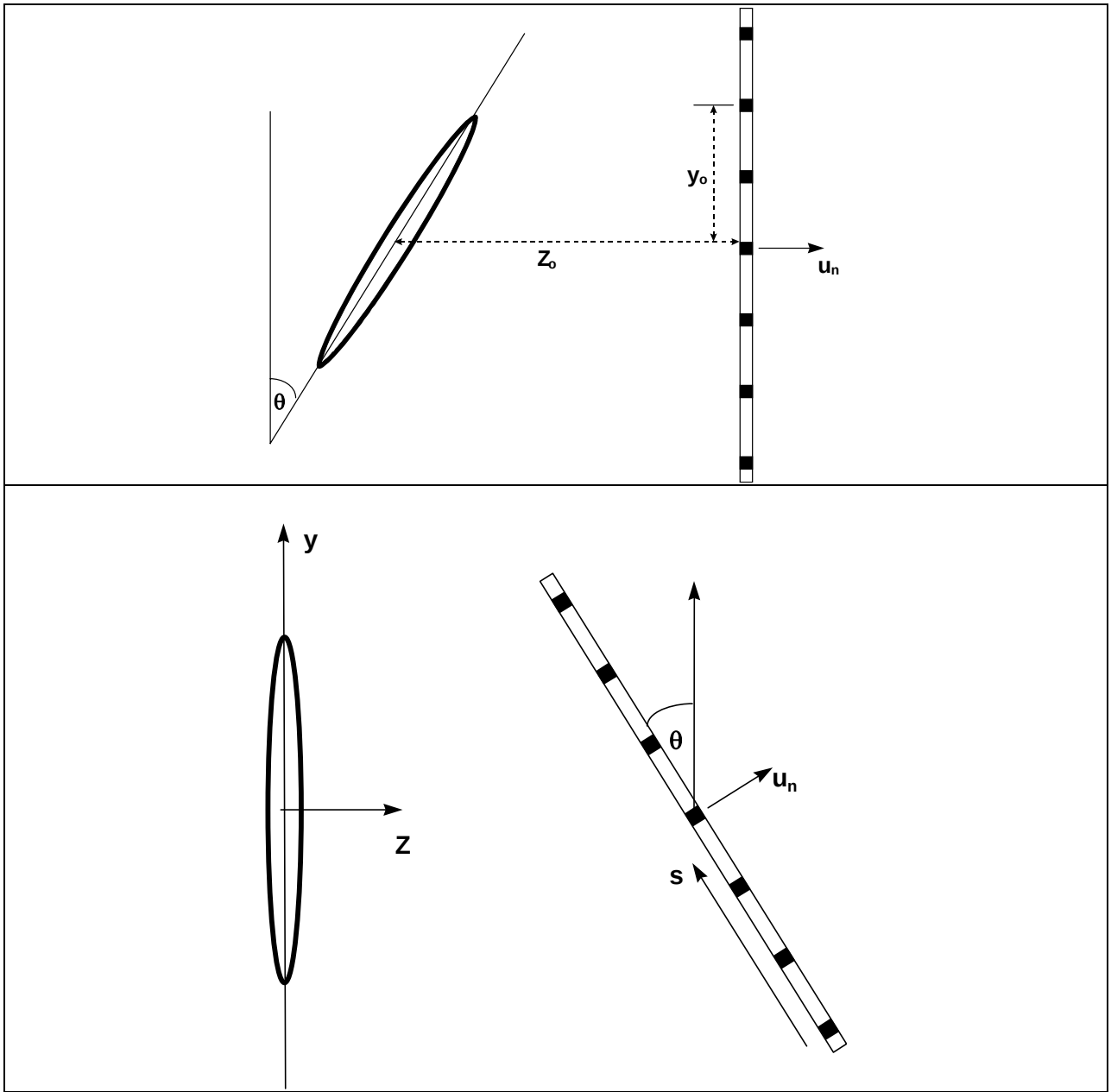


**Figure 34. Geometry for fracture with dip**

Since the two spatial derivatives are given by

$$\frac{dZ}{ds} = -\sin\gamma$$

and

$$\frac{dy}{ds} = \cos\gamma$$

the tilt derivatives can be reduced to

$$\frac{\partial u_n}{\partial s} = \sin\gamma\cos\gamma\left[-\frac{\partial u_Z}{\partial Z} + \frac{\partial u_y}{\partial y}\right] - \sin^2\gamma\frac{\partial u_y}{\partial Z} + \cos^2\lambda\frac{\partial u_Z}{\partial y}$$

and

$$\frac{\partial u_p}{\partial s} = -\sin\gamma\frac{\partial u_x}{\partial Z} + \cos\gamma\frac{\partial u_x}{\partial y}\ .$$

If the fracture is taller than it is long, then a and b should be switched and the appropriate derivatives are

$$\frac{\partial u_n}{\partial s} = \sin\gamma\cos\gamma\left[-\frac{\partial u_Z}{\partial Z} + \frac{\partial u_x}{\partial x}\right] - \sin^2\gamma\frac{\partial u_x}{\partial Z} + \cos^2\gamma\frac{\partial u_Z}{\partial x}$$

and

$$\frac{\partial u_p}{\partial s} = -\sin\gamma\frac{\partial u_y}{\partial Z} + \cos\gamma\frac{\partial u_y}{\partial x}\ .$$

The final issue is the correct geometric parameters to characterize the distance from the fracture to the tiltmeters. Referring to the unrotated schematic at the top of **Figure 34**, it can be found from geometry considerations that

$$\hat{x} = x$$

$$\hat{y} = Z_o\sin\gamma + y_o\cos\gamma$$

and

$$\hat{Z} = Z_o\cos\gamma - y_o\sin\varphi\ ,$$

where the variables with hats are the correct distances to use in the analysis. Of course, if the fracture is taller than it is long, then the x and y variable need to be reversed so that

$$\hat{x} = Z_o\sin\gamma + x_o\cos\gamma$$

$$\hat{y} = y\ ,$$

where the vertical distance from the crack centerline to the tiltmeter of interest is now $x_o$.

These equations complete the analysis of downhole tilt data for any fracture of any geometry, as long as it is far from the free surface.

### D. Microseismic Model

For this initial development, the microseismic events are assumed to be normally distributed in some sensible manner about the fracture. If true, then they should have some characteristic height and length that are functions of the actual fracture height and length, an overall azimuth and dip that is consistent with the actual fracture, and an edge-on distribution that envelopes the fracture (assuring that the microseismic events are at the right distance).

Starting with 3D locations obtained from the current velocity model, the (x, y) coordinates are then used to determine the microseismic azimuth from directional statistics, and from this azimuth, edge ($b_i$) and side ($r_i$) projections are obtained. The dip is obtained from the edge projection, again using circular statistics and the side projection data provide means and variances of the event locations for height and length calculations. From this approach, an azimuth, a dip, an average center depth, characteristic length parameters, and characteristic height parameters can be extracted from the microseismic data.

The terms characteristic length and height parameters refer to the variances of those values. If the fracture is symmetric (assumed here), then the average projected horizontal distance of the microseismic events from the treatment well will be zero (equal distribution on both sides of the well). Similarly, an edge-on projected distribution will have a zero mean (if centered on the well). The vertical event locations will be distributed about the center depth of the fracture.

What is needed however is some way to relate the standard deviation of event distances to the fracture length and the standard deviation of event depths (about the center) to the fracture height. Preliminary testing has shown that characteristic heights and lengths that are about 60% of the actual height and length provide microseismic distributions that mirror actual distributions. However, this may not be a general rule and will require continual testing.

A second aspect of the distribution is the potential that the velocity structure is not correct and the events are not centered in any way on the actual treatment well. This is handled by assuming that there is a virtual wellbore at a point where the perpendicular line to the fracture azimuth which runs through the actual wellbore intersects the fracture azimuth line. This point is well defined by the data and the well location.

Given all of this information, a probability for that event location based on height, length, azimuth, and dip can be obtained from

$$P(x_i, y_i, z_i) = \frac{1}{\sqrt{2\pi}\sigma_z}\exp\left[\frac{-(z_i - z_c)^2}{2\sigma_z^2}\right] \cdot \frac{1}{\sqrt{2\pi}\sigma_r}\exp\left[\frac{-(r_i - r_c)^2}{2\sigma_r^2}\right] \cdot \frac{1}{\sqrt{2\pi}\sigma_b}\exp\left[\frac{-(b_i - b_c)^2}{2\sigma_b^2}\right]$$

where $z_c$, $r_c$, and $b_c$ are the means and $\sigma_z$, $\sigma_r$, and $\sigma_b$ are the standard deviations of the distributions vertically, along the side projection, and along the edge projection, respectively, and the three separate variables are assumed to be independent.

There are actually two probabilities required for each event. The first is the probability of the event location relative to the "model" and the second is the probability of the event location relative to the event distribution. If the difference in these two probabilities is zero, then the model is perfectly aligned with the event data and accurately represents the microseismic data. In general there will always be differences and the goal is to minimize these differences in some least square approach.

### E. Inversion Process

The inversion process is one that has previously been used to invert tiltmeter data alone, but has now been modified to add microseismic distribution data. Essentially, the tilt distribution as a function of the vertical sensor location ($z$) is given as

$$\frac{\partial u}{\partial z}(z) = F\left(h, L, \Delta P, y_c, \alpha_f, \delta_f, w_{dis}, E, \nu\right) ,$$

where $h$ is the fracture total height, $L$ is the wing length (symmetry is assumed), $\Delta P$ is the net pressure, $y_c$ is the vertical depth to the center of the fracture, $\alpha_f$ is the azimuth of the fracture relative to the monitoring position, $\delta_f$ is the inclination of the fracture (complement of the dip), $w_{dis}$ is the separation between the monitor well and the injection well, $E$ is Young's modulus, and $\nu$ is Poisson's ratio. The geometric parameters are shown in **Figure 35**. It is generally expected that $w_{dis}$, $E$, and $\nu$ are known and these are not usually free parameters in the inversion. The sense of $\alpha_f$ is such that a fracture azimuth normal to the line between the monitor and injection wells is 0° while a fracture directly approaching the monitor well is 90°. Any of the first six parameters may be known and used as constraints on the results. To facilitate the inversion, all of the free parameters are mapped onto the real axis, but this is more of a convenience than a necessity.

The Levenberg/Marquardt algorithm seeks to minimize the function

$$G = \sum_n \left\{ \left.\frac{\partial u}{\partial z}\right|_{calc} - \left.\frac{\partial u}{\partial z}\right|_{obs} \right\}^2$$

in an efficient manner by determining optimum values of the unknown parameters. $n$ is the number of tilt observations. The formulation for a dislocation model would be the same, except that the dislocation opening, $b$, would be used instead of the crack internal pressure, $\Delta P$.

The microseismic event locations, both because of the nature of the microseismic origins and ubiquitous noise, are distributed in some manner about a fracture length, height, azimuth, and dip. The microseismic distribution can be added into this formulation by minimizing the difference between the observed distribution about the model and the expected distribution about the model, as characterized by the self-distribution of events as described above. In this way, the function to be minimized can be written as

$$G = \sum_n \left\{ \left.\frac{\partial u}{\partial z}\right|_{calc} - \left.\frac{\partial u}{\partial z}\right|_{obs} \right\}^2 + W_m \sum_m \left\{ P_{expected}\left(x_i, y_i, z_i\right) - P_{obs}\left(x_i, y_i, z_i\right) \right\}^2$$

where $W_m$ is a weighting function that can be used to increase or decrease the effect of the microseismic data.

Besides the model parameters for the tiltmeter data, the microseismic data now includes the effect of velocities, which can also be extracted from the inversion. To extract the velocities, however, it is also necessary to have a location algorithm in the inversion. Assuming the arrival times and azimuths are correct, then a velocity can also be found which allows the microseismic and tiltmeter data to optimally match. For the case of a constant velocity structure, the location algorithm can be a simple regression on the distance equation. For a more complex velocity structure, a forward model and grid-search algorithm is applied to obtain the re-located points. In such a case, it is necessary to invert for all of the velocities.

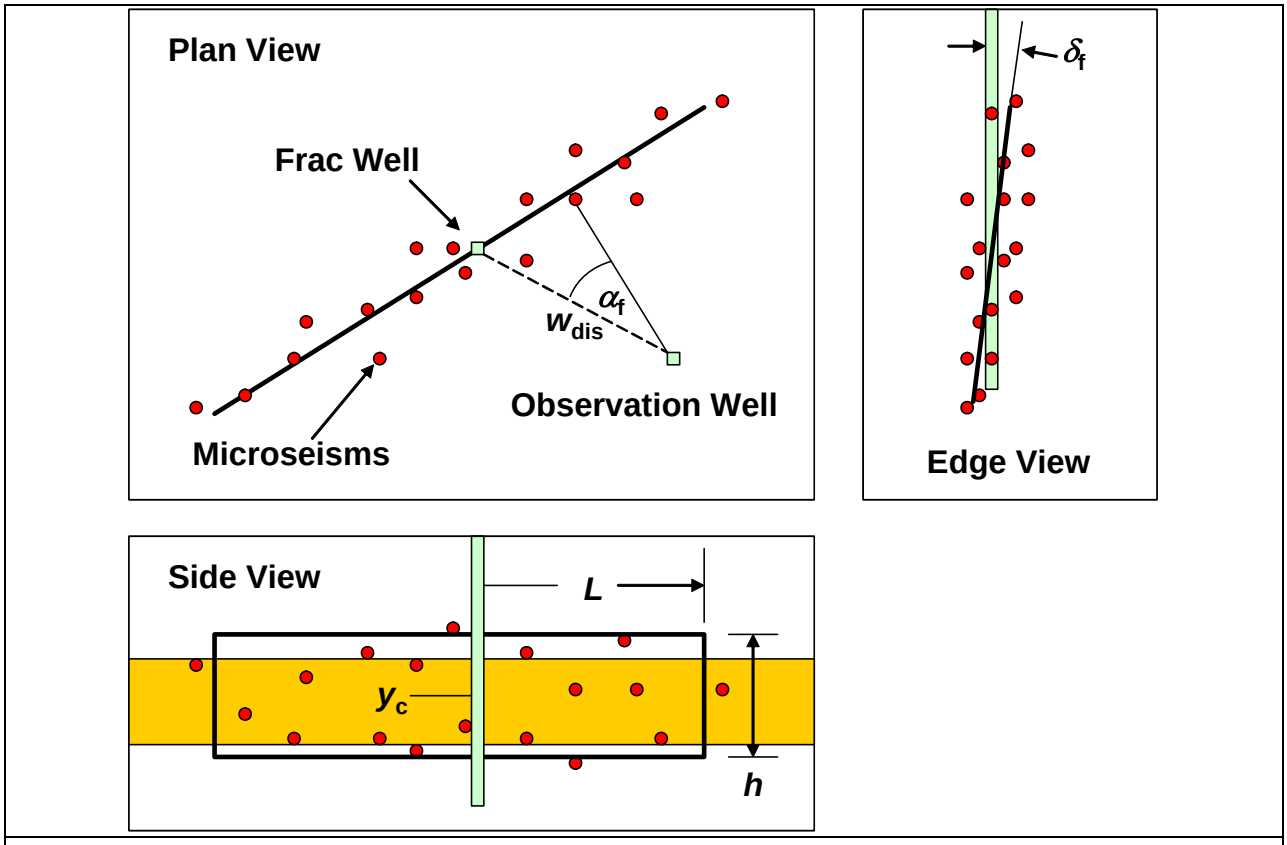


**Figure 35. Geometry of fracture model Inversion**

Using a probability function for the microseismic data is not intended to imply any particular geophysical behavior, but rather it is simply a convenient method for: (1) assessing whether a microseismic event fits the current model parameters, (2) treating the microseismic data like a true distribution with outliers, and (3) developing an efficient function to be minimized jointly with the tiltmeter data.

### F. Example Synthetic Data Set

The example synthetic data set is for a fracture 250 ft in wing length, 80 ft in height, pressurized at 500 psi and monitored from a well 500 ft away, directly normal to the fracture. The Young's modulus is 4,000,000 psi and Poisson's ratio is 0.2. The fracture azimuth is N45°E and is centered at 5,000 ft. For this initial test, it is assumed that the velocities are correct and the microseismic data are accurate. **Figure 36** shows this geometry.

There are 100 microseismic data points with random error of ± 20 ft and 20 tiltmeter measurements that are exact. The microseismic locations were used to extract directional statistics with a length standard deviation of 157 ft, a half-height standard deviation of 22.3 ft, and an edge standard deviation of 12.6 ft.

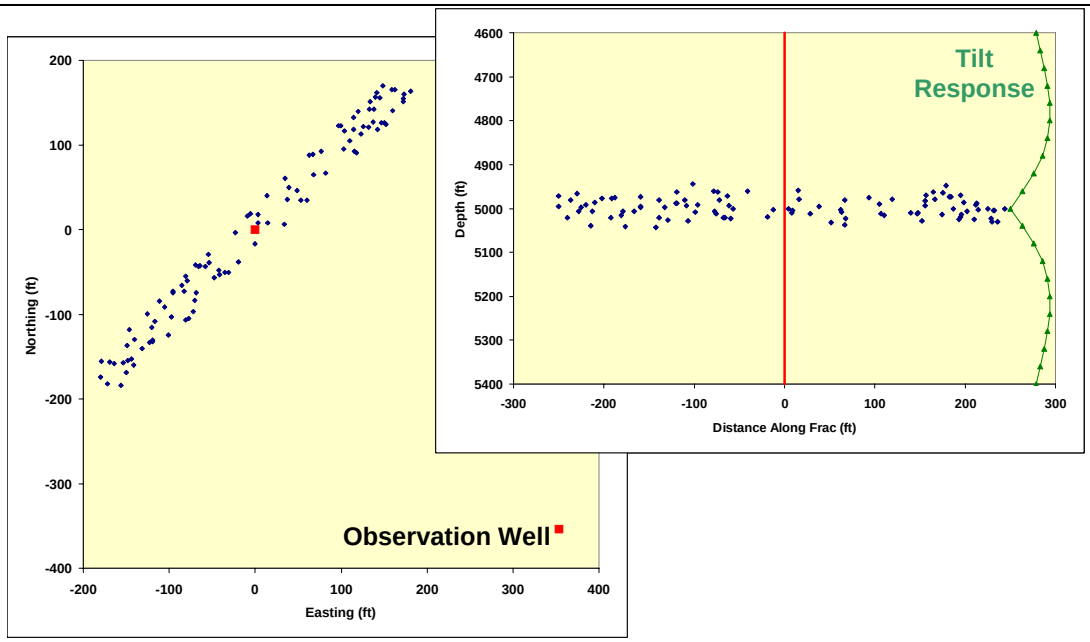


**Figure 36. Synthetic data set for testing joint inversion**

Using an equal weighting on the microseismic probability, the inversion quickly arrived at the following results:

| | |
|---|---|
| Length | 252.8 |
| Height | 71.5 |
| Azimuth | -0.3° |
| Dip | 0.4° (from vertical) |
| Pressure | 617 psi |
| Center | 4998.4 |

With the exception of the pressure, all of the results are very close to the synthetic fracture from which they were derived. If the weighting is changed so that it is 2 orders of magnitude weighted towards the microseismic data, then the inversion returns the microseismic statistics (with no realistic pressure and possible problems with dip). If the weighting is changed so that it is 2 orders of magnitude weighted towards the tiltmeters, then the inversion returns the tiltmeter results. However, it has trouble getting only tiltmeter results because there are so many free parameters (with a little noise, it probably would not find the solution). With both data sets, however, the inversion is extremely stable and all parameters appear to be derived with ease. In addition, we can look at various weightings and develop some uncertainty estimates based on those weightings (grading from all tiltmeters, to both, to all microseisms), as well as added value with the additional array.

A more instructive example is to take the input data shown in **Figure 36**, mislocate it by applying the wrong velocity, and then invert the mislocated data. **Figure 37** shows the mislocated microseismic data (left) and the locations recovered after the inversion (right). **Table 1** shows a comparison of the model values and the recovered inverted parameters. In this example, the pressure and dip are assumed known (applied constraints) and the velocity model is constant, so only one of the two velocities can be found (*e.g.*, the location depends upon $V_pV_s/\{V_p\text{-}V_s\}$). The advantage of having some tiltmeter data is that it can be used to improve the microseismic locations. Similarly, some microseismic locations can help to improve the results from noisy tiltmeter data. If no constraints were used in this example, the results would have been $h$=71.6, $L$=253, $\Delta P$=614, azimuth=45°, dip=3.1°, center depth=4998.3, and $V_p$=15,020 ft/sec, which are fairly accurate results, but nevertheless show the value of having some information on which to ground the inversion.

**Table 1. Synthetic Inversion Results**

| Parameter | Model | Inverted |
|---|---|---|
| Length (ft) | 250 | 252 |
| Height (ft) | 80 | 79.7 |
| Center Depth (ft) | 5000 | 4999.5 |
| Azimuth (deg) | 45 | 45 |
| $V_p$ (ft/sec) | 15,000 | 15,010 |
| $V_s$ (ft/sec) | 8,000 | NA |
| Pressure (psi) | 500 | NA |
| Dip (deg) | 0.0 | NA |

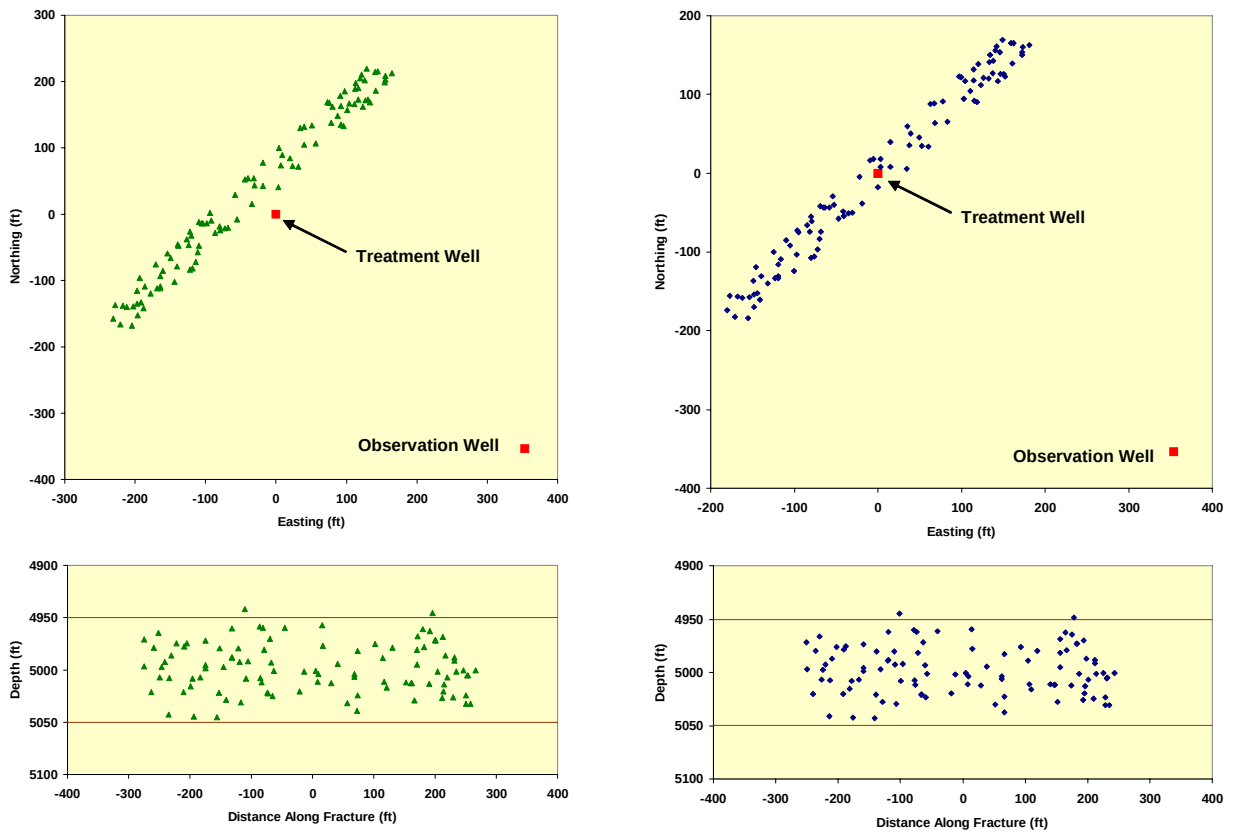


**Figure 37. Mislocated and inverted event locations for velocity case**

## G. M-Site Example

Perhaps the best test case for a combined microseismic and tiltmeter data set is the data from the DOE & GRI sponsored M-Site experiments.[8] At M-Site, both tiltmeters (6 levels) and tri-axial accelerometers (30 levels) were cemented in a monitor well approximately 300 ft from a series of fractures conducted in two intervals. The geologic setting is a fluvial environment, in which comprehensive fracturing experiments were carried out in two intervals. The test zone of interest for this evaluation was labeled the "B" sandstone at a depth of approximately 4,525 to 4,560 ft.[9-11]

Numerous injections were performed in the B sandstone, with one particular minifrac providing a good data set for testing this approach. The minifrac was pumped at 22 bpm, injecting a total volume of 400 bbl of a 40-lb linear gel. During the test, over 100 microseisms were detected and located and excellent quality (high signal-to-noise-ratio) tiltmeter data were also obtained on all six tiltmeters.

**Figure 38** shows a plan view of the microseismic data and a side view of the combined microseismic and tiltmeter data, along with the theoretical tilts. Approximately 20 of the microseismic events are from a second monitor well that has a 5-level wireline receiver array. For this case, the microseismic locations are assumed to be correct, so the inversion provides a fracture geometry that gives a best-fit of the microseismic distribution with the measured tilts. However, the wide distribution of microseismic events does not lend itself to useful evaluation of the dip, so the dip was constrained to a vertical fracture (known from the testing). The bottomhole pressure was also measured and used as a constraint (1,300 psi).

**Table 2** gives a comparison of the joint inversion results compared to the previous reported results for individual technologies. The original tiltmeter results used an analytic model with homogeneous formation properties,[9] whereas the original FE (finite element) results used variable layer properties.[11]

The major difference in the various results lies primarily in the height estimates. A combined analysis yields a height that is somewhat greater than the height estimates from separate measurement techniques. When combined, the requirements of matching azimuth and center position, as well as length and height, require a greater height to best fit all of the data, subject to the constraints as well as the weighting and other factors (that is, the microseismic distribution suggests a higher center whereas the tiltmeters suggest a lower center).

Weighting is an issue that is still being investigated, as it plays a significant role in the type of results obtained. A small microseismic weighting produces an azimuth that is oriented closer to the observation well and a somewhat smaller fracture height, yielding a better fit of the tilt data. A larger microseismic weighting (as used here) fits the microseismic events better and matches the event azimuth, but the fit of the tilt data is somewhat weaker. Interestingly, the primary difference observed by changing the weighting is a rotation of the fracture azimuth. In this case, the fracture azimuth is known precisely from core-through tests, so a weighting that matched the known azimuth was preferred. Alternately, the same results could be obtained by using an azimuth constraint.

**Table 2. M-Site B Sandstone Comparison**

| Parameter | Original μseismic | Original Tiltmeter | Original FE Tilt | Joint Inversion |
|---|---|---|---|---|
| Center (ft) | NA | NA | 4542 | 4547 |
| Height (ft) | 80±20 | 67 | 75-80 | 94.9 |
| Length (ft) | 230/375 W/E | 425 | NA (2D) | 327.4 |
| Azimuth | N74W | NA | NA | N74W |
| Dip | NA | 0° fixed | 0° fixed | 0° fixed |
| Press. (psi) | NA | 1300 | 1300 | 1300 |

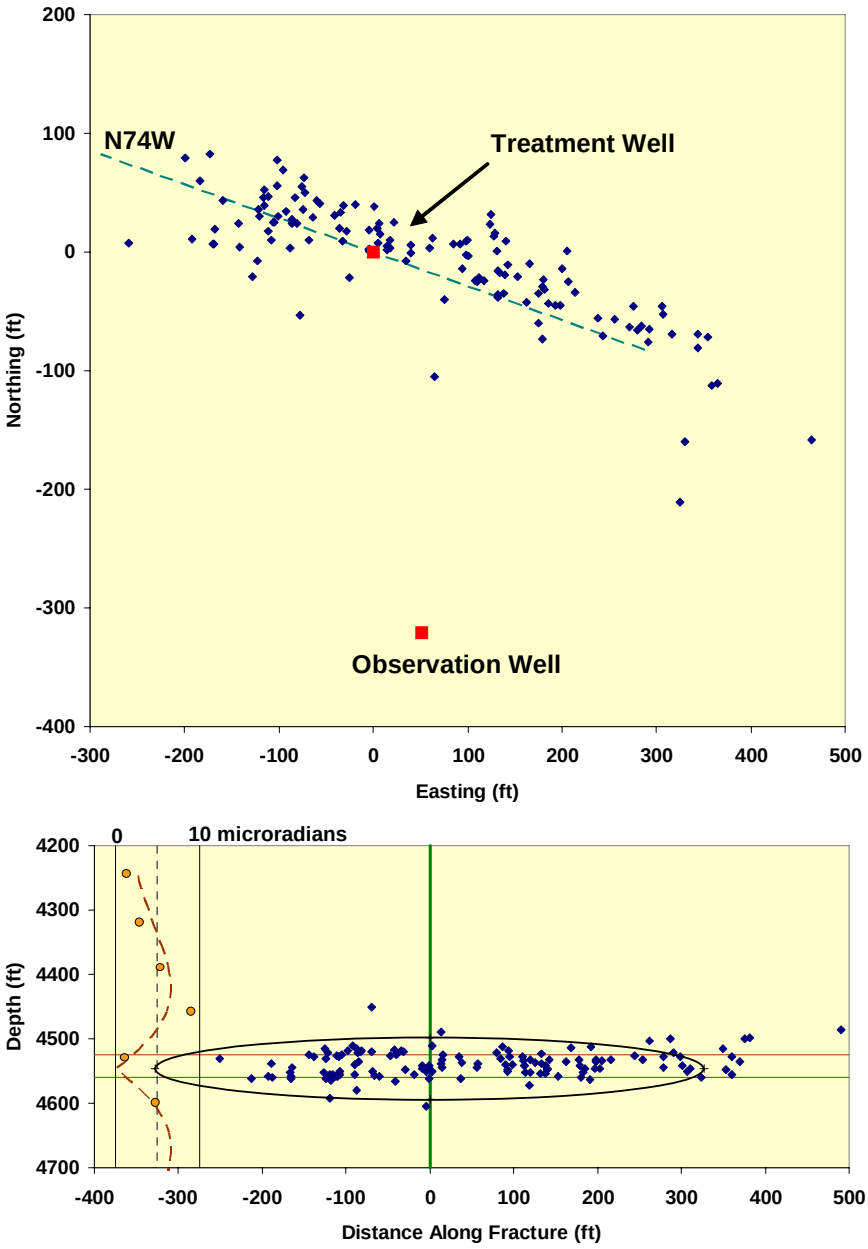


**Figure 38. Microseismic and tiltmeter data from M-Site with inverted results**

Taking the process one step farther, the microseismic data can be re-located as part of the inversion process. However, only the events from the cemented receivers are used in this analysis, since the large number of arrivals makes these data considerably more accurate. The original location analysis at M-Site used a constant velocity medium because of the fluvial environment and the large number of receivers (velocity effects wash out).[10] In a homogeneous velocity medium, only one of the velocities is independent, so the P-wave velocity was taken as a constraint at $V_p$ = 15,000 ft/sec and the S-wave velocity was determined in the inversion. **Figure 39** shows a plan-view and side-view map of the microseismic locations and the tiltmeter fit for the re-location case.

The results are very similar to those shown in **Figure 38** (although there are fewer events), with the primary difference being some additional estimated length. The final results are a N72°W azimuth, $L$ = 400 ft, $h$=89 ft, and center at 4,548 ft. The S-wave velocity was found to be 8,600 ft/sec, compared to the original 8,750 ft/sec.

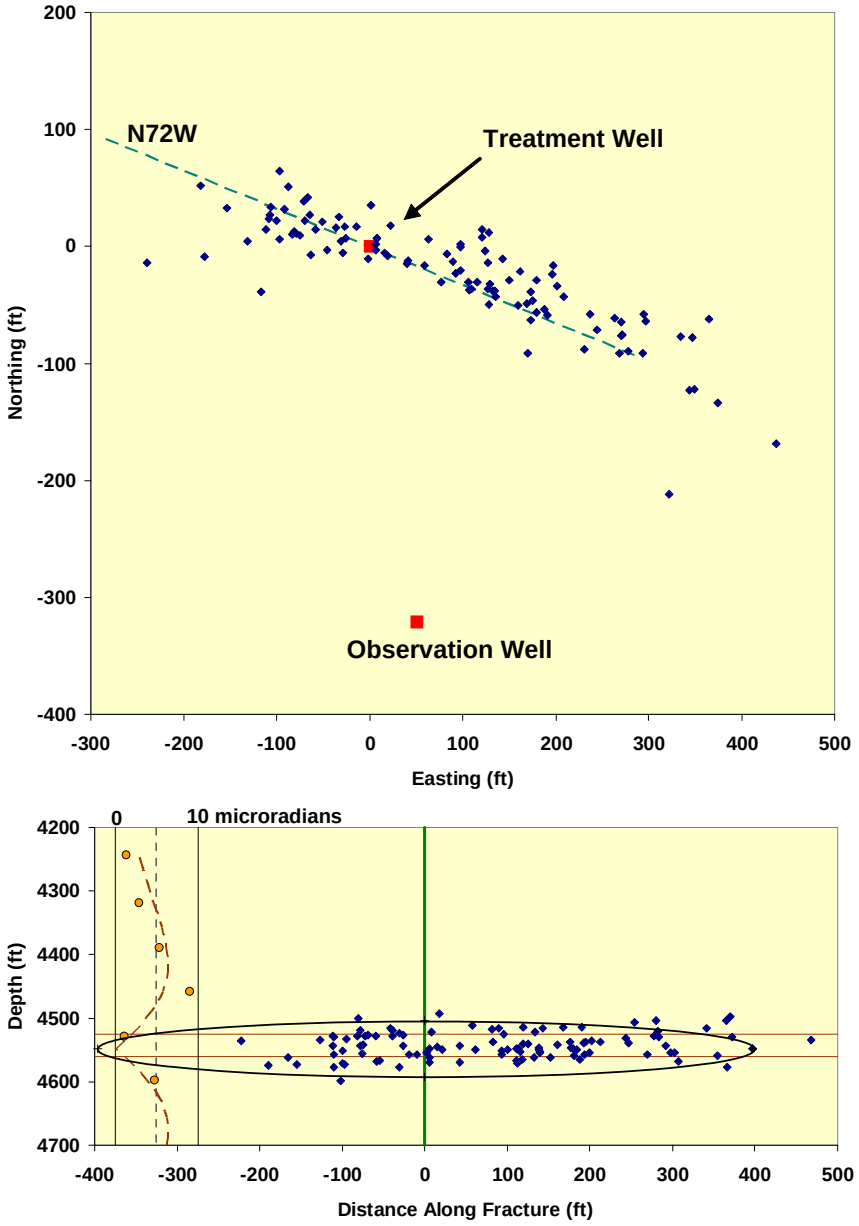


**Figure 39. Microseismic and tiltmeter data from M-Site with inverted results with velocity**

### H. Mounds Drill Cutting Injection Experiment Example

The Mounds Drill Cuttings Injection Experiment[12,13] was another test in which both microseismic and tiltmeter data were obtained.[14-16] Experiments at this site simulated the behavior expected to occur in

repeat injections of solid-loading slurries into various formations for disposal of drill cuttings. A series of small injections (50 to 100 bbl) were performed in two different intervals, but the one of interest here is the Atoka Shale.

Monitoring of the Atoka Shale injections, into a perforated interval at 1,940 to 1,960 ft depth, was performed with an 8-level tiltmeter array in an observation well at a distance of 140 ft and with a 5-level microseismic array at a distance of 250 ft. However, the microseismic data was very sparse in the Atoka tests, so most of the inferences about fracture geometry were made from the downhole tiltmeters or from a surface tiltmeter array.

There were 20 injections into the Atoka Formation over a three-day period and the fifth injection was chosen as one having good quality tiltmeter data. Additionally, since this injection was early in the overall testing, it is not expected that there was too much complexity yet due to the development of a disposal domain.

**Figure 40** shows the plan-view and side-view maps of the inversion results, assuming the microseismic data are located correctly. During the whole first day of testing in the Atoka (eight injections) there were only about a dozen microseisms observed. However, the downhole tiltmeters had responses as large as 50 microradians and the surface tiltmeters also obtained good quality data.

Constraints on the inversion included a measured net pressure of 425 psi and a vertical fracture. The microseismic data were highly weighted so that the inverted azimuth approximately matched the azimuth derived from the microseism, which were weak by themselves, but matched the azimuth measured by surface tiltmeters. **Table 3** shows a comparison of the results from this joint inversion with previously reported data. The main effect of the joint inversion is to allow the fracture to shift up or down, although this does depend to some extent on how highly the microseismic data are weighted (a small weighting yields a deeper center location).

There was no attempt made to relocate the microseismic data in this example since it was so sparse of a data set. Note that the limited microseismic data do not match the tiltmeter geometry very well, but these few events are actually taken from all of the eight injections on that day and are used primarily for azimuth and also for some general control of height and length.

**Table 3. Comparison of Mounds Atoka Results**

| Parameter | Original Tilt | Alternate Tilt | Joint Inv. |
|---|---|---|---|
| Center (ft) | 1974 | 1914 | 1935 |
| Length (ft) | 239.5 | 173 | 165 |
| Height (ft) | 79.6 | 101 | 116 |
| Azimuth (deg) | N73W | N75W | N71W |
| Dip (deg) | 1° | 0° (fixed) | 0° (fixed) |

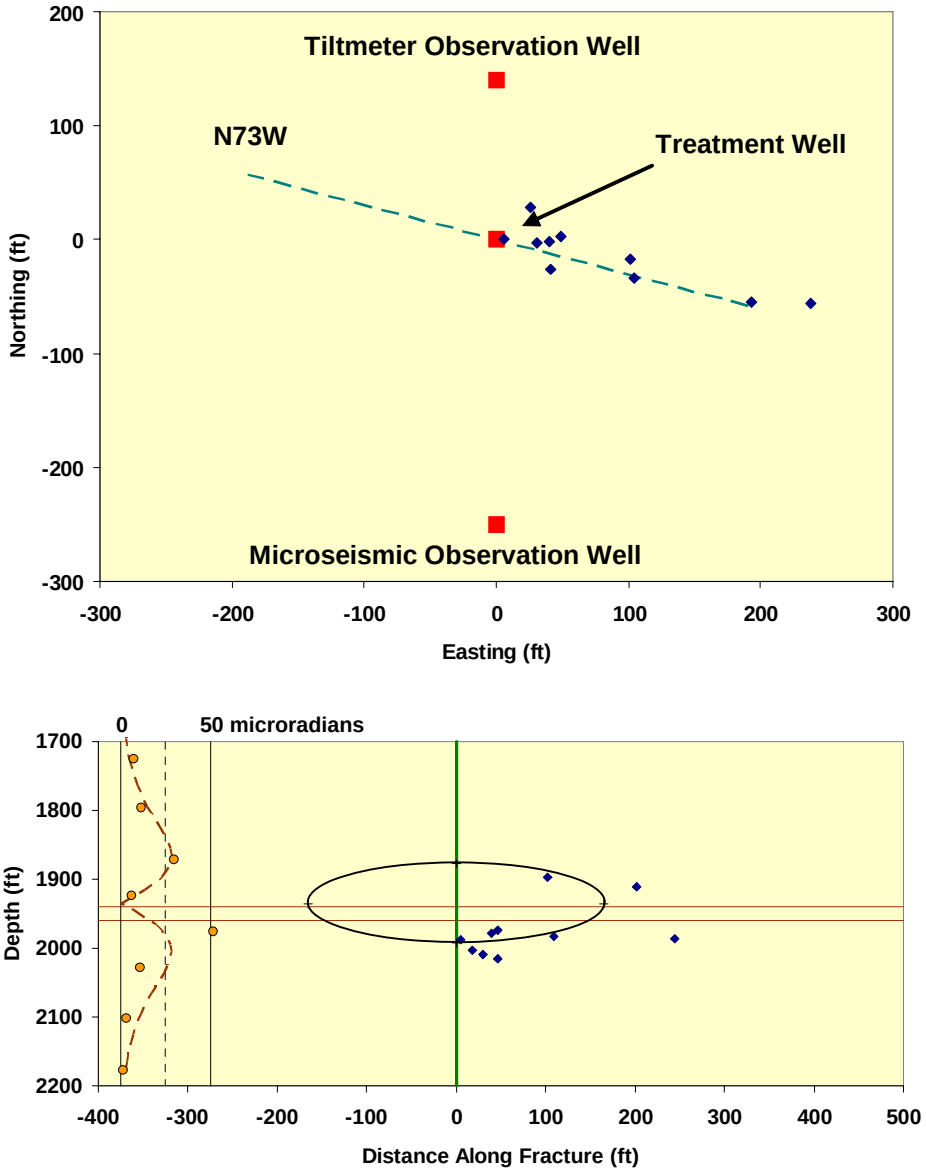


**Figure 40. Mounds Atoka fracture inversion with poor microseismic data**

### 3.6.2 Uncertainty Analysis

In order to develop joint analysis techniques for microseismic and tiltmeter mapping, it is helpful to have methods to assess uncertainty of the measurements. For microseismic mapping, the uncertainty can be determined explicitly if the formation has a constant velocity. However, for real-world problems where there is a significant velocity structure that cannot be ignored in analysis, the determination of uncertainty is not easily determined. The problem occurs because the determination of microseismic event locations in a non-homogeneous velocity structure is solved using a grid search routine that compares the observed travel times with calculated travel times for the given velocity structure (*e.g.*, Vidale[17] and Nelson and Vidale[18]). The approach is simple and extremely effective, in that it is guaranteed to always find the

absolute best-fit point, but it is not conducive to generating information on errors. In fact, the current accepted approach to error analysis is a Monte Carlo technique that would be much too cumbersome for practical application.

However, a method has been devised to take the grid-search results and estimate the standard errors of the grid-search location procedure using a modification of the approach that results from analysis in a homogeneous formation. Initial tests of the approach show reasonable agreement with test cases developed to assess the error.

In examining uncertainty in microseismic locating, it has always been expected that the size of the total residual (misfit or difference between observed and calculated times) is a qualitative representation of the standard error and hence can be used for uncertainty estimates. However, previous studies show that under controlled conditions (*e.g.*, for a constant velocity model), the residual of the best-fit location provides a gross over-estimate of the positional uncertainty. A current hypothesis is that most of the residual is due to the uncertainty in the origin time and the positional uncertainty is only a small fraction of that number. Thus, the problem now is to figure out some straightforward way to estimate positional uncertainty given the non-usability of the residual.

A significant effort was spent examining the residuals as a function of position and origin time, and numerous test cases were constructed to see if there was some obvious way to partition the residual into an origin-time component and a positional component. The information that is available includes the solution location ($t_o$, $z_o$, and $r_o$), the calculated travel times for the best-fit point, the receiver locations, and the observed arrival times. No reliable relationships were found between any combinations of these from which positional uncertainty could be derived.

One possible solution, however, is to take a similar approach as that obtained in the regression solution where accurate errors and uncertainties can be established. For background, the error analysis for the regression is shown and then the modification of that approach is given. Finally, some results follow.

### A. Constant Velocity Model

The location analysis for a constant velocity model uses a joint p-s regression to calculate the elevation of and distance to the microseism. It starts with the equations for distance squared in order to get rid of the square root, giving a P-wave equation,

$$V_p^2\left(t_{pi}-t_o\right)^2=\left(r_o\right)^2+\left(z_i-z_o\right)^2\ ,$$

and an S-wave equation,

$$V_s^2\left(t_{si}-t_o\right)^2=\left(r_o\right)^2+\left(z_i-z_o\right)^2\ ,$$

where the $V_p$ and $V_s$ are the P- and S-velocities, $r$ refers to the horizontal distance, $z$ refers to the elevation, $t$ is the time, the subscript "$o$" denotes the origin location and the subscript "$i$" denotes the i$^{th}$ receiver. The equation to be minimized is a combination of the two of them,

$$F=w_p\sum_n\left[V_p^2\left(t_{pi}-t_o\right)^2-\left(r_o\right)^2-\left(z_i-z_o\right)^2\right]^2 + w_s\sum_m\left[V_s^2\left(t_{si}-t_o\right)^2-\left(r_o\right)^2-\left(z_i-z_o\right)^2\right]^2\ ,$$

The *n* and *m* variables are the numbers of P-wave and S-wave arrivals respectively. Variables $w_p$ and $w_s$ are weighting functions which can be used if one of the phases has less certainty than the other. The result of the minimization is the location coordinate, ($r_o$, $z_o$, $t_o$), which places the microseism in a two-dimensional vertical plane at the time the microseism occurred.

The solution of these equations for $r_o$, $z_o$, and $t_o$ is quite complicated, as all of the terms need to be multiplied out to extract and solve for the variables. However, this approach was chosen because it allows us to use any collection of P-wave and S-wave data that is available. It is not necessary to have both P- and S-data on the same level, nor is it even necessary to have any data from either phase (although there must be three arrival times to solve the equations). The second advantage to using this approach is that it lends itself to fast uncertainty analyses using standard regression methods. To use standard methods, however, it is first necessary to transform the regression equation to standard form. Given the following substitutions:

$$y_i = z_{pi}^2 - V_p^2 t_{pi}^2, \qquad \text{for P-waves;}$$

$$y_i = z_{si}^2 - V_s^2 t_{si}^2 + t_o^2\left(V_p^2 - V_s^2\right), \qquad \text{for S-waves;}$$

$$x_{1i} = z_{pi}\ , \qquad \text{for P-waves;}$$

$$x_{1i} = Z_{si}\ , \qquad \text{for S-waves;}$$

$$x_{2i} = V_p^2 t_{pi}\ , \qquad \text{for P-waves;}$$

$$x_{2i} = V_s^2 t_{si}\ , \qquad \text{for S-waves.}$$

The distance equation can now be written as

$$y_i = a_o + a_1 x_{1i} + a_2 x_{2i}\ ,$$

where

$$a_o = V_p^2 t_o^2 - r_o^2 - z_o^2\ ,$$
$$a_1 = 2z_o\ , \text{ and}$$
$$a_2 = -2t_0\ .$$

This equation is now in a standard format for multiple regression. Note that while this equation appears much easier to solve than the one actually used, it would require an iterative solution since $t_o$ is in the $y_i$ term. Thus the direct solution is preferred and is used in practice.

We can now take averages and normalize the equation to get

$$Y_i = a_1 X_{1i} + X_{2i}\ ,$$

where

$$\bar{x}_1 = \sum_j x_{1i}$$
$$\bar{x}_2 = j\sum_p x_{2i}$$
$$Y_i = y_i - a_o - a_1\bar{x}_1 - a_2\bar{x}_2$$
$$X_{1i} = x_{1i} - \bar{x}_1$$
$$X_{2i} = x_{2i} - \bar{x}_2$$

and j is the total number of arrival times in the regression. Since the variances of $a_1$ and $a_2$ are simple, *i.e.*,

$$S_{a1} = \frac{\sigma\sum_j X_{2i}^2}{\sum_j X_{1i}^2\sum_j X_{2i}^2 - \sum_j X_{1i}X_{2i}}$$
$$S_{a2} = \frac{\sigma\sum_j X_{1i}^2}{\sum_j X_{1i}^2\sum_j X_{2i}^2 - \sum_j X_{1i}X_{2i}}$$

with $\sigma$ being the deviations mean square,

$$\sigma^2 = \frac{\sum_p \left(Y_i - \hat{Y}_i\right)^2}{p-3} \ ,$$

and $\hat{Y}_i$ obtained from $X_{1i}$ and $X_{2i}$, the variance and/or standard deviations of $z_o$ and $t_o$ are found readily as

$$\sigma_{z_o} = \frac{1}{2}S_{a1}$$
$$\sigma_{t_o} = \frac{1}{2}S_{a2}$$

from the definitions of $a_1$ and $a_2$.

The determination of the variance of $r_o$ is considerably more difficult since the definition of $a_o$ involves several terms and squares of those terms. However, the equation can be re-setup as

$$y_i = V_{pi}^2\left(t_{pi} - t_o\right)^2 = r_o^2 + \left(z_{pi} - z_o\right)^2 = r_o^2 + x_i$$

for the P-wave, with a similar term for the shear wave. This can now be rewritten as a standard linear regression format,

$$y_i = \alpha + \beta x_i \ .$$

In this case, the variance of $\alpha$ is the variance of the $y_i$, so the $y_i$ can be used to estimate the variance of the square of $r_o$.

### B. Application to Vidale/Nelson Grid Search

The distance equation above is not suitable for the case with variable velocity structure because the travel path is actually an assemblage of travel paths through the different layers with different velocities. However, it seems reasonable to assume that for the case of mildly varying velocity structure, a velocity characteristic of each receiver-source pair can be used. In such a case, the calculated travel times and known distances can be used to extract "pseudo-velocities" as

$$\tilde{V}_{pi} = \frac{\sqrt{r_o^2 + (z_i - z_o)^2}}{t_{pi}^{calc}}$$

and

$$\tilde{V}_{si} = \frac{\sqrt{r_o^2 + (z_i - z_o)^2}}{t_{si}^{calc}} \ .$$

In addition to these pseudo-velocities, it is also necessary to calculate the squared sum of these velocities (for use with the $t_o$ terms).

After this calculation, the analysis is the same except that these new velocities are used. The results will be accurate for any constant-velocity analysis, should be reasonable for small velocity variations, and the only question is what happens when the velocity model has large contrasts.

Given the standard deviations for $r_o$ and $z_o$, the code then finds the time contour that best reflects these errors. In practice, the code finds the residual at four points ($+s_r$, $-s_r$, $+s_z$, and $-s_z$) and then uses the maximum of these to estimate the one standard deviation misfit contour. The difference between this misfit time and the minimum residual (that is, the one standard deviation residual for position) is used to determine the two and three standard deviation misfits. Each of these contours can then be plotted.

### C. Test Case

The synthetic test case that was used to evaluate the residuals in the first place was now used to see how the results would work. This case used a symmetric receiver array (12 levels), spaced 40 ft apart, with a source at a distance of 800 ft and located vertically in the center of the array. The P- and S-velocities are 15,000 ft/sec and 9,000 ft/sec. There is ±1 msec random error added to the calculated travel times.

Using the old formulation for error estimates, the total misfit residual was 0.598 msec and the contour out to twice this value extended many 10's of feet. The residual contours for this approach are shown in **Figure 41**. The contours extend out three standard deviations in the plot.

Using the new approach, the height error is 10.6 ft and the distance error is 8.6 ft. These numbers agree well with those obtained statistically (11.2 and 5.6) for 18 realizations, and those from the regression directly (10.6 and 8.6 also). Using these values, the one standard deviation positional misfit contour is 0.0036 msec greater than the residual, a far cry from the 0.598 msec greater that would come from assuming that the residual is representative of the positional error. **Figure 42** shows the misfit contours out to three standard deviations now.

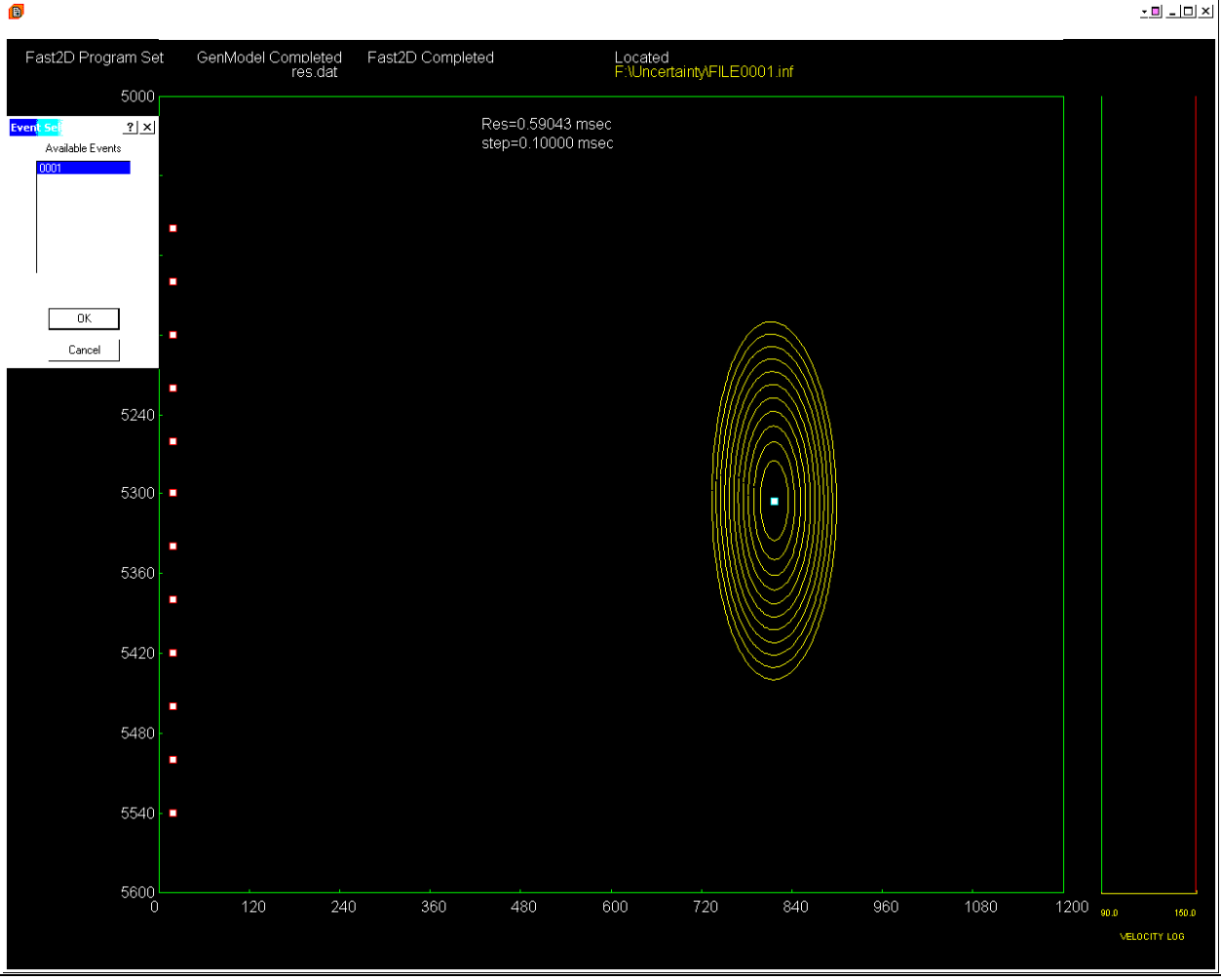


**Figure 41. Residual contours from 0.6 to 1.7 msec**

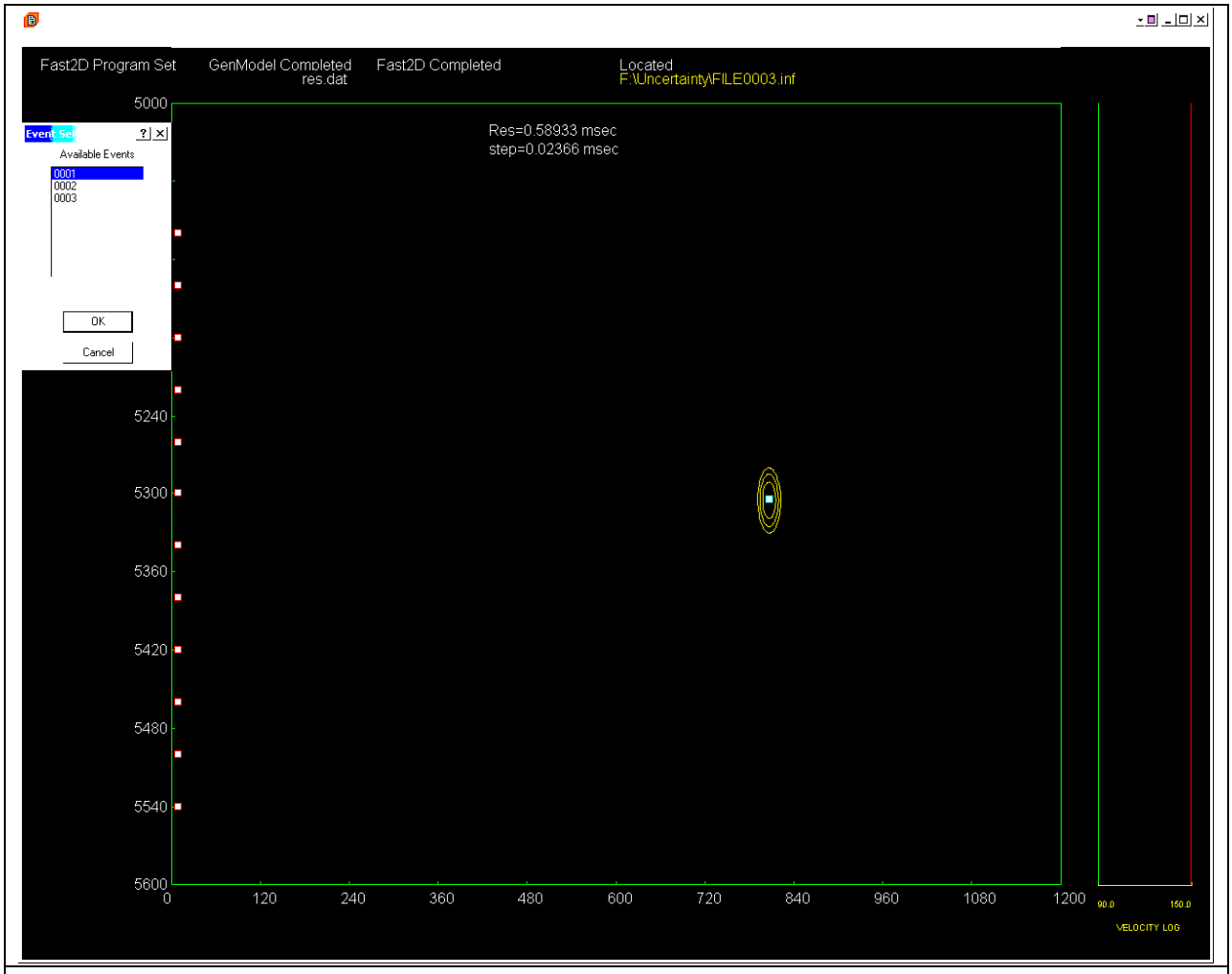


**Figure 42. Uncertainty contours out three standard deviations using new approach**

This approach now provides a relatively simple way to estimate the errors associated with any microseismic event, and this error analysis can be used in more advanced joint inversion procedures where the errors can be coupled into the inversion process.

# 4. Microseismic Source Mechanism Characterization

The microseism that is generated during the fracturing (or other) process contains significant information about its source that can be gleaned from the data under certain conditions. In particular, the fault plane orientation and the direction of slippage are both potentially determinable if the microseism can be observed from several different locations. These are the source mechanisms.

As an example, the theoretical equation for a double-couple source, which is a good approximation of a fault slippage or microseismic event, for the case of a horizontal fault plane slipping in the x direction (see **Figure 43**) is given below. Basically, it is a displacement function, *u(x, t)*, as a function of the source moment, $M_o$, the distance away, $r$, the velocities, $V_p$ and $V_s$, the density, $\rho$, and the time, $t$. The various $\mathbf{A}^{\mathbf{i}}$ vectors represent the radiation pattern and include terms for the near field (N), intermediate field (IP and IS), and the far field (FP and FS). These are the components that a hodogram would provide directional information about.

$$u(x,t) = \frac{1}{4\pi\rho}\mathbf{A}^{\mathbf{N}}\frac{1}{r^4}\int_{r/V_p}^{r/V_s} \tau M_o(t-\tau)d\tau$$
$$+\frac{1}{4\pi\rho V_p^2}\mathbf{A}^{\mathbf{IP}}\frac{1}{r^2}M_o\left(t-\frac{r}{V_p}\right)+\frac{1}{4\pi\rho V_s^2}\mathbf{A}^{\mathbf{IS}}\frac{1}{r^2}M_o\left(t-\frac{r}{V_s}\right)$$
$$+\frac{1}{4\pi\rho V_p^3}\mathbf{A}^{\mathbf{FP}}\frac{1}{r}\dot{M}_o\left(t-\frac{r}{V_p}\right)+\frac{1}{4\pi\rho V_s^3}\mathbf{A}^{\mathbf{FS}}\frac{1}{r}\dot{M}_o\left(t-\frac{r}{V_s}\right)$$

$$\mathbf{A}^{\mathbf{N}} = 9\sin 2\theta\cos\phi\,\hat{\mathbf{r}} - 6(\cos 2\theta\cos\phi\,\hat{\boldsymbol{\theta}} - \cos\theta\sin\phi\,\hat{\boldsymbol{\varphi}})$$
$$\mathbf{A}^{\mathbf{IP}} = 4\sin 2\theta\cos\phi\,\hat{\mathbf{r}} - 2(\cos 2\theta\cos\phi\,\hat{\boldsymbol{\theta}} - \cos\theta\sin\phi\,\hat{\boldsymbol{\varphi}})$$
$$\mathbf{A}^{\mathbf{IS}} = -3\sin 2\theta\cos\phi\,\hat{\mathbf{r}} + 3(\cos 2\theta\cos\phi\,\hat{\boldsymbol{\theta}} - \cos\theta\sin\phi\,\hat{\boldsymbol{\varphi}})$$
$$\mathbf{A}^{\mathbf{FP}} = \sin 2\theta\cos\phi\,\hat{\mathbf{r}}$$
$$\mathbf{A}^{\mathbf{FS}} = \cos 2\theta\cos\phi\,\hat{\boldsymbol{\theta}} - \cos\theta\sin\phi\,\hat{\boldsymbol{\varphi}}$$

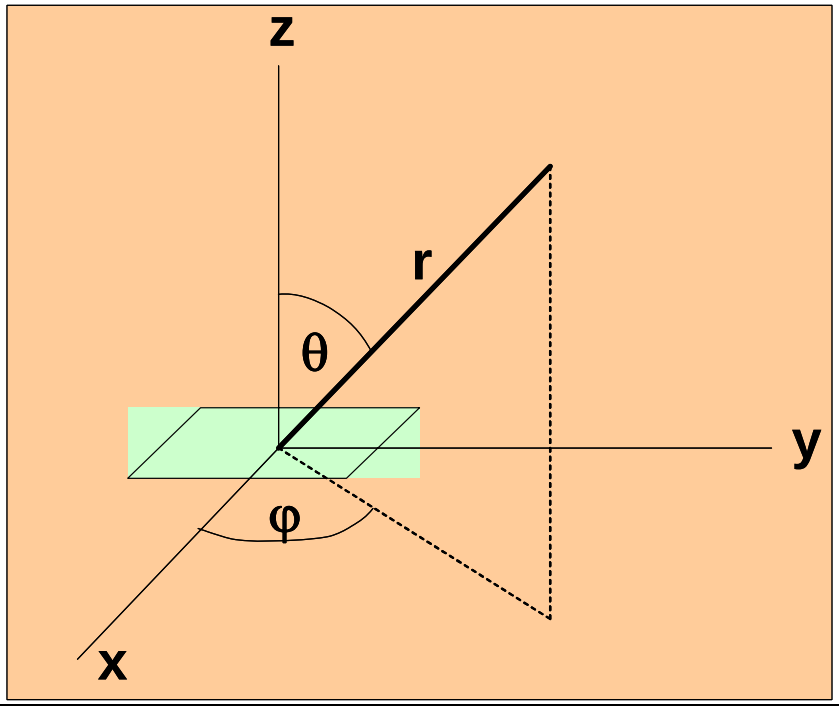


**Figure 43. Schematic of angles for double couple source**

In microseismic monitoring, it is almost always assumed that the monitoring location is far enough away that only the far field components are of importance. In such a case, the radiation pattern, that is the amplitude as a function of angle(s), is reduced to

$$\mathbf{A}^{FP} = \sin 2\theta \cos\varphi \hat{\mathbf{r}}$$
$$\mathbf{A}^{FS} = \cos 2\theta \cos\varphi \hat{\boldsymbol{\theta}} - \cos\theta \sin\varphi \hat{\varphi}$$

The variation of the P-wave amplitude as a function of depth and azimuthal angle ($\varphi$) is shown in **Figure 44**. Note that the P-wave changes sign as the fault plane is crossed.

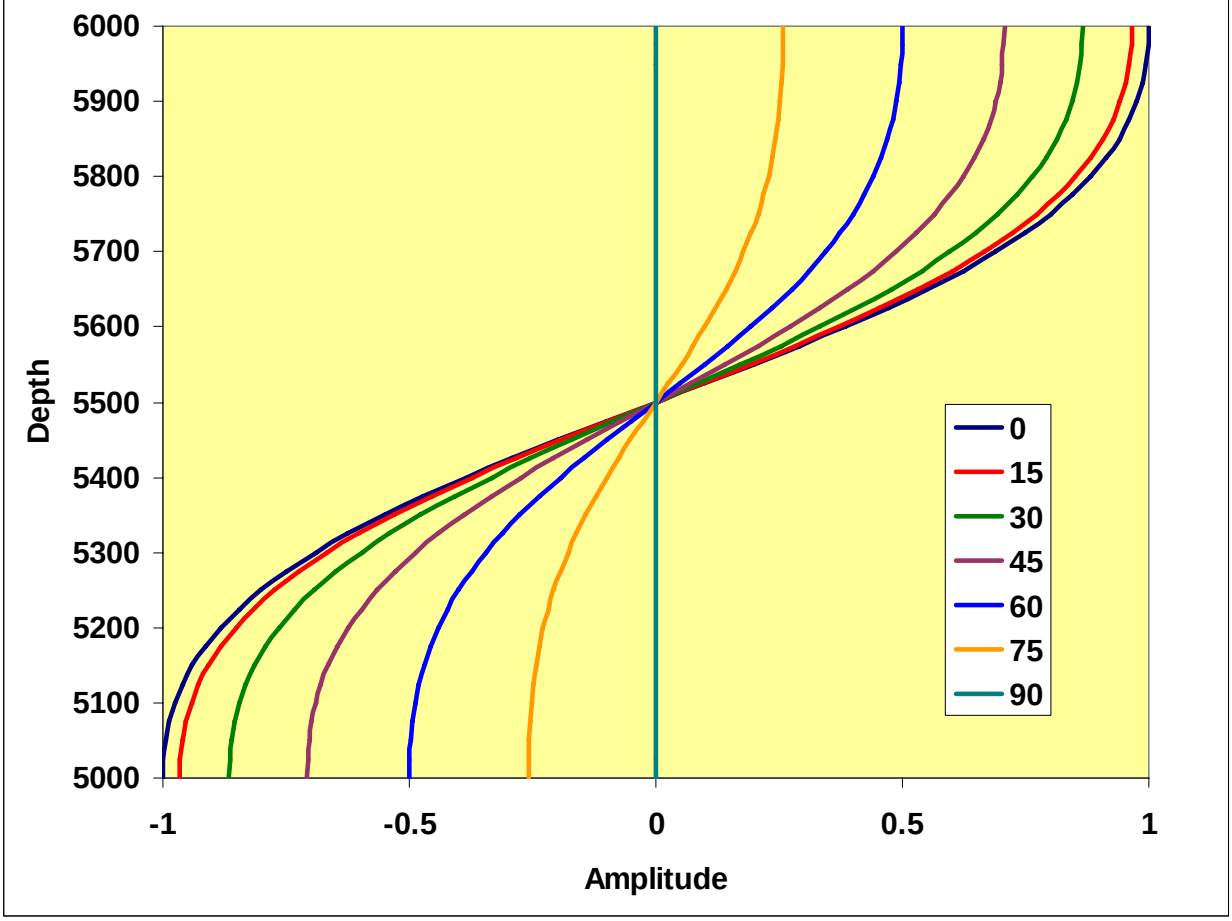


**Figure 44. Variation of P-wave amplitude with depth and as a function of azimuthal angle ($\varphi$)**

The variation of the $S_h$-wave amplitude as a function of depth and azimuthal angle ($\varphi$) is shown in **Figure 45**. The $S_h$ wave is that component of the S-wave in the $\varphi$ direction.

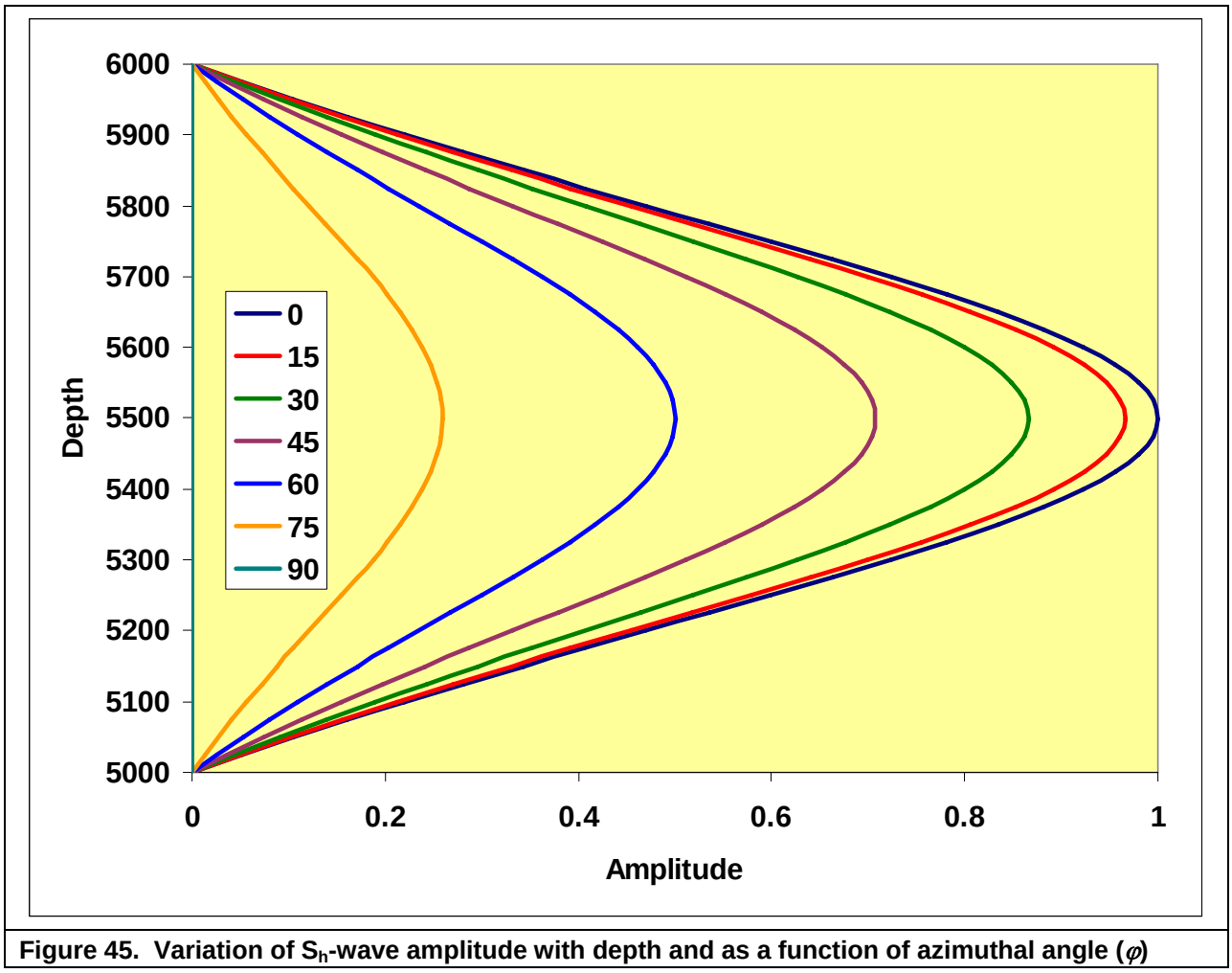


**Figure 45. Variation of $S_h$-wave amplitude with depth and as a function of azimuthal angle ($\varphi$)**

The variation of the $S_v$-wave amplitude as a function of depth and azimuthal angle ($\varphi$) is shown in **Figure 46**. The $S_h$ wave is that component of the S-wave in the $\varphi$ direction.

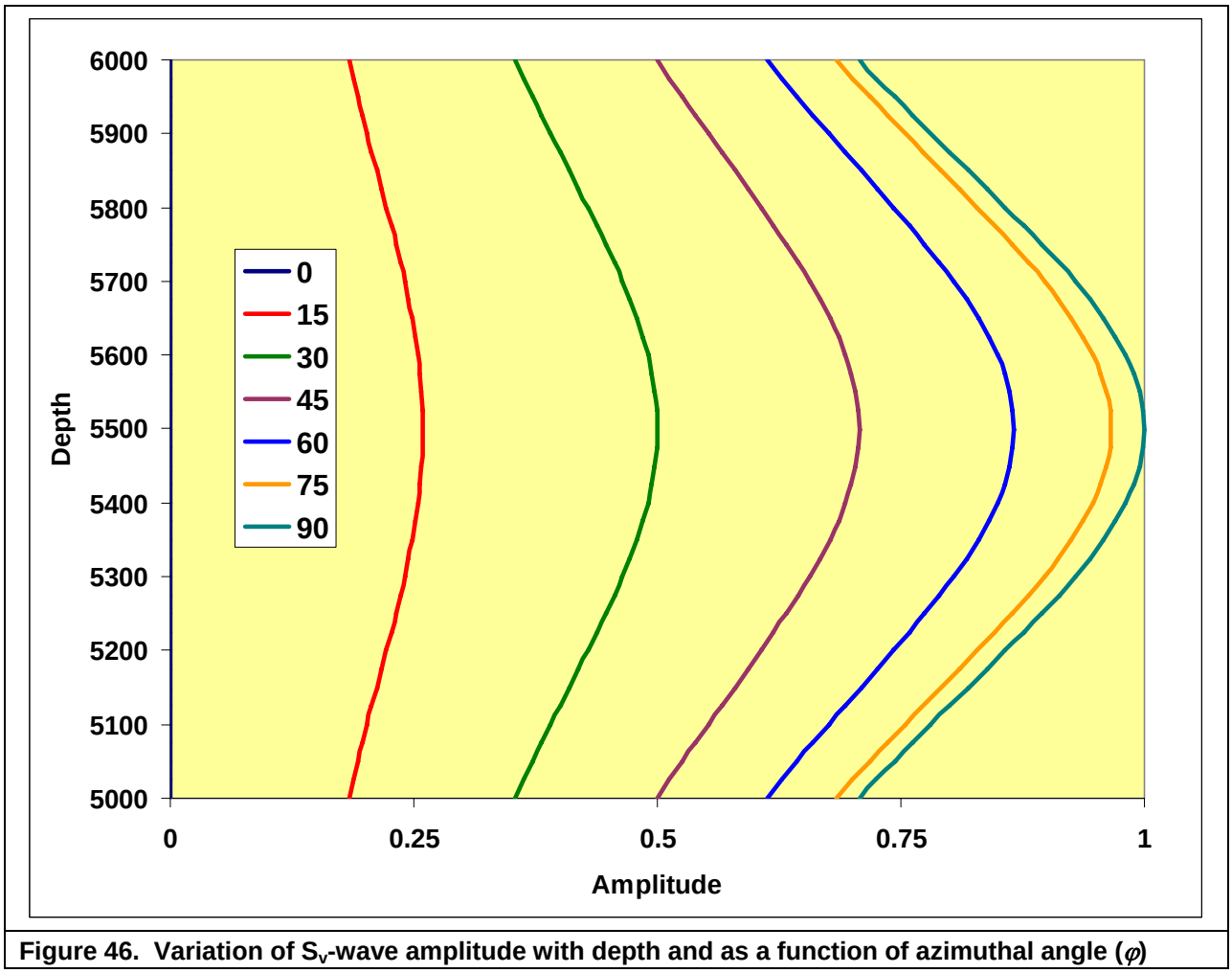


**Figure 46. Variation of $S_v$-wave amplitude with depth and as a function of azimuthal angle ($\varphi$)**

These curves show that there is a very large variability in amplitudes that depend upon the monitoring location relative to the fault plane and the slip direction. By using ratios of S/P, $S_h$/P, and $S_v$/P, it is possible to invert observed data to estimate the source mechanisms, with some caveats and uncertainties depending upon conditions. This is the objective of this work.

## 4.1 Improvements in the Source Mechanism Approach

The basic approach to determining source mechanism information is to use the array-wide data to estimate the focal mechanism vector (***fmv***) of the slippage. The ***fmv*** is the pair of vectors that define (1) the normal to the plane of slippage, which would be vertical in **Figure 43**, and (2) the direction of slip, which would be in the y direction in **Figure 43**. The importance of treating this arrangement as a pair of vectors is that a reversal in the two vectors would have exactly the same radiation pattern. In other words, a fault plane normally pointing in the y direction in **Figure 43** having slippage in the z direction would give exactly the same results. It is the vector pair of the ***fmv*** that provides all of the key information necessary to fully evaluate the slippage characteristics.

Two approaches to determining the ***fmv*** have been developed and evaluated. One is an algorithm that uses data in the frequency domain, the other one is a time-domain methodology. Testing and application has shown that the time-domain approach is more suitable for this analysis and all further work has progressed in the time domain.

As noted above, the amplitude ratios of the various phases have information in them that can be used to extract information about the radiation pattern and thus the ***fmv***. To do this, an inversion process is required to take measured amplitude ratios and output the ***fmv***. This inversion was available prior to the start of this project, but there were considerable limitations in its application. To enhance its capabilities, a method for the estimation of the vector mean and variance was developed and integrated into the existing inversion code and then applied to existing data sets.

Test results on a Barnett Shale data set indicated that existing codes yielded orientation angle estimates with a mean standard deviation of 8° to 10° when individual vector polarity reversals were accounted for and assuming that the solution grid sampling interval and amplitude ratio measurement errors were the primary cause of the observed orientation angle variance. To improve this result, the solution grid sampling interval was reduced from 6° to 3°. The maximum permissible deviation from a double couple dislocation was reduced from 3° to less 0.5°. A module for the estimation of the P/Sh relative polarities was added to the data attributes acquisition code, and the use of these data as an additional constraint was integrated into the inversion code to mitigate a problem that arises due to a polarity reversal issue.

The revised codes were re-applied to the Barnett Shale data set referenced above. The test results indicated that the revised codes yield orientation angle estimates with a mean standard deviation of ~6° and the occurrence of apparent polarity reversals was significantly reduced.

### 4.1.1 Application to Dual-Monitor Well Tests

The increasing use of two dual-monitor well sensor arrays for the acquisition of microseismic data during hydraulic fracturing dictated the requirement for modification of existing software tools to use these data for ***fmv*** orientation estimates. Completion of this task did not require the incorporation of new methods into the existing tool set, but did require a substantial level of effort to modify the take-off angle, data attributes acquisition, and inversion tools to operate on either one or two dimensional arrays and return and/or display one or two dimensional output files.

The microseismic data acquired during a Lower Barnett Shale stimulation was used for the initial trials of the dual-well software. While the dual-well takeoff angle and data attributes passed their performance tests, the performance test of the inversion tool yielded ambiguous results, primarily because of the narrow effective takeoff angle apertures (~4°) resulting from the placement of the monitor well sensor arrays in the high velocity zone above the low velocity Lower Barnett stimulation zone. Remedial actions were deferred until dual-well data acquired in a medium characterized by a simple velocity structure were acquired and processed so that a fair evaluation of software could be performed; unfortunately, no dual-well tests outside of the Barnett Shale were available for analysis during the period of this project.

### 4.1.2 Extensional and Compressional Environments

The original Solution Grid Generation Tool returned approximately orthogonal vector pairs in a focal hemisphere centered on the direction of a horizontal axis that is presumed to be the local direction of the minimum principal stress. While this configuration is applicable to data acquired in structurally extensional geologic environments (typical of most – but not all – sedimentary basins in which we produce oil and gas), the minimum principal stress direction in structurally compressive geologic environments can be vertically oriented.

After examination of the problem, it was determined that to efficiently address both cases, the solution grid hemisphere should be centered on a vertically directed axis. The Solution Grid Generation Tool was revised to return distinct orthogonal vector pairs, both of which intersect the upper focal hemisphere and one of which is spaced at 3° intervals across its entire surface. A performance test demonstrated that the revised Solution Grid Generation Tool yielded the expected results and returns ~160,000 possible solution vector pairs. Application to one data set in such an environment yielded impressive results.

### 4.1.3 Order Ambiguity Problem

The changes to the Solution Grid Generation Tool identified above dictated the requirement for substantive changes in the module used for the order ambiguity resolution to ensure that ***fmv*** orientation estimates could be made for microseismic data acquired in either structural environment. An examination of the changes necessary to acquire the capability to resolve the order ambiguity associated with ***fmv*** orientation estimates derived from microseismic data acquired in compressive structural environments indicated that a simple expansion of the method embodied in the module was impractical. Consequently, a different technical approach was devised. This approach is derived from the methods used in earthquake seismology to determine the local principal stress directions and relative magnitudes from a suite of ***fmv*** orientation estimates. It requires the user to specify either a compressional or an extensional structural environment as well as approximate orientations of the local principal stresses. Two possible stress states are associated with each structural environment. A module that embodies this method was written and integrated into the inversion tool for test purposes.

The revised inversion code was applied to a previously acquired set of data attribute profiles derived from microseismic data recorded during a hydraulic fracturing stimulation in a compressive structural environment. During the first test of the new order ambiguity resolution module, 71 out of a sample population containing 184 solution vector pairs (~ 38%) were rejected because the occurrence of dual stress state compatibility prevented the determination of their respective orders. By “dual stress state compatibility” it is meant that one of the vectors in the pair is identified as the source plane normal in one stress state, while the other vector in the pair is identified as the source plane normal in the second stress state.

Two specific actions were taken to address the dual stress state compatibility issue. The first was to develop a tool for the determination of the density distribution of a sample population of unit vectors and that is independent of the order and polarity of the vectors. The second was to develop a module for the estimation of three seismic metrics that may be used to characterize a particular ***fmv*** pair and that can be used to find the dual stress state solution that most resembles the metrics characterizing uniquely ordered ***fmv*** pairs in the sample population. Applying these tools to the 71 vector pairs in the dual stress state category resulted in the reassignment of 37 vector pairs to unique stress state category.

### 4.1.4 Related Source Location Populations

The observation of linear clusters of microseismic epicenters is not uncommon when the monitored hydraulic fracturing stimulation is executed in a naturally fractured rock formation. A simple hypothesis for the explanation of the occurrence of this phenomenon is based upon the following assumptions.

The microseismic sources activated by the stimulation are constrained to lay on large scale fracture planes whose orientations are determined by the orientations of the contemporaneous principal stress directions.

The large scale fracture planes are orthogonal to the plane defined by the maximum and minimum principal stress directions.

If these assumptions are valid, then it should be possible to determine the location, seismic extent, and the orientation of the large scale fractures that act as the principal elements of the fluid flow paths activated during a hydraulic fracturing stimulation. Development and utilization of the tools necessary to make these determinations would more closely align microseismic hydraulic fracture diagnostics service company capabilities with client's needs for quantitative information about the network of connected natural fractures in the vicinity of the treatment well, since it is likely that this network strongly influences the recoverability rate and the ultimate, economically feasible recovery volume for the stimulated well.

The assumptions listed above imply that the microseismic source locations should plot as multiple straight lines when resolved in the plane defined by the local maximum and minimum principal stress directions characterizing each stress state. Moreover, the projections of the unit vectors normal to the microseismic source planes, when viewed in the same plane, are expected to be either normal to their respective source location lines or make an acute angle with this line that is predictable from a linear friction model with a frictional sliding coefficient in the range of 0.6 to 0.8. Finally, the normal to the plane defined by the estimated focal mechanism vector pair associated with each microseismic source is expected to be sub-parallel to the intermediate principal stress direction characterizing its particular stress state. An exploratory test was designed to determine if these properties could be identified in an integrated microseismic source-location/*fmv* pair data set.

The 79 ***fmv*** pairs in the Reverse-Thrust subset of the sample population acquired in a compressive structural environment were first searched using the previously identified (Task 2.2.1, Subtask D) density distribution tool. This search resulted in the identification of three different microseismic source arrays with failure planes favorably oriented for two-dimensional reactivation. Resolution of the source location vectors of the events in these arrays into the plane orthogonal to the intermediate stress direction revealed that a large majority of the source locations were distributed in tight clusters along lines that defined the directions favorably oriented for two-dimensional reactivation in the reverse-thrust structural environment. Finally it was found that the normals to the ***fmv*** planes for the events in these clusters were roughly sub-parallel to the estimated intermediate principal stress direction.

The favorable exploratory test results justified the development of a software tool set to characterize the large scale natural fractures reactivated by a hydraulic fracturing stimulation. The software tool set was designed to incorporate the use of the density distribution tool to identify the locations of microseismic sources whose failure plane normals contribute to the occurrence of significant peaks in the density distribution. A software tool was designed and developed to:

- Resolve the source location vectors of the events contributing to the previously determined density peaks into the plane orthogonal to the intermediate principal direction
- Separately display the source location distributions of the events contributing to each density peak
- Permit the user to identify and interactively select the source locations that contribute to separate, distinct linear clusters
- Use linear regression methods to determine the slope and intercept of the linear clusters and to compute the Analysis of Variance statistics characterizing the "goodness of fit" at the 90% confidence
- Save the linear regression results for each linear cluster in each density peak

A separate tool was designed and developed to operate on the linear regression results returned by the interactive tool. It uses this information to determine the orientation, location, and seismically perceptible

extent of the natural fractures as defined in an ENZ Cartesian coordinate referenced to a point chosen by the user. It then creates a 3-dimensional visualization of the inferred natural fractures.

Application of the software tools resulting from the completion of this new software tool to the exploratory test data set resulted in the identification and determination of the orientation and location of eight natural fractures with seismically perceptible dimensions of several hundred feet. Five of these fractures were favorably oriented for reverse fault movement, three were favorably oriented for sub-horizontal thrust fault movement, and two of these fractures appeared to intersect the perforated interval of the treatment well. The existence of these two sub-horizontal fractures was partially confirmed by client data that indicated the occurrence hydrocarbon shows at depths close to where these fractures appear to intersect the treatment well.

### 4.1.5 Improvements in Signal-To-Noise Ratios

One of the initial objectives of the project was to improve signal-to-noise ratio (SNR) through some combination of hardware, software and procedures. Initial thoughts ranged from sensor improvements to filtering and other digital-signal-processing approaches. However, it was found that significant improvements in the SNR could be obtained by stacking receivers, and no further work on other methodologies was conducted.

# 5. Technology Transfer

The primary method of technology transfer is commercialization of this product. Pinnacle is in the process of developing a full hybrid array for application in both offset-well and treatment-well tests. This hybrid array is expected to be available for use in the second quarter of 2007.

In addition to the commercial product, Pinnacle has written an SPE paper on the joint inversion and a *Gas Tips* article on the hybrid concept. The SPE paper is titled "Improving Hydraulic Frac Diagnostics by Joint Inversion of Downhole Microseismic and Tiltmeter Data" by N.R. Warpinski, L.G. Griffin, E.J. Davis, Pinnacle Technologies Inc., and T. Grant, National Energy Technology Laboratory, paper number SPE 102690, presented at the 2006 Annual Technical Conference and Exhibition in San Antonio, Texas, September 2006. The *Gas Tips* article is titled "Hydraulic Fracture Mapping with Hybrid Microseismic/Tiltmeter Arrays" published in October 2006.

Other technology transfer media include this final report and previous monthly or other updates to DOE, as well as a final presentation for DOE.

# 6. Conclusions

The project has successfully completed the development of an advanced fracture mapping system that includes both microseismic receivers and tiltmeters in a combined downhole array. The combined system takes advantage of the best features of both technologies, yielding a superior mapping result compared to either technology by itself. This combined result is obtained by using both sets of data in a "joint" inversion of the results, that is, an inversion that jointly applies both data sets to a single model of the process.

From a hardware perspective, the combined mapping system was obtained by fabricating new housings for the tiltmeters that could be linked to the microseismic system and allow for pass through of the additional wires required for microseismic operation. In addition, a method to use two separate telemetry systems (fiber optic for the microseismic system and electrical for the tiltmeter array) was developed and applied.

In addition, improvements to the signal-to-noise ratio (SNR) were attempted both by developing accelerometers and by stacking tools. The accelerometers were successfully integrated into the microseismic receivers, but unfortunately had elevated noise levels. Independent work is still ongoing to solve noise problems with the accelerometers and these may eventually be used to improve the SNR. Stacking of multiple receivers was performed successfully and this approach yielded a significant improvement in SNR. Stacking of three tools (essentially three separate tools connected together) gave improvements of about a factor of 2 in SNR by reducing digitization noise, resonance effects, and random noise (*e.g.*, gas bubbles impinging on tools).

From an analysis standpoint, a joint inversion was developed that uses a mechanical fracture model for the tiltmeter with a microseismic distribution about the mechanical model. In this way, both sets of data are referenced to a "model" and deviations of the data from the model are handled by changing the model to best fit the data. The model includes not only fracture parameters (*e.g.*, length, height, azimuth and dip), but also the velocity structure of the formation so that microseismic events are correctly located.

Finally, methods were advanced for assessing fault slippage planes and deducing information about stress levels and fault orientations. This was done by analyzing the microseisms from an earthquake perspective based on the measured response at each receiver in the array. These methods allow for some evaluation of reservoir characteristics based upon the microseismic response.

# References

1. Wright, C. A.: "Tiltmeter Fracture Mapping: From the Surface and Now Downhole," *Petr. Eng. Int*. (1998) **71**, 50.

2. Warpinski, N.R., Branagan, P.T., Peterson, R.E., Wolhart, S.L. and Uhl, J.E.: "Mapping Hydraulic Fracture Growth and Geometry Using Microseismic Events Detected by a Wireline Retrievable Accelerometer Array," paper SPE 40014 presented at the 1998 Gas Technology Symposium, Calgary, March 15-18.

3. Green, A.E. and Sneddon, I.N.: "The Distribution of Stress in the Neighbourhood of a Flat Elliptic Crack in an Elastic Solid," *Proc. Camb. Phil. Soc*., **46**, pp. 159-163, 1950.

4. Okada, Y.: "Internal Deformation Due to Shear and Tensile Faults in a Half-Space," *Bulletin of the Seismological Society of America*, (April 1992) **82,** 1018.

5. Whittaker, E.T. and Watson, G.N.: *A Course of Modern Analysis*, Cambridge, 1927.

6. Abramowitz, M. and Stegun, I.A.: *Handbook of Mathematical Functions*, Dover Publications, New York, 1970.

7. Sih, G.C. and Liebowitz, H.: "Mathematical Theories of Brittle Fracture," in *Fracture*, Liebowitz, ed., II, Academic Press, New York, p.137, 1968.

8. GRI CD: "*GRI/DOE Multi-Site Hydraulic Fracture Diagnostics Project*," S. Wolhart (manager), Gas Research Institute Report GRI-99/0117, Chicago (May 1999).

9. Branagan, P.T., Warpinski, N.R., Engler, B.P. and Wilmer, R.: "Measuring the Hydraulic Fracture-Induced Deformation of Reservoir and Adjacent Rocks Employing a Deeply Buried Inclinometer Array: GRI/DOE Multi-Site Project," paper SPE 36451 presented at the 1996 SPE Annual Technical Conference and Exhibition, Denver, October 6-9.

10. Warpinski, N.R., Wright, T.B., Uhl, J.E., Engler, B.P., Drozda, P.M. and Peterson, R.E.: "Microseismic Monitoring of the B-Sand Hydraulic Fracture Experiment at the DOE/GRI Multi-Site Project," paper SPE 36450 presented at the 1996 SPE Annual Technical Conference and Exhibition, Denver, October 6-9.

11. Engler, B.P. and Warpinski, N.R.: "Hydraulic Fracture Imaging Using Inclinometers at M-Site: Finite-Element Analyses of the B-Sandstone Experiments," GRI Topical Report, GRI-97/0361, Chicago (December 1997).

12. GRI CD: "*Mounds Drill Cuttings Injection Project*," S. Wolhart (manager), Gas Research Institute Report GRI-99-0173, Chicago (June 1999).

13. Moschovidis, *et al*.: "The Mounds Drill Cuttings Injection Field Experiment," Proceedings of the 37th U.S. Rock Mechanics Symposium, Vail (June 6-9, 1999) 1017.

14. Warpinski, N.R. and Engler, B.P.: "Assessment of Downhole Tiltmeter Fracture Monitoring at the Mounds Drill Cuttings Injection Test," Sandia National Laboratories Report, SAND2001-1054, Albuquerque (April 2001).

15. Griffin, L.G., Wright, C.A., Davis, E.J., Weijers, L. and Moschovidis, Z.A.: "Tiltmeter Mapping to Monitor Drill Cuttings Disposal," Proceedings of the 37th U.S. Rock Mechanics Symposium, Vail (June 6-9, 1999) 1033.

16. Warpinski, N.R., Branagan, P.T., Wolhart, S.L., Moschovidis, Z.A. and Mahrer, K.D.: "Microseismic Monitoring of the Mounds Drill Cuttings Injection Tests," Proceedings of the 37th U.S. Rock Mechanics Symposium, Vail (June 6-9, 1999) 1025.

17. Vidale, J.E.: "Finite Difference Calculation of Travel Times," *Bull. of the Seismological Society of America*, **78**, 1988, 2062.

18. Nelson, G.D. and Vidale, J.E.: "Earthquake Locations by 3D Finite Difference Travel Times," *Bull. of the Seismological Society of America*, **80**, April 1990, 395.

# Appendix A—Technical Articles


SPE 102690

# Improving Hydraulic Frac Diagnostics by Joint Inversion of Downhole Microseismic and Tiltmeter Data

N.R. Warpinski, SPE, L.G. Griffin, SPE, E.J. Davis, SPE, Pinnacle Technologies Inc., and T. Grant, National Energy Technology Laboratory



This paper was prepared for presentation at the 2006 SPE Annual Technical Conference and Exhibition held in San Antonio, Texas, U.S.A., 24–27 September 2006.



## Abstract

Downhole microseismic and downhole tiltmeter mapping are the primary direct diagnostic techniques for monitoring the geometry of hydraulic fractures at depth. Although these techniques have seldom been used together because of a lack of available monitor wells, the advent of new hybrid arrays having both microseismic receivers and downhole tiltmeters has now made application of both technologies from a single well possible. This paper discusses algorithms for joint inversion of the combined data along with the development of hybrid arrays for combined tiltmeter and microseismic. Examples from several data sets show how the combined results can be used to improve velocity models and obtain better constrained-height estimates, as well as improved confidence in other fracture geometry parameters.

## Introduction

Diagnosis of hydraulic fracture behavior and geometry and accurate design of fracture treatments usually require much more information about the geology, stress, permeability, rock moduli, and other parameters than is customarily available. As a result, it has fallen on fracture diagnostics to provide a more detailed understanding of the overall behavior of propagating hydraulic fractures, particularly in complex or unconventional environments. The subsequent incorporation of these direct measurements of fracture dimensions into hydraulic fracture simulators then enables the creation of customized calibrated models that can be used as predictive tool for specific areas.

While there are numerous fracture diagnostic techniques available to the industry, high-resolution mapping of hydraulic fractures is primarily performed with either the microseismic technique using downhole receiver arrays or downhole tiltmeter monitoring. These two techniques measure different properties and different characteristics of the hydraulic fracture, potentially yielding alternate perspectives of the results of a treatment. In general, these two types of measurements have not been performed on the same tests because each requires its own observation well.

Improvements in borehole technology, telemetry, and computational capabilities have now made it possible to combine both of these technologies in a single diagnostic array, allowing both types of information to be obtained in a single observation well. The microseismic data provides a detailed map of micro-earthquakes that are induced by the hydraulic fracturing process, whereas the tiltmeters provide an integrated measure of the actual rock deformation. Separately, they both give important information about fracture growth process and the resultant geometry. Jointly, however, they can provide a much more complete, or composite, view of the fracture. This is particularly true if the two data sets can be jointly analyzed, or inverted, to give a single overall view of the fracture.

The previously described coupling of tiltmeters and microseismic receivers, analyzed by joint inversion techniques, has been the focus of a US DOE funded project on fracture diagnostics. This paper describes some initial approaches taken in obtaining both tiltmeter and microseismic data during a fracture treatment and also some analysis methods that have been used to jointly analyze the data.

## Downhole Tiltmeter and Microseismic Technologies

Downhole tiltmeter mapping and microseismic mapping using downhole receivers are the two fracture monitoring technologies that can provide high-resolution monitoring of hydraulic fracture growth and behavior. A brief overview of each of these technologies is discussed separately below.

**Downhole Tiltmeter Mapping.** Tiltmeters[1,2] are extremely accurate measuring devices that use a sophisticated bubble sensor – much like a carpenter's level – to detect changes in the angular position of the sensor. Sensitivities of these sensors are typically in the nanoradian ($10^{-9}$ radians) range, equivalent to 0.2 inch movement over a 3,000 mile span. A measurement of the angular position, which is equivalent to the gradient of displacement orthogonal to the displacement direction, provides all the information needed to determine how the earth is deforming in response to some process.

Tiltmeters only measure the tilt along a single axis, so a full tilt measurement (magnitude and angle) requires two

orthogonal sensors. The reference direction for tiltmeters is determined by gravity, nominally directly downward. These sensors can be used in both surface and downhole applications to measure earth movements that are induced by some deformation process, such as a hydraulic fracture. Surface tiltmeters have been employed to map fractures for over three decades, but the downhole application of this technology[1,3-7] is relatively recent. The advantage of being downhole is that the sensors are much closer to the process so the signals are larger and more facets of the process are resolvable. Still, offset well applications typically require high sensitivity tiltmeters (e.g., tens of nanoradian) unless the monitoring well is very close to the process or the induced deformations are large.

Hydraulic fractures produce a well-defined tilt signature that can be inverted using an appropriate model to deduce fracture geometry parameters. For downhole applications, either a dislocation model or a crack model give the same results when the monitor position is greater than about one hydraulic fracture characteristic dimension (usually the height). The dislocation models that have been rigorously checked and catalogued by Okada[8] are normally used for tiltmeter analyses because of their versatility, but the 3D ellipsoidal fracture of Green and Sneddon[9] is also used and is more accurate at monitoring positions very close to the hydraulic fracture.

**Microseismic Mapping.** Microseismic monitoring is the detection and location of earthquakes that are induced by downhole injection or production processes.[10-12] The approach is similar to standard earthquake seismology, except that it is generally applied with downhole receiver systems instead of surface seismic stations.

Microseismic monitoring has been performed for several-decades, but this technology has recently expanded because of improvements in receiver technology, telemetry, and processing capabilities. The application of this technology consists of placing an array of triaxial geophone or accelerometer receivers downhole, fixing them in place and orienting them, recording seismic data during the fracturing process, finding earthquake "events" within the data, locating those events, and interpreting the overall results.[13-16]

The microseisms associated with hydraulic fractures are very small earthquakes that are induced by changes in either (or both) pore pressure and stress due to the inflating of the hydraulic fracture and leakoff of the fracturing fluids.[17] These earthquakes are shear slippages that generally occur along existing failure planes. Such failure planes could be faults, natural fractures, bedding planes, shale dewatering features, and various other discontinuities in the rocks. These microseisms form a "cloud" around the hydraulic fracture, outlining its shape and azimuth.

Detecting and separating the microseisms from the background seismic noise requires commonplace event-detection programs that are readily available.[18] To locate these "events" with a single vertical array of sensors (the typical application), it is necessary to determine arrival times of the P wave (compressional wave) and the S wave (shear wave), as well as determine the particle motion of either the P wave, S wave or both. Location schemes include regressions or grid-search procedures, depending on the velocity model and geometry.

## Hybrid Tiltmeter/Microseismic Arrays

Both tiltmeters and microseismic monitoring technologies are limited by noise and distance. Microseismic monitoring also requires an accurate velocity model of the rocks between the events and the receivers, while tiltmeter modeling requires a model for the process that is occurring (e.g., a dislocation or a crack model). The use of hybrid arrays[19] consisting of both tiltmeters and microseismic receivers probably cannot help very much with the distance problem, but it certainly can help mitigate effects of noise on both systems, improve the velocity structure (microseismic), and sharpen up results from a less-than-ideal model (tiltmeter).

Downhole tiltmeter arrays are generally run into a wellbore on a wireline and use magnetic coupling of the sensor tools (although they were originally run on centralizers). Microseismic receiver arrays are generally run into a wellbore on a wireline and employ either clamp arms or other types of mechanisms to solidly couple the receiver to the wellbore to assure high-frequency response. A hybrid system can take many forms, but the most convenient is to package the tiltmeter system into a housing that connects directly to a seismic receiver, thus assuring a positive clamping of both tools.

In such a geometry, the primary issues are wiring and telemetry, although the supply of sufficient power and limitations on total tool-string weight are also important factors. Microseismic monitoring requires high-speed sampling (e.g., ¼ msec sampling to capture the high frequencies typical of these microseisms) and multi-level tri-axial systems will need telemetry rates of several megabits per second to send all of the data to the surface. Tiltmeter data, on the other hand, only requires low-speed sampling (e.g., 1-10 Hz), so the initial hybrid system has kept the two telemetry systems separate. To achieve the desired high-speed telemetry rates, the microseismic receivers are run on a fiber-optic wireline, but these wirelines are manufactured in a seven-conductor design, so there are six additional copper wires for power and other needs. The wiring of this system has been reconfigured so that two wires are available for the tiltmeter power and telemetry (the rest are used by the microseismic system for power, clamping, and other needs). At the surface, data from both systems are processed separately, prior to final data analysis.

## Joint Inversion Of Hybrid Data

The ultimate joint inversion of microseismic and tiltmeter data would consist of a poro-thermo-mechanical model of the fracture/rock system that predicts zones of microseismic activity as well as tiltmeter response. One such model has previously been developed for microseismic predictions,[17] but its use is unfortunately not appropriate for anything but a full-blown science project because of a lack of sufficient input data (all 3 stresses, pore pressure, moduli, permeabilities, poro-elastic parameters, etc. for all layers) to ever provide meaningful results in a typical fracturing application. Other such models also exist in different forms (e.g., Settari et al.[20]).

However, simpler approaches can also be developed that concentrate on extracting geometry parameters and potentially some formation parameters such as velocities. There are many ways to formulate such a model with varying degrees of complexity, but one relatively straighforward approach is given here for initial application of this technology.

The approach used for these initial studies consists of a 3D ellipsoidal fracture model for the tilts coupled with a distributional model for the microseismic data. The distributional model treats the microseism as a set of arrival times (P and S waves) and azimuths (from particle-motion analyses) that can be located or re-located using updated velocities to yield distributions of events about mean values of azimuth, dip, height, and length. A Levenberg/Marquardt non-linear solver (e.g., as discussed in Warpinski & Engler[21]) performs the inversion for fracture parameters and formation velocities. The 3D ellipsoidal fracture model was used here instead of the dislocation model because it was already set up for this inversion procedure from previous work.[21]

The equations associated with the tilt response in the 3D crack model are given in Warpinski,[22] based on the original Green and Sneddon formulation.[9] Essentially, the tilt distribution as a function of the vertical sensor location ($z$) is given as

$$\frac{\partial u}{\partial z}(z) = F\left(h, L, \Delta P, y_c, \alpha_f, \delta_f, w_{dis}, E, \nu\right), \qquad (1)$$

where $h$ is the fracture total height, $L$ is the wing length (symmetry is assumed), $\Delta P$ is the net pressure, $y_c$ is the vertical depth to the center of the fracture, $\alpha_f$ is the azimuth of the fracture relative to the monitoring position, $\delta_f$ is the inclination of the fracture (complement of the dip), $w_{dis}$ is the separation between the monitor well and the injection well, $E$ is Young's modulus, and $\nu$ is Poisson's ratio. The geometric parameters are shown in Figure 1. It is generally expected that $w_{dis}$, $E$, and $\nu$ are known and these are not usually free parameters in the inversion. The sense of $\alpha_f$ is such that a fracture azimuth normal to the line between the monitor and injection wells is 0° while a fracture directly approaching the monitor well is 90°. Any of the first six parameters may be known and used as constraints on the results. To facilitate the inversion, all of the free parameters are mapped onto the real axis, but this is more of a convenience than a necessity.

The Levenberg/Marquardt algorithm seeks to minimize the function

$$G = \sum_n \left\{ \left.\frac{\partial u}{\partial z}\right|_{calc} - \left.\frac{\partial u}{\partial z}\right|_{obs} \right\} \qquad (2)$$

in an efficient manner by determining optimum values of the unknown parameters. $n$ is the number of tilt observations. The formulation for a dislocation model would be the same, except that the dislocation opening, $b$, would be used instead of the crack internal pressure, $\Delta P$.

The microseismic event locations, both because of the nature of the microseismic origins and ubiquitous noise, are distributed in some manner about a fracture length, height, azimuth, and dip. Handling of the distributional characteristics of the azimuth and dip are straightforward, as the mean and variance are readily obtained from directional statistics (e.g., Mardia[23]). Approaches to handle the length and height distributions are less clear and will continue to be investigated as more combined data sets are obtained (see later discussion).

For this initial development, the microseismic events are assumed to be normally distributed about some characteristic height and length that are functions of the actual fracture height and length. Preliminary testing has shown that characteristic heights and lengths that are about 60% of the actual height and length provide microseismic distributions that mirror actual distributions.

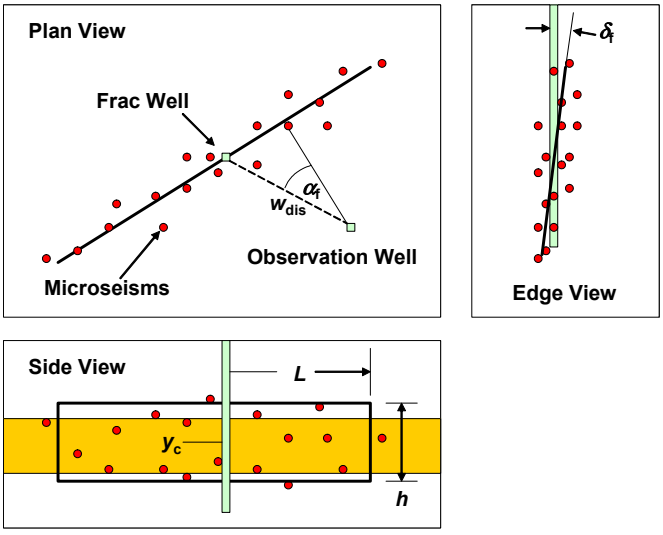


**Figure 1. Geometry of Fracture Model Inversion.**

The procedure for processing the microseismic data is to start with 3D locations obtained from the current velocity model. The (x, y) coordinates are then used to determine the microseismic azimuth from directional statistics[23], and from this azimuth edge ($b_i$) and side ($r_i$) projections are obtained. The dip is obtained from the edge projection, again using circular statistics and the side projection data provide means and variances of the event locations for height and length calculations. Finally, a probability for that event location based on height, length, azimuth, and dip can be obtained from

$$P(x_i, y_i, z_i) = \frac{1}{\sqrt{2\pi}\sigma_z}\exp\left[\frac{-(z_i - z_c)^2}{2\sigma_z^2}\right] \cdot \frac{1}{\sqrt{2\pi}\sigma_r}\exp\left[\frac{-(r_i - r_c)^2}{2\sigma_r^2}\right] \cdot \frac{1}{\sqrt{2\pi}\sigma_b}\exp\left[\frac{-(b_i - b_c)^2}{2\sigma_b^2}\right] \qquad (3)$$

where $z_c$, $r_c$, and $b_c$ are the means and $\sigma_z$, $\sigma_r$, and $\sigma_b$ are the standard deviations of the distributions vertically, along the side projection, and along the edge projection, respectively, and the three separate variables are assumed to be independent.

An expected probability for this event can also be obtained by using the current model azimuth, dip, characteristic length

and characteristic height to obtain projections and then variances. However, the distributions associated with the current model are distributed differently and take into account the azimuth of the model and the center location of the model, as well as height and length. This expected probability can be compared with the current location probability to update the model. The Levenberg/Marquardt algorithm now seeks to minimize the combined function

$$G = \sum_n \left\{ \left.\frac{\partial u}{\partial z}\right|_{calc} - \left.\frac{\partial u}{\partial z}\right|_{obs} \right\} + W_m \sum_m \left\{ P_{expected}(x_i, y_i, z_i) - P_{obs}(x_i, y_i, z_i) \right\} \quad (4)$$

where $W_m$ is a weighting function that can be used to increase or decrease the effect of the microseismic data.

Besides the model parameters for the tiltmeter data, the microseismic data now includes the effect of velocities, which can also be extracted from the inversion. To extract the velocities, however, it is also necessary to have a location algorithm in the inversion. Assuming the arrival times and azimuths are correct, then a velocity can also be found which allows the microseismic and tiltmeter data to optimally match. For the case of a constant velocity structure, the location algorithm can be a simple regression on the distance equation. For a more complex velocity structure, a forward model and grid-search algorithm is applied to obtain the re-located points. In such a case, it is necessary to invert for all of the velocities.

Using a probability function for the microseismic data is not intended to imply any particular geophysical behavior, but rather it is simply a convenient method for (1) assessing whether a microseismic event fits the current model parameters, (2) treating the microseismic data like a true distribution with outliers, and (3) developing an efficient function to be minimized jointly with the tiltmeter data.

## Data Analysis

Three types of analyses have been performed to date. The analyses include evaluations of synthetic data, joint microseismic and tiltmeter data from a single well where the combined sensors were cemented in place, and joint analysis of microseismic data from separate wells. In addition, data from a hybrid-array test in a treatment well have also been examined to assess the performance of the hybrid system.

**Synthetic Data.** Synthetic data was used to test the behavior of the model, understand the capabilities of the inversion under ideal conditions, and evaluate distributional approaches. Figure 2 shows an example of a synthetic microseismic and tiltmeter data set that was used for initial evaluation of the joint inversion. The tiltmeter data are based on a fracture with $L$=250 ft, $h$=80 ft, $P$=500 psi, $\nu$=0.2, and $E$=4x10$^6$ psi as monitored from a monitor well 500 ft away placed normal to the fracture azimuth. The microseismic data are randomly distributed within an envelope that is somewhat larger than the fracture dimensions.

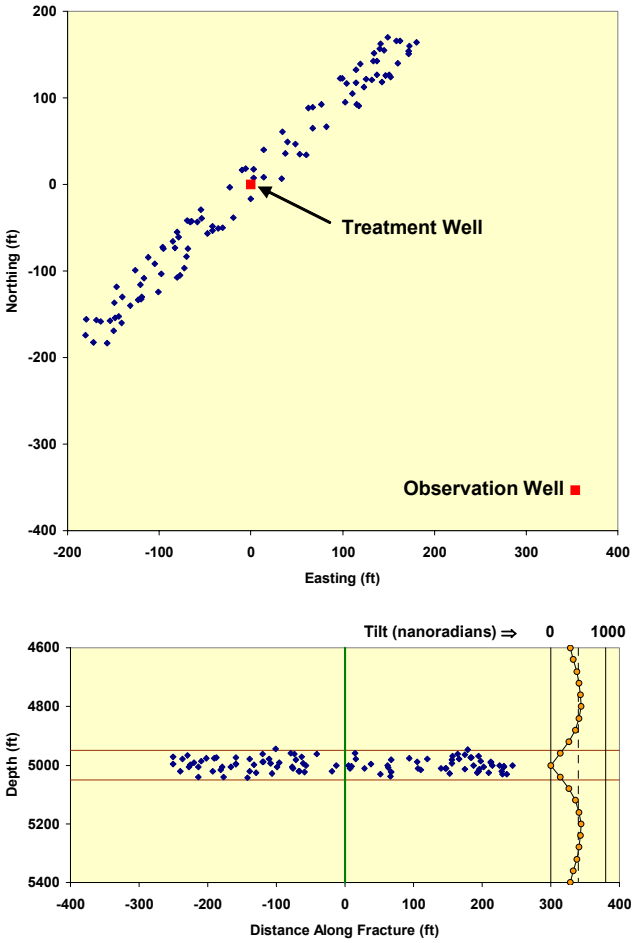


**Figure 2. Example synthetic data.**

A direct inversion of these data returns the input dimensions of the fracture to three decimal places and is not particularly interesting. A more instructive example is to take the input data shown in Figure 2, mislocate it by applying the wrong velocity, and then invert the mislocated data. Figures 3 and 4 show the mislocated microseismic data and the locations recovered after the inversion, respectively. Table 1 shows a comparison of the model values and the recovered inverted parameters. In this example, the pressure and dip are assumed known (applied constraints) and the velocity model is constant, so only one of the two velocities can be found (e.g., the location depends upon $V_pV_s/\{V_p\text{-}V_s\}$). The advantage of having some tiltmeter data is that it can be used to improve the microseismic locations. Similarly, some microseismic locations can help to improve the results from noisy tiltmeter data. If no constraints were used in this example, the results would have been $h$=71.6, $L$=253, $\Delta P$=614, azimuth=45°, dip=3.1°, center depth=4998.3, and $V_p$=15,020 ft/sec, which are fairly accurate results, but nevertheless show the value of having some information on which to ground the inversion.

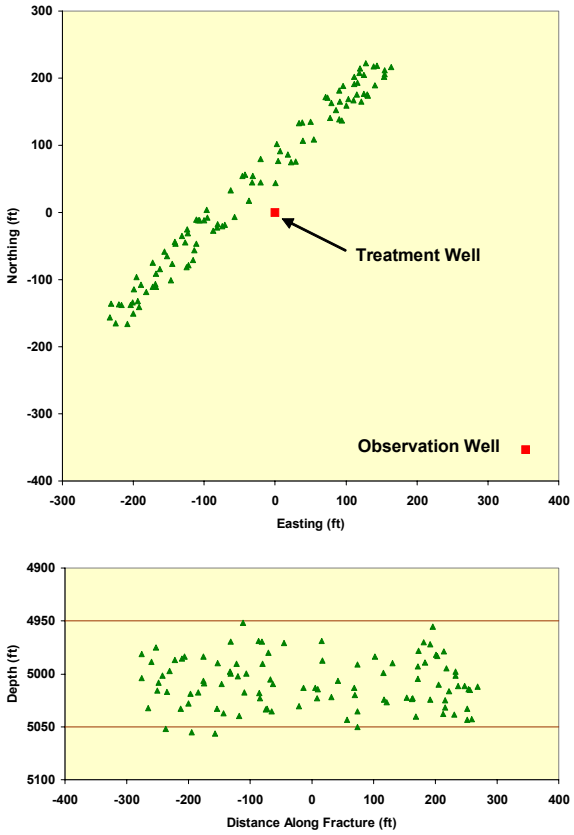


**Figure 3. Mislocated microseismic data.**

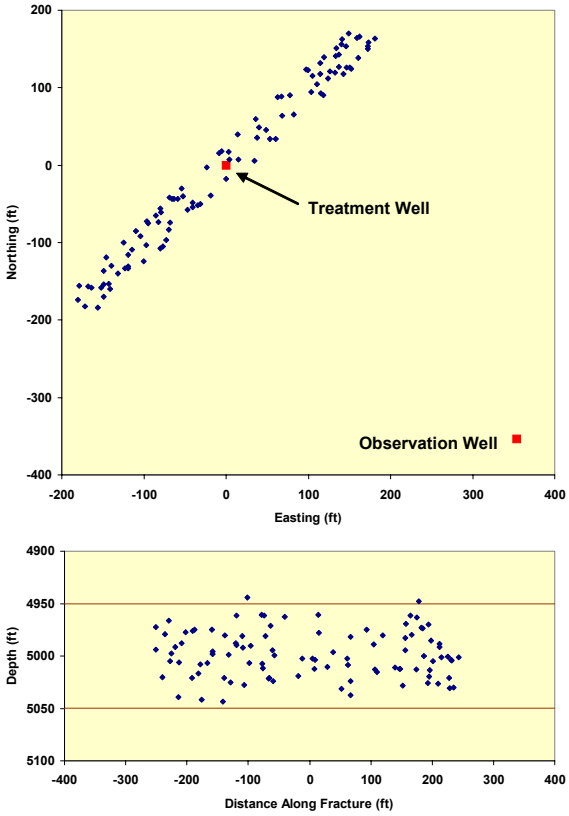


Figure 4. Recovered microseismic results.

Table 1. Synthetic Inversion Results

| Parameter | Model | Inverted |
|---|---|---|
| Length (ft) | 250 | 252 |
| Height (ft) | 80 | 79.7 |
| Center Depth (ft) | 5000 | 4999.5 |
| Azimuth (deg) | 45 | 45 |
| $V_p$ (ft/sec) | 15,000 | 15,010 |
| $V_s$ (ft/sec) | 8,000 | NA |
| Pressure (psi) | 500 | NA |
| Dip (deg) | 0.0 | NA |

**M-Site Data.** Perhaps the best test case for a combined microseismic and tiltmeter data set is the data from the DOE & GRI sponsored M-Site experiments.[24] At M-Site, both tiltmeters (6 levels) and tri-axial accelerometers (30 levels) were cemented in a monitor well approximately 300 ft from a series of fractures conducted in two intervals. The geologic setting is a fluvial environment, in which comprehensive fracturing experiments were carried out in two intervals. The test zone of interest for this evaluation was labeled the "B" sandstone at a depth of approximately 4525 to 4560 ft.[4,25,26]

Numerous injections were performed in the B sandstone, with one particular minifrac providing a good data set for testing this approach. The minifrac was pumped at 22 bpm, injecting a total volume of 400 bbl of a 40 lb linear gel. During the test, over 100 microseisms were detected and located and excellent-quality (high signal-to-noise-ratio) tiltmeter data were also obtained on all six tiltmeters.

Figure 5 shows a plan view of the microseismic data and a side view of the combined microseismic and tiltmeter data, along with the theoretical tilts. Approximately 20 of the microseismic events are from a second monitor well that has a 5-level wireline receiver array. For this case, the microseismic locations are assumed to be correct, so the inversion provides a fracture geometry that gives a best fit of the microseismic distribution with the measured tilts. However, the wide distribution of microseismic events does not lend itself to useful evaluation of the dip, so the dip was constrained to a vertical fracture (known from the testing). The bottom-hole pressure was also measured and used as a constraint (1300 psi).

Table 2 gives a comparison of the joint inversion results compared to the previous reported results for individual technologies. The original tiltmeter results used an analytic model with homogeneous formation properties,[4] whereas the original FE (finite element) results used variable layer properties.[26]

The major difference in the various results lies primarily in the height estimates. A combined analysis yields a height that is somewhat greater than the height estimates from separate measurement techniques. When combined, the requirements of matching azimuth and center position, as well as length and height, require a greater height to best fit all of the data, subject to the constraints as well as the weighting and other factors (that is, the microseismic distribution suggests a higher center whereas the tiltmeters suggest a lower center).

Weighting is an issue that is still being investigated, as it plays a significant role in the type of results obtained. A small

microseismic weighting produces an azimuth that is oriented closer to the observation well and a somewhat smaller fracture height, yielding a better fit of the tilt data. A larger microseismic weighting (as used here) fits the microseismic events better and matches the event azimuth, but the fit of the tilt data is somewhat weaker. Interestingly, the primary difference observed by changing the weighting is a rotation of the fracture azimuth. In this case, the fracture azimuth is known precisely from core-through tests, so a weighting that matched the known azimuth was preferred. Alternately, the same results could be obtained by using an azimuth constraint.

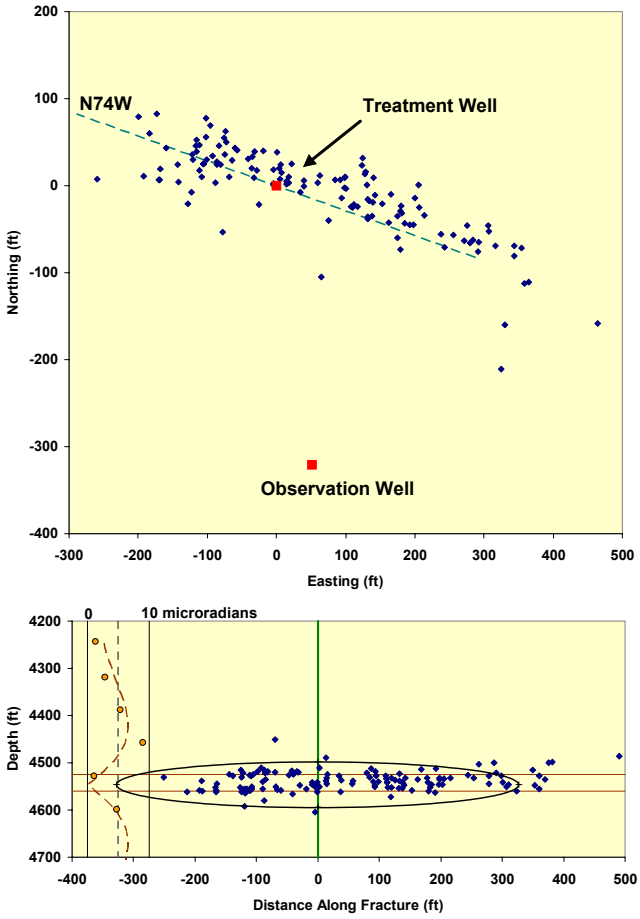


**Figure 5. M-Site combined tiltmeter and microseismic test.**

Table 2. M-Site B Sandstone Comparison

| Parameter | Original µseismic | Original Tiltmeter | Original FE Tilt | Joint Inversion |
|---|---|---|---|---|
| Center (ft) | NA | NA | 4542 | 4547 |
| Height (ft) | 80±20 | 67 | 75-80 | 94.9 |
| Length (ft) | 230/375 W/E | 425 | NA (2D) | 327.4 |
| Azimuth | N74W | NA | NA | N74W |
| Dip | NA | 0° fixed | 0° fixed | 0° fixed |
| Press. (psi) | NA | 1300 | 1300 | 1300 |

Taking the process one step farther, the microseismic data can be re-located as part of the inversion process. However, only the events from the cemented receivers are used in this anlaysis, since the large number of arrivals make these data considerably more accurate. The original location analysis at M-Site used a constant velocity medium because of the fluvial environment and the large number of receivers (velocity effects wash out).[25] In a homogeneous velocity medium, only one of the velocities is independent, so the P-wave velocity was taken as a constraint at $V_p$ = 15,000 ft/sec and the S wave velocity was determined in the inversion. Figure 6 shows a plan-view and side-view map of the microseismic locations and the tiltmeter fit for the re-location case.

The results are very similar to those shown in Figure 5 (although there are fewer events), with the primary difference being some additional estimated length. The final results are a N72°W azimuth, $L$ = 400 ft, $h$=89 ft, and center at 4548 ft. The S-wave velocity was found to be 8,600 ft/sec, compared to the original 8,750 ft/sec.

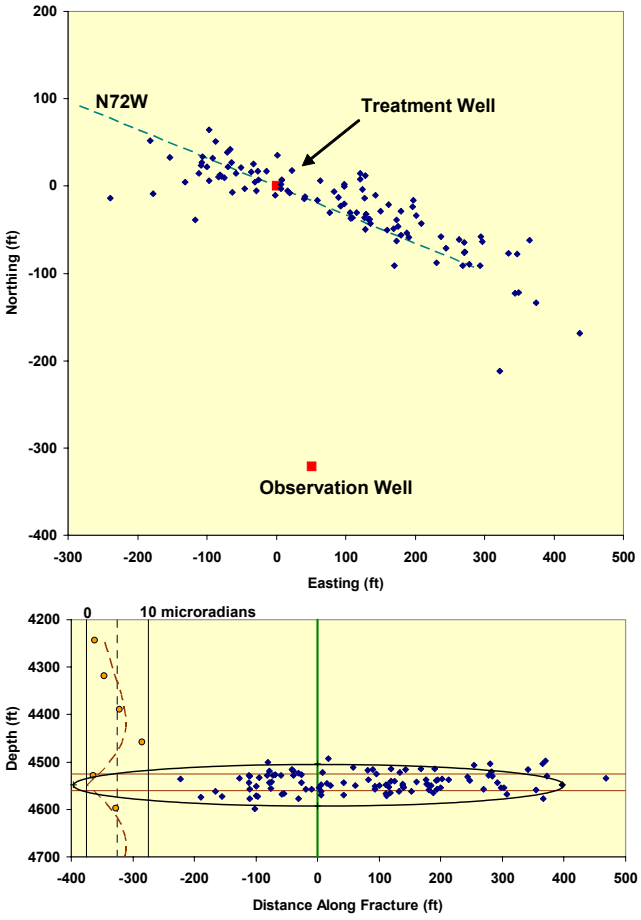


**Figure 6. M-Site re-located results.**

**Mounds Data.** The Mounds Drill Cuttings Injection Experiment[27,28] was another test in which both microseismic and tiltmeter data were obtained.[21,29,30] Experiments at this site simulated the behavior expected to occur in repeat injections of solid-loading slurries into various formations for disposal of drill cuttings. A series of small injections (50 – 100 bbls) were

performed in two different intervals, but the one of interest here is the Atoka shale.

Monitoring of the Atoka shale injections, into a perforated interval at 1940 to 1960 ft depth, was performed with a 8-level tiltmeter array in an observation well at a distance of 140 ft and with a 5-level microseismic array at a distance of 250 ft. However, the microseismic data was very sparse in the Atoka tests, so most of the inferences about fracture geometry were made from the downhole tiltmeters or from a surface tiltmeter array.

There were 20 injections into the Atoka formation over a 3 day period and the 5th injection was chosen as one having good quality tiltmeter data. Additionally, since this injection was early in the overall testing, it is not expected that there was too much complexity yet due to the development of a disposal domain.

Figure 7 shows the plan-view and side-view maps of the inversion results, assuming the microseismic data are located correctly. During the whole first day of testing in the Atoka (8 injections) there were only about a dozen microseisms observed. However, the downhole tiltmeters had responses as large as 50 microradians and the surface tiltmeters also obtained good-quality data.

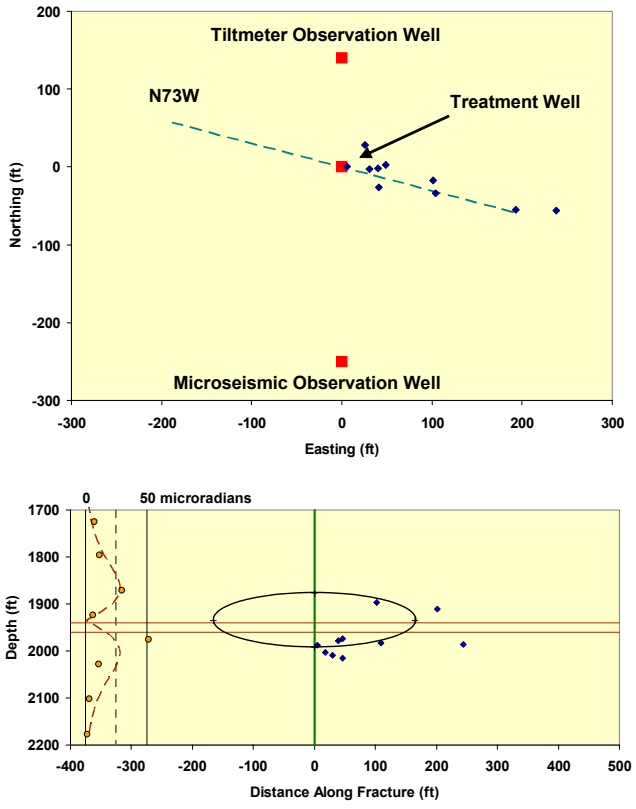


**Figure 7. Mounds Atoka results – injection number 9.**

Contraints on the inversion included a measured net pressure of 425 psi and a vertical fracture. The microseismic data were highly weighted so that the inverted azimuth approximately matched the azimuth derived from the microseism, which were weak by themselves, but matched the azimuth measured by surface tiltmeters. Table 3 shows a comparison of the results from this joint inversion with previously reported data. The main effect of the joint inversion is to allow the fracture to shift up or down, although this does depend to some extent on how highly the microseismic data are weighted (a small weighting yields a deeper center location).

There was no attempt made to relocate the microseismic data in this example since it was so sparse of a data set. Note that the limited microseismic data do not match the tiltmeter geometry very well, but these few events are actually taken from all of the eight injections on that day and are used primarily for azimuth and also for some general control of height and length.

Table 3. Comparison of Mounds Atoka results

| Parameter | Original Tilt | Alternate Tilt | Joint Inv. |
|---|---|---|---|
| Center (ft) | 1974 | 1914 | 1935 |
| Length (ft) | 239.5 | 173 | 165 |
| Height (ft) | 79.6 | 101 | 116 |
| Azimuth (deg) | N73W | N75W | N71W |
| Dip (deg) | 1° | 0° (fixed) | 0° (fixed) |

## Fielding A Hybrid Array

An initial fielding of a hybrid array was performed at an unspecified site in a coalbed methane reservoir. However, this test was a treatment-well hybrid array[31], which does not lend itself readily to the joint inversion because the treatment-well tiltmeter data is primarily usable (at this time) for fracture height measurements.

The hybrid array consisted of five microseismic tools and three tiltmeter tools run together and locked in place with the microseismic clamp arms. Figure 8 shows an example of the tiltmeter data obtained on the three tiltmeter tools in the hybrid array. Injection started at about 14:02, at which time there was considerable movement and rezeroing of the tiltmeter tools in the flowstream. Once pumping stabilized (at about 14:08), the tiltmeters showed a gradual change that resulted in the total tilt change at the end of pumping as displayed on the left-hand side of the plot.

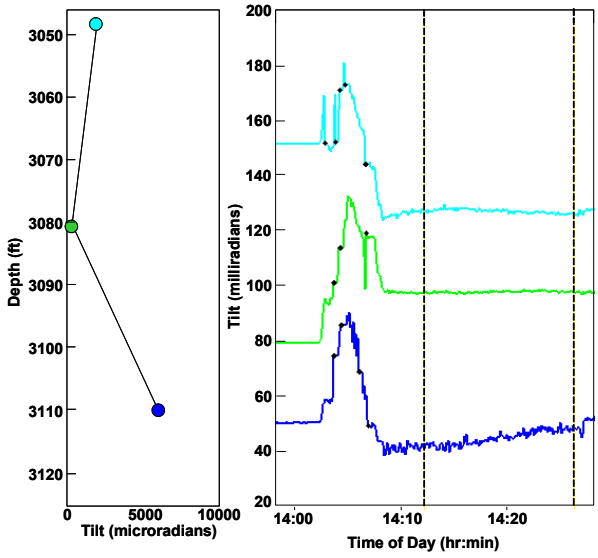


**Figure 8. Example hybrid tiltmeter data (3 levels).**

The tilts observed in Figure 8 are insufficient to describe the fracture top and bottom; however they are consistent with measurements the previous day using a larger number of tiltmeters to diagnose height growth (top at around 3050 ft and other tilt peaks reflecting potential secondary fractures in the vicinity of the perforations at ~3120 ft).

Figure 9 shows example treatment well microseismic data from the 5-level array in the hybrid system. Because it is treatment-well data, it is noisier and rings somewhat due to the moving fluids. Nevertheless, these events can be analyzed and located to provide fracture azimuth and height, as well as length for some cases (e.g., where the fracture is relatively short), as Bailey and Sorem[31] have shown.

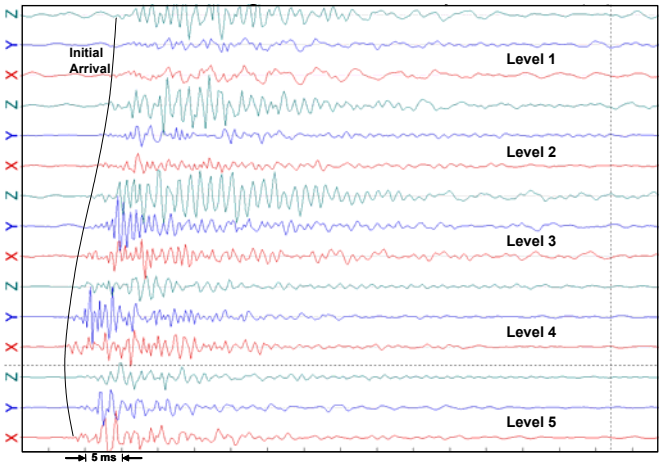


**Figure 9. Example hybrid microseismic data – 5 levels.**

## Discussion

Downhole microseismic and tiltmeter monitoring are the two primary diagnostic techniques available at this time to map fractures and infer growth patterns. The two technologies measure very different effects of the fracturing process. Tiltmeters measure direct deformation that is the summed effect of induced fracture or fractures, while the microseismic array detects and locates microearthquakes induced by changes in stress and pore pressure. Combining the two technologies gives a more comprehensive view of the fracture and its behavior.

These two technologies have routinely been run separately in offset wells dedicated to a particular array, but such an approach limits their application because of the need for additional monitoring wells. A hybrid array containing both types of sensors solves this problem.

Inferences of fracture geometry and growth pattern have generally relied on separate analyses of the two technologies. Such an approach is useful as it provides some level of comfort when the two analyses match up, but results from the two technologies may not match well for numerous reasons, such as distance of monitoring, noise, poor viewing location, and many others. In these case in particular, performing a joint inversion of the data is a sensible step to extract the best possible information from the data.

Developing a joint inversion is relatively straightforward from the tiltmeter side, as long as there is a clear understanding of the mechanism causing the deformation (e.g., a pressurized hydraulic fracture). From the microseismic side, however, the analysis is less direct. Certainly a complete mechanical model of the changes in stress and pressure due to the fracture could be coupled with the existing natural fracture planes and the required rock properties, but the detailed information required to exercise such a model is never available except in rare cases when a comprehensive scientific experiment is being performed (e.g., the Multiwell experiment[33] and M-Site[22]). Using the microseismic data in a distributional sense appeared to be a reasonable compromise to minimize the amount of input data required to perform the joint inversion. This approach does allow for re-location of the microseismic events if the compressional and shear velocities are not constrained, but does not require any other poro-mechanical properties and stresses.

The distributional approach assumes that the microseismic data should pass throught the treatment wellbore, be aligned with the fracture azimuth, be correctly vertically centered, and be distributed in some reasonable manner along the length. The distribution with respect to the model is straightforward, since the azimuth height, length, center depth, and dip are parameters of the model. The model distribution is compared with the actual distribution at any iteration, where the actual distribution is centered about its own vertical center, regression azimuth, and the location of a virtual wellbore that is a projection of the treatment-well location on the microseismic azimuth plane. The objective of the inversion is to find parameters such that the locations of the microseisms match the model parameters as closely as the weighting requires.

Nevertheless, it is the weighting and two characteristic distribution factors (for height and length) that are still very subjective and are currently being investigated as more data are obtained. The effect of the weighting is obvious, but how to apply it in an appropriate manner is less clear. Choosing a large microseismic weighting returns the microseismic results; choosing a low weighting returns the tiltmeter model results. Methods to normalize the individual data sets are now being investigated in order to obtain more predictable behavior as the weighting is adjusted.

The characteristic height and length factors, which are the ratios of the distributional standard deviations to the "true" height and length, appear to be fairly constant (~0.6) for a well-distributed data set like the synthetic data shown in the first example. However, for an asymmetric distribution like the M-Site data, the standard deviation is considerably smaller and a lower factor is required to match the data. For these analyses, the factors were adjusted at the beginning of the inversion to yield an acceptable starting geometry of the microseismic data. However, better ways to select these parameters need to be determined and investigation into this process is continuing. The solution may potentially be the application of a different distribution function that more closely matches microseismic data.

In spite of the subjectiveness of the distributional factors, the results are not found to change much when factors are varied by reasonable amounts. Typical changes in height and length were found to be less than 10% when the factors were dropped from 0.6 to 0.3 to better match an asymmetric data set. This result suggests that these parameters are not that

critical in most data sets, although they certainly could have a significant effect under some conditions.

As noted earlier, this distributional approach is not meant to imply any specific geophysical behavior or process other than expecting the microseisms to be distributed about the fracture in all dimensions. It is simply a convenient method of matching the microseismic event distribution with the current model so that the model can be related to both the tiltmeter data (directly through the deformation behavior) and the microseismic data.

Finally, a hybrid array offers considerable potential for obtaining accurate data to calibrate the velocity model for microseismic monitoring. The velocities along the ray paths of interest (mostly horizontal, as opposed to the vertical ray paths obtained from dipole sonic logs) can be obtained as an inversion parameter that is constrained by the deformation observed by the tiltmeter.

## Conclusions

Hydraulic fracture mapping technology is rapidly becoming a critical element in the development of unconventional resources such as tight-gas sands, gas shales, and coalbed methane. In technology plays such as these, information about the created fracture is essential to optimizing recovery and maximizing the economic returns. Technologies that can improve information about the induced fracture geometry and growth have the potential to significantly influence development strategies and economic decisions.

Hybrid downhole tiltmeter and microseismic arrays combine two technologies into one system to maximize information and minimize the footprint of the monitoring procedures. The use of one monitoring well instead of two significantly reduces costs to the operator and also provides the potential to obtain more information, such as when only one monitoring well is nearby.

A joint inversion offers a methodology for extracting a single result from a combined tiltmeter and microseismic data set, rather than two separate answers that may or may not be entirely consistent. It is still valuable to obtain separate results (to evaluate consistency of the data), but the combined answer has the potential to provide more accurate and more complete results. In addition, the hybrid approach provides considerable potential for calibrating the velocity model for the microseismic analysis.

The joint inversion process is still somewhat subjective due to weighting and distributional issues that are not well defined. As additional data and experience are gained, it is expected that some of these issues will be circumvented.

## Acknowledgments

The authors would like to acknowledge the support of the US DOE under contract DE-FC26-04NT42108 for the development of hybrid arrays and the joint inversion of combined tiltmeter and microseismic data sets. We would also like to thank the large number of people (far too many to name individually) within Pinnacle who have helped to develop the hybrid array system.

## Nomenclature

$b$ = dislocation width, L, ft.
$b_i$ = edge projection of i$^{th}$ microseism, L, ft.
$b_c$ = microseismic center edge projection, L, ft.
$E$ = Young's modulus, m/Lt$^2$, psi.
$G$ = function to be minimized.
$h$ = fracture height, L, ft.
$L$ = fracture length, L, ft.
$n$ = number of tiltmeter data points.
$P$ = Probability distribution.
$\Delta P$ = average net pressure in fracture, m/Lt$^2$, psi.
$r_c$ = microseismic center length projection, L, ft.
$r_i$ = length projection of i$^{th}$ microseism, L, ft.
$u$ = deformation displacement, L, ft.
$V_p$ = compressional velocity, L/t, ft/sec.
$V_s$ = shear velocity, L/t, ft/sec.
$w_{dis}$ = monitor well distance, L, ft.
$x$ = coordinate axis, usually east, L, ft.
$x_i$ = $x$ coordinate position of i$^{th}$ microseism, L, ft.
$y$ = coordinate axis, usually north, L, ft.
$y_c$ = vertical center of fracture, L, ft.
$y_i$ = $y$ coordinate position of i$^{th}$ microseism, L, ft.
$z$ = vertical coordinate axis, L, ft.
$z_c$ = microseismic vertical center position, L, ft.
$z_i$ = $z$ coordinate position of i$^{th}$ microseism, L, ft.
$\alpha_f$ = fracture azimuth, deg.
$\delta_f$ = fracture inclination, deg.
$\nu$ = Poisson's ratio.
$\sigma_b$ = distribution standard deviation about edge, L, ft.
$\sigma_r$ = distribution standard deviation about length, L, ft.
$\sigma_z$ = distribution standard deviation about depth, L, ft.

## References

1. Wright, C. A.: *Tiltmeter fracture mapping: from the surface and now downhole", Petr. Eng. Int.* (1998) **71**, 50.
2. Wright, C.A., Davis, E.J., Minner, W.A., Ward, J.F., Weijers, L., Schell, E.J. and Hunter, S.P.: "*Surface Tiltmeter Fracture Mapping Reaches new Depths – 10,000 Feet and Beyond?*", paper SPE 39919 presented at the 1998 SPE Rocky Mountain Regional Conference, Denver, April 5-8.
3. Warpinski, N.R., Branagan, P.T., Engler, B.P., Wilmer, R., and Wolhart, S.L.: "*Evaluation of a Downhole Tiltmeter Array for Monitoring Hydraulic Fractures*", Proceedings. 36th U.S. Rock Mechanics Symposium, Columbia University, NY (1997) June 29 - July 2.
4. Branagan, P.T., Warpinski, N.R., Engler, B.P., Wilmer, R.: "*Measuring the Hydraulic Fracture-Induced Deformation of Reservoir and Adjacent Rocks Employing a Deeply Buried Inclinometer Array: GRI/DOE Multi-Site Project*", paper SPE 36451 presented at the 1996 SPE Annual Technical Conference and Exhibition, Denver, Oct. 6-9.
5. Warpinski, N.R., Branagan, P.T., Peterson, R.E., Fix, J.E., Uhl, J.E., Engler, B.P. and Wilmer, R.: "*Microseismic and Deformation Imaging of Hydraulic Fracture Growth and Geometry in the C Sand Interval, GRI/DOE M-Site Project*", paper SPE 38573 presented at the 1997 SPE Annual Technical Conference and Exhibition, San Antonio October 5-8.
6. Wright, C. A., E. J. Davis, G. M. Golich, J. F. Ward, S. L. Demetrius, W. A. Minner, and L. Weijers: "*Downhole tiltmeter fracture mapping: Finally measuring hydraulic fracture dimensions",* paper SPE 46194 presented at the 1998 SPE Western Regional Conference, Bakersfield, May 10-13.

7. Warpinski, N.R., Steinfort, T.D., Branagan, P.T. and Wilmer, R.H.: "*Apparatus and Method for Monitoring Underground Fracturing*", United States Patent 5,934,373, Aug 10, 1999.
8. Okada, Y.: "*Internal Deformation Due to Shear and Tensile Faults in a Half-Space", Bulletin of the Seismological Society of America*, (Apris 1992) **82** 1018.
9. Green, A. E., and I. N. Sneddon: "*The distribution of stress in the neighbourhood of a flat elliptic crack in an elastic solid*", *Proceedings Cambridge Philosophical Society*, (1950) **46** 159.
10. Albright, J.N. and Pearson, C.F.: "*Acoustic Emissions as a Tool for Hydraulic Fracture Location: Experience at the Fenton Hill Hot Dry Rock Site*", *SPEJ* (August 1982) **22** 523.
11. Aki, K., Fehler, M., Aamondt, R.L., Albright, J.N., Potter, R.M., Pearson, C.M. and Tester, J.W.: "*Interpretation of Seismic Data from Hydraulic Fracturing Experiments at the Fenton Hill, New Mexico, Hot Dry Rock Geothermal Site*", *Journal of Geophyscial Research* (February 10, 1982) **87** 936.
12. Pearson, C.: "*The Relationship between Microseismicity and High Pore Pressures during Hydraulic Stimulation Experiments in Low Permeability Granitic Rocks*", *Journal of Geophyscial Research* (September 1981) **86** 7855.
13. Warpinski, N.R., Branagan, P.T., Peterson, R.E., Wolhart, S.L. and Uhl, J.E.: "*Mapping Hydraulic Fracture Growth and Geometry Using Microseismic Events Detected by a Wireline Retrievable Accelerometer Array*", paper SPE 40014 presented at the 1998 Gas Technology Symposium, Calgary, March 15-18.
14. Vinegar, H.J., Wills, P.B., De Martini, D.C., Shlyapobersky, J., Deeg, W.F.J., Adair, R.G., Woerpel, J.C., Fix, J.E. and Sorrells, G.G.: "*Active and Passive Seismic Imaging of a Hydraulic Fracture in Diatomite*" *JPT* (January 1992) **44** 28.
15. Withers, R.J., Perkins, T.K. and Keck, R.G.: "*A Field Demonstration of Hydraulic Fracturing for Solids Waste Disposal, Part Two: Real Time Passive Seismic Monitoring System and Data Analysis*", in *Deep Injection Disposal of Hazardous and Industrial Waste*, J.A. Apps and C.F. Tsang, eds., Academic Press, San Diego, (1996) 705.
16. Griffin, L.G., Sullivan, R.B., Wolhart, S.L., Waltman, C.K., Weijers, L. and Warpinski, N.R.: "*Hydraulic Fracture Mapping of the High-Temperature, High-Pressure Bossier Sands in East Texas*", paper SPE 84489 presented at the 2003 SPE Annual Technical Conference and Exhibition, Denver, Oct 5-8.
17. Warpinski, N. R., Wolhart, S. L, and Wright, C. A..: "*Analysis and Prediction of Microseismicity Induced by Hydraulic Fracturing*", paper SPE 71649 presented at the 2001 SPE Annual Technical Conference and Exhibition, New Orleans, Sept 30 –October 3.
18. McEvilly, T.V. and Majer, E.L.: "*ASP: An Automated Seismic Processor for Microearthquake Networks*", *Bulletin of the Seismological Society of America*, (February 1982) **72** 303.
19. Wright, C., Davis, E., Griffin, L., Fisher, K., King, G., Warpinski, N., Ward, J. and Sampson, E.: "*Seismic Mapping Tool Incorporating Seismic Receivers and Tiltmeters*", US Provisional Patent Application 60/553,876, Filed March 16, 2004.
20. Settari, A. and Sullivan, R.B., Walters, D.A. and Wawrzynek, P.A.: "*3-D Analysis and Prediction of Microseismicity by Coupled Geomechanical Modeling*", paper SPE 75714 presented at the 2002 SPE Gas Technology Symposium, Calgary, April 30 – May 2.
21. Warpinski, N.R., and Engler, B.P.: "*Assessment of Downhole-Tiltmeter Fracture Monitoring at the Mounds Drill Cuttings Injection Test*", Sandia National Laboratories Report, SAND2001-1054, Albuquerque (April 2001).
22. Warpinski, N.R.: "*Analytic Crack Solutions for Tilt Fields Around Hydraulic Fractures*", *Journal of Geophysical Research* (Oct 10, 2000) **115**, 23462.
23. Mardia, K.V.: *Statistics of Directional Data*, Academic Press, Orlando, 1972.
24. GRI CD: "*GRI/DOE Multi-Site Hydraulic Fracture Diagnostics Project*", S. Wolhart (manager), Gas Research Institute Report GRI-99/0117, Chicago (May 1999).
25. Warpinski, N.R., Wright, T.B., Uhl, J.E., Engler, B.P., Drozda, P.M. and Peterson, R.E.: "*Microseismic Monitoring of the B-Sand Hydraulic Fracture Experiment at the DOE/GRI Multi-Site Project*", paper SPE 36450 presented at the 1996 SPE Annual Technical Conference and Exhibition, Denver, October 6-9.
26. Engler, B.P. and Warpinski, N.R.: "*Hydraulic Fracture Imaging Using Inclinometers at M-Site: Finite-Element Analyses of the B-Sandstone Experiments*", GRI Topical Report, GRI-97/0361, Chicago (December 1997).
27. GRI CD: "*Mounds Drill Cuttings Injection Project*", S. Wolhart (manager), Gas Research Institute Report GRI-99-0173, Chicago (June 1999).
28. Moschovidis et al.: "*The Mounds Drill Cuttings Injection Field Experiment*", Proceedings of the 37th U.S. Rock Mechanics Symposium, Vail (June 6-9, 1999) 1017.
29. Griffin, L.G., Wright, C.A., Davis, E.J., Weijers, L. and Moschovidis, Z.A.: "*Tiltmeter Mapping to Monitor Drill Cuttings Disposal*", Proceedings of the 37th U.S. Rock Mechanics Symposium, Vail (June 6-9, 1999) 1033.
30. Warpinski, N.R., Branagan, P.T., Wolhart, S.L., Moschovidis, Z.A. and Mahrer, K.D.: "*Microseismic Monitoring of the Mounds Drill Cuttings Injection Tests*", Proceedings of the 37th U.S. Rock Mechanics Symposium, Vail (June 6-9, 1999) 1025.
31. Wright, C., Davis, E., Ward, J., Samson, E., Wang, G., Griffin, L., Demetrius, S., and Fisher, K.: "*Treatment Well Tiltmeter System*", US Patent 7,028.722, April 18, 2006.
32. Bailey, J.R., and Sorem, W.A.: "*Logging Tool Enables Fracture Characterization for Enhanced Field Recovery*", paper SPE 95909 presented at the 2005 SPE Annual Technical Conference and Exhibition, Dallas, Oct 9-12.
33. Northrop, D.A., and Frohne, K.-H.: "*The Multiwell Experiment – A Field Laboratory in Tight Gas Reservoirs*", *JPT* (June 1990) 772.


## SI Metric Conversion Factors

| | |
|---|---|
| ft × 3.048* | E-01 = m |
| psi × 6.894 757 | E+00 = kPa |

# Hydraulic Fracture Mapping With Hybrid Microseismic/ Tiltmeter Arrays

By Norm Warpinski,
*Pinnacle Technologies*

*A project to develop a new method for fracture mapping combines the best features of two of the most widely used current mapping technologies – downhole tiltmeters and microseismic monitoring. The new "hybrid" array provides an improved capability for monitoring and interpreting fracture growth.*

Hydraulic fracturing is employed in almost all U.S. onshore natural gas wells to improve the deliverability of the well and economics of the development.

The application of hydraulic fracturing is particularly important in unconventional gas reservoirs, where economics may be marginal even with a successful stimulation. In such reservoirs, the application of new technology to characterize, access, stimulate and produce the reservoir is critical for optimization of the stimulation treatments and field development. Many of these resources can be characterized as "technology plays," where economic development would be impossible without some of the advanced technology employed.

One of these new technologies is hydraulic fracture mapping, which is frequently used to provide information about the growth and geometric features of the fracture. This type of mapping is a subset of fracture diagnostics, which encompasses all technologies used to derive information about the fracture and its effectiveness. Fracture diagnostics include logging and tracers to provide near wellbore information, pressure analyses and pressure-history matching with a model, and well testing and production analyses among others. Fracture mapping could be defined as the process of determining fracture geometry through direct measurements of geophysical properties influenced or altered by the fracturing process.

## Fracture mapping technologies

There are only three proven types of fracture diagnostics that can measure far-field fracture geometries: surface tiltmeter mapping, downhole tiltmeter mapping and microseismic mapping. To explain these technologies, it is necessary to describe the sensors used to make the measurements.

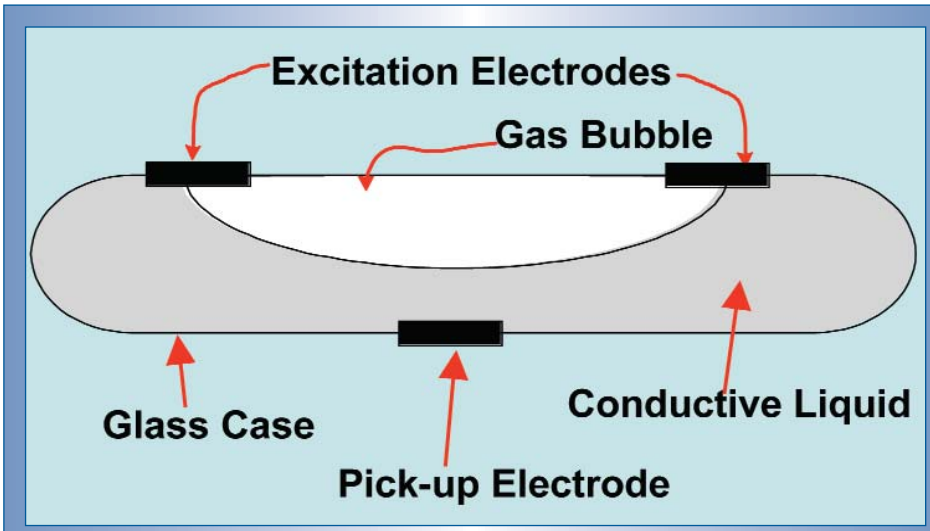


*Figure 1. A schematic of a tilt sensor is shown above.*

## Sensors

Tiltmeters are sensitive devices that measure the slightest deformation of the ground, much like a carpenter level. However, the tiltmeters used in hydraulic fracture mapping are designed for higher sensitivities and can measure tilts as small as 1 nanoradian. Figure 1 shows a schematic of a tiltmeter sensor, which uses a conductive fluid and suitably placed electrodes to achieve the required precision. Arrays of tiltmeters are used to measure the deformation around a fracture induced by the opening of the fracture. This deformation is measured and then inverted for the size and shape of the fracture that created the deformation.

Microseismic mapping is performed with an array of tri-axial seismic receivers, which detect small earthquakes induced by the changes in stress and pore pressure caused by the fracturing process. The geophones or accelerometers in these receivers need to be sensitive and also have higher frequency capabilities than typical VSP receivers, as the microseisms are generally small, high-frequency events. The receiver array detects the microseisms, and P (compressional) and S (shear) arrivals are determined during processing. By appropriate ray tracing, the distance and elevation to the microseism can be determined. The particle motion of the P and S waves (the reason why tri-axial receivers are required) provides the information on the direction to the microseismic source. Since these microseisms are generated in

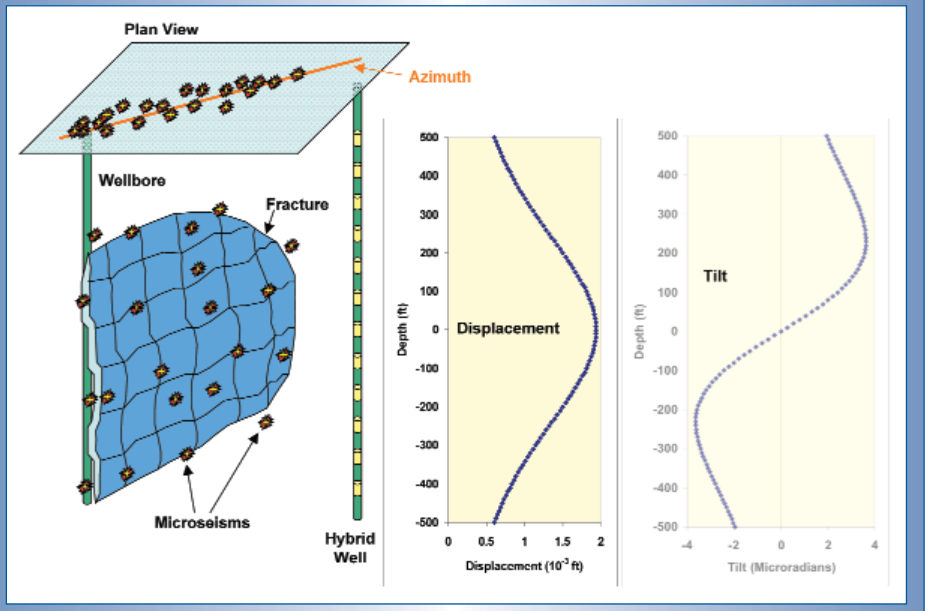


*Figure 2. An example of tilt and microseismic measurements.*

a zone surrounding the fracture, the overall shape and size of the fracture can be evaluated from the spatial distribution of the microseisms.

## Mapping technologies

Surface tiltmeter mapping is a significant reconnaissance tool for mapping fracture azimuths and dip (especially valuable for evaluating horizontal vs. vertical fractures), but being far away from the fracture (at the surface), geometric parameters such as height or length can only be obtained for shallow fractures. Surface tiltmeters are often used in conjunction with downhole tiltmeters and microseismic mapping, but they are not integral to the hybrid system.

If an array of these tiltmeters are placed downhole across from the fracture, more information about the height, width and fracture center can be obtained. In many circumstances, fracture length can also be determined from downhole tiltmeters, along with dip and possibly azimuth. Figure 2 shows an example of the deformation that occurs alongside a vertical fracture and the subsequent tilt that would be measured in an offset well. The shape of the tilt field provides information on height, dip and center while the amplitude of the tilts also helps specify width and length.

Microseismic mapping is also performed with downhole arrays, but it relies on detecting microearthquakes caused by the deformation measured with the tiltmeters and by leakoff of fracturing fluid. Because hundreds of these earthquakes may be created, there is potential for obtaining detailed structural information about the fracture that would otherwise be impossible to obtain. Figure 2 also shows an example of the typical microseismic activity that might be observed in such a fracture.

## Hybrid microseismic/tiltmeter array

In most fracture mapping situations, there is at most one monitor well close enough to be useful for microseismic or downhole tiltmeter mapping. In such cases, it is necessary to choose one of these two technologies based upon the type of information required. However, there is no guarantee *a priori* that the selected technology will actually yield better results. For example, tiltmeters are insensitive to seismic noise, as induced by nearby drilling or fracturing equipment on the same pad, while microseismic receivers may be "deafened" by the noise to the point that few or no microseisms can be detected. On the other hand, microseisms gain an advantage as the monitoring distance increases because resolution from the tilt measurements decreases with distance. There are numerous similar advantages and disadvantages of these two technologies that interplay under various circumstances, leading an observer to the conclusion that it would be optimal to have both technologies in a single array in the monitoring well. This is the rationale behind the hybrid array concept.

A project to develop hybrid arrays has been ongoing for more than 2 years. The first part of this project is developing the necessary hardware and equipment for fielding these two arrays on the same wireline and sending both sets of data to the surface simultaneously. Fortunately, the microseismic arrays are fielded on fiber-optic wirelines that also have six electrical conductors for power and other uses. The optical fiber is necessary for the high-density telemetry requirements of a microseismic array, such as 12 levels x 3 channels x 4,000 samples/sec x 4 byte data x 8 bits = 4,608,000 bits/sec, run with even a minimum number of tools. Use of 15 or 20 receivers would increase this accordingly. However, because the data telemetry is handled easily by the fiber alone, there are free conductors that can be used independently for the tiltmeter data, which is run multiplexed (only two conductors needed). While a combined telemetry system is the ultimate solution, this separate-system approach was envisioned to be one that could prove up the hybrid system in the shortest time.

Given this separate-system approach, the primary hardware needs were crossovers between tools and a method to pass the microseismic telemetry and power lines through the tiltmeters. This was accomplished by constructing a new tiltmeter housing with space for additional lines and new end caps and connectors to mate with the microseismic receivers. Other issues included getting appropriate power downhole to all tools and ensuring all telemetry remained functional. Surface equipment remained the same for each set of tools.

## Joint inversion of hybrid data

The result of a hybrid-array monitoring test would be a tiltmeter map and a microseismic map, each of which would show its own perspective of the fracture geometry. In many cases, these two maps will not agree because of: some inability of one or the other to clearly "see" the fracture; some degree of complexity that cannot be easily reconciled by the tiltmeter model; non-seismic intervals that do not produce microseisms yet still have deformation; or any number of plausible causes. In these cases, the best result will likely be one that provides a best-fit solution for both data sets. Since the tiltmeter results require an inversion (fitting the data to a model) to produce the fracture parameters, a sensible approach is to tie the microseismic data to that same model and determine how well the event locations match the model, that is, jointly inverting the data.

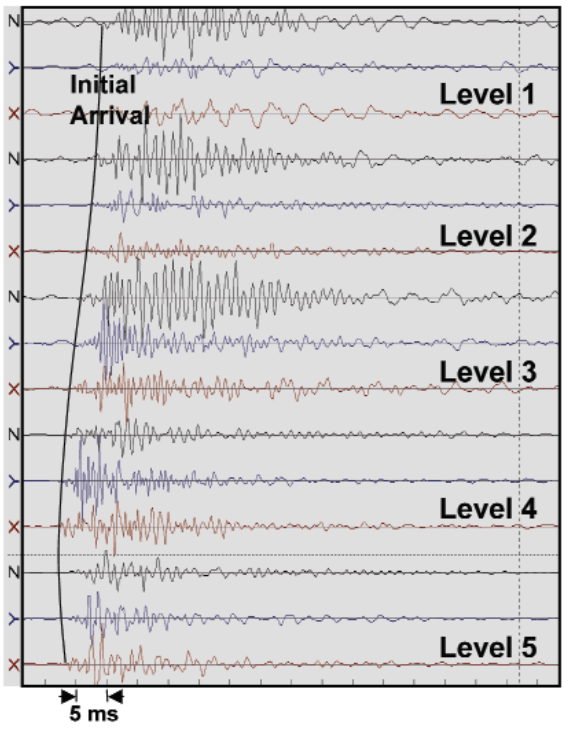


*Figure 3. An example of microseismic data from hybrid-array test.*

As noted above, inversion of the tiltmeter data is straightforward. A model of the process is selected (or several models together, as would occur with multiple fractures), a forward model calculation is made with some initial conditions, the observed data is compared with the forward model calculation, and a decision is made on how to change the model to better fit the data. This process is repeated until the model adequately fits the data.

The uncertain part is how to adequately factor in the microseismic data. The ultimate approach would be to construct a structural model of fracture deformation and leakoff, calculate the stress perturbations and pore pressure changes around the fracture, determine the normal and shear stress on existing failure planes (fracture and faults), calculate where slippage is likely to occur and then use the slippage zone as an envelope that must contain the microseisms. Unfortunately, this approach is complicated and requires data about the reservoir that is seldom available (all three stresses, pore pressure, fracture sets, faults, coefficient of friction, poroelastic parameters, permeabilities of the matrix and fractures, etc.) and guessing these parameters would not be a good way to improve mapping results.

There are simpler approaches, which are not structural, but still require the microseismic data to adequately fit the model. One such approach is distributional, that is, the microseismic events must be distributed in some reasonable way about the model fracture. When they do not distribute adequately about the model, the model is in error and must be changed, similar to the way the tiltmeter inversion changes the model to match the tilt data. The primary questions here are: how to handle the distribution and what parameters to invert.

In the simplest sense, the microseismic distribution about its own center of mass is compared with the distribution about the fracture model. If the model and microseism co-align, then the model is "correct;" if not, the model is changed. An initial approach is to find the standard deviations of the events about its vertical center as an estimate of the fracture height (times a multiplying parameter), the standard deviation of the events horizontally about projected well location as an estimated fracture length (also with a multiplying parameter) and a similar distribution about its edge-on width. Also available from the distributional analysis is an azimuth, the center of the fracture, and the fracture dip.

It was recognized that this approach could also allow for inversion of the velocities of the formation. Assuming the picked arrival times of the P and S waves are correct and the polarization is accurate, (for example, the data are good; the interpretation is the issue), the formation velocities are then the remaining parameters that can result in movement of microseismic locations. Yet formation velocities are not always precisely known in many situations. An inversion that not only finds the best model geometry, but also finds optimized velocities that provide an overall best fit of the total data set, is clearly a desirable result. Such is the approach taken in the joint inversion investigated here.

## Treatment-well hybrid array

In addition to the offset-well approach given above, it is clear that a hybrid array run in the treatment well offers the potential for considerable information about the fracture if no nearby monitoring wells are available. Treatment well microseismic arrays are typically run with rigid interconnects and a gyro tool to orient the string. Adding tiltmeters to this string adds the potential for additional new information and corroborating information. For example, if the tiltmeters – bi-axial devices that will provide a direction of the deformation if the sensors are oriented – are now oriented, then the orientation of the tilt defines the

fracture azimuth, which can be compared with the azimuth derived from the locus of microseismic data. Treatment-well tiltmeters are primarily a height-measurement system, which can be compared with the microseismic height.

## Initial prototype field test

Two protype hybrid arrays were tested in wells to work out final details and evaluate problems last year and early this year, but the first fielding of an array in a fracture-monitoring test was conducted in May in a coalbed methane field in Colorado. This test had five microseismic receivers and three tiltmeters run together on a fiber-optic wireline. Several minifracs and calibration injections (no proppant) were monitored with the tools in various positions relative to the perforated interval.

Figure 3 shows an example of the type of microseismic event detected after shut in (there is generally too much noise to hear events during pumping). This example shows an arrival on five levels of an event that is about horizontal with level 4 at a distance of a little more than 100ft.

Figure 4 shows an example of the tilt data (right side) from one of the calibration tests and a graph of the tilt changes vs. depth during the shut-in period. An examination of the changes in these measurements (center) suggests the fracture bottom was somewhere in the vicinity of the lower tiltmeter (about 3,110ft) giving a large tilt response, and the fracture center was near 3,080ft with not much change in the tilt. The fracture top could not be clearly identified with only the three available tiltmeters. The left side shows a histogram of the observed microseismic heights, which agrees fairly well with the limited tiltmeter data.

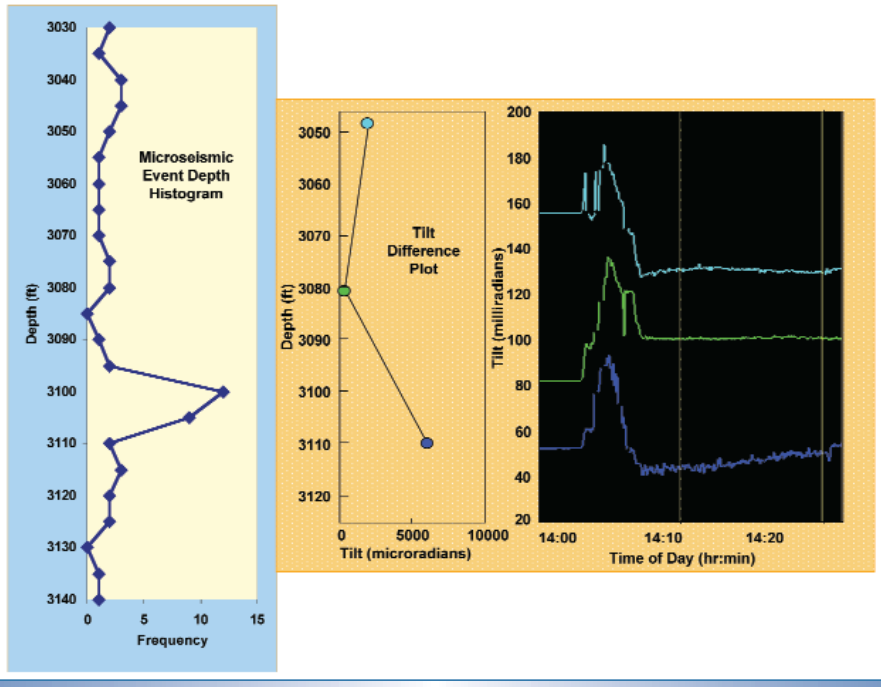


*Figure 4. An example of tiltmeter data from hybrid array test, compared with microseismic events.*

## Conclusions

The hybrid tiltmeter project has been used to develop combined tiltmeter/microseismic mapping arrays that can be used for obtaining the most precise fracture mapping measurements possible. These arrays have been tested in the field and shown that both data sets can be obtained simultaneously in the same well.

A method for jointly inverting the two data sets has also been developed. In addition to a microseismic map and a tiltmeter map, the joint inversion provides an estimate of fracture dimensions that is a combination of the two. ✧

***Acknowledgments***

The authors and Pinnacle Technologies would like to thank the U.S. Department of Energy, through the National Energy Technology Laboratory in Pittsburgh and Morgantown, Pa., for their support of this work under contract No. DE-FC26-04NT42108.

***References***

1. Wright, C. A.: *Tiltmeter Fracture Mapping: From the Surface and now Downhole,* Petroleum Engineer International (1998) 71, 50.

2. Warpinski, N.R., Branagan, P.T., Peterson, R.E., Wolhart, S.L. and Uhl, J.E.: *Mapping Hydraulic Fracture Growth and Geometry Using Microseismic Events Detected by a Wireline Retrievable Accelerometer Array,* SPE paper No. 40014 presented at the Gas Technology Symposium, Calgary, March 15-18, 1998.

3. Wright, C., Davis, E., Griffin, L., Fisher, K., King, G., Warpinski, N., Ward, J. and Samson, E.: *Seismic Mapping Tool Incorporating Seismic Receivers and Tiltmeters,* US Provisional Patent Application 60/553,876, Filed March 16, 2004.

4. Warpinski, N.R., Griffin, L.G., Davis, E.J., and Grant, T., *Improving Hydraulic Frac Diagnostics by Joint Inversion of Downhole Microseismic and Tiltmeter Data,* SPE paper No. 102690 presented at the SPE Annual Technical Conference and Exhibition, San Antonio, Sept 24-27.

5. Bailey, J.R., and Sorem, W.A.: *Logging Tool Enables Fracture Characterization for Enhanced Field Recovery,* SPE Paper No. 95909 presented at the SPE Annual Technical Conference and Exhibition, Dallas, Oct 9-12, 2005.

6. Wright, C., Davis, E., Ward, J., Samson, E., Wang, G., Griffin, L., Demetrius, S., and Fisher, K.: *Treatment Well Tiltmeter System,* U.S. Patent 7,028.722, April 18.